

A Low-cost Microfluidic Approach for Single Cell Analysis of Rare Cells

by Payar Radfar

Thesis submitted in fulfilment of the requirements for
the degree of

Doctor of Philosophy

under the supervision of Prof. Majid Ebrahimi Warkiani,
A/Prof. David Gallego Ortega and Prof. Dayong Jin

University of Technology Sydney
Faculty of Engineering and IT

April 2023

Certificate of Original Authorship

I, Payar Radfar, declare that this thesis is submitted in fulfilment of the requirements for the award of Doctor of Phil, in the School of Biomedical Engineering at the University of Technology Sydney.

This thesis is wholly my own work unless otherwise referenced or acknowledged. In addition, I certify that all information sources and literature used are indicated in the thesis.

This document has not been submitted for qualifications at any other academic institution. This research is supported by the Australian Government Research Training Program.

Signature:

Production Note:
Signature removed prior to publication.

Date: 30/04/2022

Impact of COVID-19 on the Completion of the Thesis

The incident of the global COVID-19 pandemic and long-term lockdowns significantly affected the work on this thesis. Unfortunately, Australia had to undertake major restriction including closing down the universities, laboratories and workplaces. Thus, the progress of the thesis faced major delays. Particularly, chapter 7 was affected the most by the campus lockdowns and limitations with access to the laboratory starting from early 2020 until end of 2021. Further information regarding the impacts on the results and future works has been provided in Chapter 7.

Acknowledgment

Firstly, I would like to acknowledge and thank my supervisor, Prof. Majid Ebrahimi Warkiani for his ongoing support and guidance throughout this project. I would like to particularly appreciate all the motivations to hard work and the opportunity to enter the biotechnology industry. The journey was filled with joy, challenges and most importantly learnings to apply my engineering knowledge for biological applications. I was so delighted to land in such environment and work under a supervisor with a great vision and problem solving. I definitely would have not achieved outcomes without his passion for science and translational work.

I would like to express my gratitude to my co-supervisor, A/Prof. David Gallego Ortega for his endless support throughout my PhD. Often it is difficult task to introduce biological concepts to researchers with engineering background, however, I am extremely grateful for David's efforts to help me broaden the impact of my research. I would like to also express my gratitude to Prof. Dayong Jin for facilitating my research and providing technical support.

I would like to extend my appreciation towards my family for their ongoing support throughout the difficult days of research. A huge thanks to my father, Parviz Radfar, and my mother, Atieh Karimi, for motivating me to continue my research with a pure focus on my studies. I would like to thank my brother, Artin Radfar, for his inspirational talks and supporting me – despite being physically far away. Also, I am extremely grateful to Romina Rahnama for her endless love and support throughout the toughest days. Being mentally prepared to tackle PhD challenges was a huge privilege supported by my family and I am grateful for that. I would like to express my gratitude towards Dr. Lin Ding who helped me throughout different stages of my degree. Additionally, I would like to appreciate the support I received from Dr. Hamidreza Aboulkheyr, Dr. Sareh Zhand, Dr. Jesus Shrestha and Steven Vasilescu. Lastly, I would like to raise my appreciation towards my colleagues and groupmates at Warkiani Lab who helped me throughout my studies. Without their support and help, I would have not been able to achieve my PhD aims and objectives.

Format of Thesis

This thesis is prepared in 7 chapters including published and under preparation publications. The first chapter provides an introduction on cancer and metastasis along with the role of Circulating Tumour Cells (CTCs) in the spread of cancer. In the second chapter an in-depth literature review on the current technologies enabling single cell analysis of CTCs. Furthermore, chapter 3 focuses on rapid microfabrication of microfluidic devices that can enable single cell encapsulation for analysis of CTCs where the clinical sample is often limited and number of CTCs are extremely rare. In chapter 4, a new methodology was introduced to capture single CTCs via a static droplet microfluidic device and retrieving them through rapid freezing of the chip for downstream molecular analysis. This enables rapid, low-cost and simple characterisation of CTCs to improve the accessibility of such single-cell analysis devices. In chapters 5, methods and tools were developed for characterising viable single CTCs based on their metabolic profile. The ability to distinguish single CTCs based on their lactate production can propose a new and reliable biomarker that would directly correlate with patients' disease conditions. Finally, in chapter 6 we explore the relation between the metabolic activity of cancer cells with their epithelial-mesenchymal transition status which is known to be a key principle for spread of cancers in the body of patients. An overall summary is provided in Chapter 7 with an insight on potential future works needed to translate the proposed devices and methodologies in clinical settings.

Author's of Publications

Directly Related Publications

1. **Radfar, P.**, Es, H. A., Salomon, R., Kulasinghe, A., Ramalingam, N., Sarafray-Yazdi, E., ... & Warkiani, M. E. (2022). Single-cell analysis of circulating tumour cells: enabling technologies and clinical applications. *Trends in Biotechnology*. DOI: [10.1016/j.tibtech.2022.02.004](https://doi.org/10.1016/j.tibtech.2022.02.004) - Impact Factor = 21.942
2. Ding, L.#, **Radfar, P.#**, Rezaei, M., & Warkiani, M. E. (2021). An easy-to-operate method for single-cell isolation and retrieval using a microfluidic static droplet array. *Microchimica Acta*, 188(8), 1-11. DOI: [10.1007/s00604-021-04897-9](https://doi.org/10.1007/s00604-021-04897-9) - Impact Factor = 6.408
3. Rezaei, M., **Radfar, P.**, Winter, M., McClements, L., Thierry, B., & Warkiani, M. E. (2021). Simple-to-operate approach for single cell analysis using a hydrophobic surface and nanosized droplets. *Analytical chemistry*, 93(10), 4584-4592. DOI: [10.1021/acs.analchem.0c05026](https://doi.org/10.1021/acs.analchem.0c05026) - Impact Factor = 8.008
4. **Radfar, P.**, Ding, L., de la Fuente, L. R., Aboulkheyr, H., Gallego-Ortega, D., & Warkiani, M. E. (2023). Rapid metabolomic screening of cancer cells via high-throughput static droplet microfluidics. *Biosensors and Bioelectronics*, 223, 114966. DOI: [10.1016/j.bios.2022.114966](https://doi.org/10.1016/j.bios.2022.114966) - Impact Factor = 12.54

Other Publications

1. **Radfar, P.**, Bazaz, S. R., Mirakhorli, F., & Warkiani, M. E. (2021). The role of 3D printing in the fight against COVID-19 outbreak. *Journal of 3D printing in medicine*, 5(1), 51-60. DOI: doi.org/10.2217/3dp-2020-0028
2. Rad, H. S., Shiravand, Y., **Radfar, P.**, Ladwa, R., Perry, C., Han, X., ... & Kulasinghe, A. (2022). Understanding the tumor microenvironment in head and neck squamous cell carcinoma. *Clinical & Translational Immunology*, 11(6), e1397. DOI: [10.1002/cti2.1397](https://doi.org/10.1002/cti2.1397)
3. Rad, H. S., Rad, H. S., Shiravand, Y., **Radfar, P.**, Arpon, D., Warkiani, M. E., ... & Kulasinghe, A. (2021). The Pandora's box of novel technologies that may revolutionize lung cancer. *Lung Cancer*, 159, 34-41. DOI: [10.1016/j.lungcan.2021.06.022](https://doi.org/10.1016/j.lungcan.2021.06.022)

4. Morshedi Rad, D., Rezaei, M., **Radfar, P.**, & Ebrahimi Warkiani, M. (2022). *Microengineered filters for efficient delivery of nanomaterials into mammalian cells. Scientific reports, 12(1), 1-11. DOI: [10.1038/s41598-022-08300-2](https://doi.org/10.1038/s41598-022-08300-2)*
5. Sadeghirad, H., Bahrami, T., Layeghi, S. M., Yousefi, H., Rezaei, M., Hosseini-Fard, S. R., **Radfar P.**, Warkiani M., O'Byrne K., Kulasinghe, A. (2022). *Immunotherapeutic targets in non-small cell lung cancer. Immunology. DOI: [10.1111/imm.13562](https://doi.org/10.1111/imm.13562)*

Table of Contents

Chapter 1 – Introduction	21
1.1 Cellular Heterogeneity	21
1.2 Cell Separation	22
1.3 Rare Cells and Their Importance	23
1.4 Overview of Cancer	24
1.5 Cancer Metastasis & Role of Circulation Tumour Cells.....	24
1.6 Role of Circulation Tumour Cells.....	25
1.7 Thesis Overview	26
1.8 Hypothesis and Aims	27
Chapter 2 – Literature Review	30
2.1 Importance of analysing CTCs	31
2.2 Cellular and molecular features of CTCs	32
2.3 Understanding tumour heterogeneity using genomic analysis of CTCs	33
2.4 CTC single-cell isolation techniques	36
2.4.1 Limited Dilution.....	39
2.4.2 Micro-pipetting & Micromanipulation	39
2.4.3 Laser-Capture Microdissection	40
2.4.4 Fluorescence Activated Cell Sorting	41
2.4.5 Droplet Generators	41
2.4.6 Nano (Micro)-Wells.....	42
2.4.7 Integrated Fluidic Circuits	43
2.4.8 Dielectrophoresis & Optofluidics.....	44
2.5 Current obstacles in single-cell isolation of CTCs.....	46
2.6 Clinical application of single-cell analysis of single/cluster CTCs in cancer targeted therapies.....	46

2.7 Concluding remarks and future perspectives	49
Chapter 3 – Rapid Fabrication of Static Droplet Microfluidic Devices for Isolation of Circulating Tumour Cells	55
3.1 Introduction.....	56
3.2 Result and Discussion	59
3.2.1 Working Principles and Device Design.....	59
3.2.2 Fabrication Approaches	59
3.3 Experimental Results.....	64
3.4 Summary and Conclusion.....	65
Chapter 4 – An Easy-to-Operate Method for Isolation and Molecular Analysis of Single Rare Cells.....	66
4.1 Introduction.....	67
4.2 Material and Methods.....	69
4.2.1 Device design and fabrication.....	69
4.2.2 Cell culture	70
4.2.3 Cells/beads loading and capture rate counting.....	70
4.2.4 Cell viability assay	71
4.2.5 Immunofluorescence staining and imaging.....	71
4.2.6 Single-cell RT-qPCR	72
4.2.7 Numerical simulation	73
4.3 Theory of static droplet array	74
4.4 Results and Discussion	76
4.4.1 Device performance - trapping.....	76
4.4.2 Retrieval through quick freezing.....	78
4.4.3 RNA analysis through RT-qPCR	81
4.4.4 Cell loss during retrieval.....	82

4.4.5 – Alternative Retrieval Approach via Highly Hydrophobic Surface	83
4.5 Conclusion	87
Chapter 5 – Rapid Metabolomic Screening of Cancer Cells via High-Throughput Static Droplet Microfluidics.....	88
5.1 Introduction.....	89
5.2 Materials and Methods	94
5.2.1 Device Design and Fabrication.....	94
5.2.2 Device Loading and Operation.....	94
5.2.3 Cell Culture and generation of syngeneic mouse models of breast cancer	95
5.2.4 Healthy Human Blood	96
5.2.5 Immunofluorescence Staining	96
5.2.6 Numerical Simulation.....	96
5.2.7 SDM Imaging and Analysis	97
5.2.8 Oestrogen Deprivation of MCF-7 Cells	97
5.2.9 Preclinical Validation.....	98
5.3 Automated Droplet Intensity Analyser	100
5.3.1 Programming Workflow.....	100
5.3.2 Image Analysis.....	101
5.3.3 Application Use Cases	102
5.4 Results and Discussion	104
5.4.1 Static Droplet Microfluidic: Concept Design and Development.....	104
5.4.2 Device and Workflow Optimisation.....	104
5.4.3 Classification of Cancer Cell Metabolic Activity at Single-Cell Resolution.....	106
5.4.4 Metabolic Classification of ER+ Breast Cancer Cells	109
5.4.5 Metabolic Classification of CTCs in Blood Samples	109

5.4.6 Pre-clinical Verification of the SDM Device utility for CTC Detection Based on Metabolic Activity	112
5.5 Conclusion	113
Chapter 6 – The Correlation of Epithelial-Mesenchymal Transition and Lactate Metabolism in Human Breast Cancer	115
6.1 Introduction.....	116
6.2 Results and Discussion	117
6.2.1 In Silico Studies	117
6.2.2 Lactate Metabolic Screening.....	121
6.3 Conclusion and Future Works	124
Chapter 7 - Conclusion and Future Work	125
References	128

List of Figures

Figure 1.1 - Cellular Heterogeneity and the Importance of it. A) An illustration of how bulk averaging can mask the gene expression of single cells. Inspired from ref. [1]. B) Importance of understanding cellular heterogeneity and sub population of cells for treatment of patients.

Figure 1.2 - Example of rare cells and resident material. Three typical example of rare cells include circulating tumour cells, stem cells and foetal cells which often can be found in bone marrow, peripheral blood, urine and/or lymph system.

Figure 1.3 - Overview of Metastatic Cascade. The process of cancer metastasis begins from a primary tumour, where a tumour cell spread the cancer through 5 major steps of invasion, intravasation, circulation, extravasation and colonization.

Figure 1.4 – Importance of Miniaturisation. Sample miniaturisation into tiny droplets in contrast to bulk analysis can facilitate a lower limit of detection through sample purification and increasing the effective concentration.

Figure 1.5 – Comparison of Miniaturisation Techniques. Static Droplet Microfluidics only relies on fluid capillary forces to fractionate the sample into sub-nanolitre droplets. In contrast conventional droplet microfluidic that relies on multiple syringe pumps, microscope and complicated setup and operation.

Figure 2.1 - Schematic illustration of the role of CTC in cancer metastasis in various forms and the current workflow for analysis of them. A) Overall outlook of tumour progression with key biological steps of metastasis through intravasation, circulation and extravasation. B) Various CTC assemblies recognised as single cells and clusters [2]. C) Typical workflow for isolation of CTCs including sample collection, CTC enrichment and single-cell characterisation. Created with Biorender.

Figure 2.2 - Single-cell Isolation Techniques. Single-cell Isolation techniques discussed in this review are primarily categorised into conventional and micro-engineering devices. The conventional systems include limited dilution using a handheld laboratory pipette, micromanipulation using a micro-pipette on a robotic arm to allow precise manipulation/handling of liquid, micro-pipetting using a thin capillary pipette under a

microscope, mass cytometry that determines cellular properties via antibodies labelled with metal ion tags, Fluorescent Activated Cell Sorting (FACS) that uses cell surface biomarkers to isolate and deposit single-cells into wells, Laser Capture Microdissection (LCM) that takes advantage of the energy of the laser beam to detach the cell of interest from a slide. Micro-engineering devices include; hydrodynamic traps that utilise fluidic resistances to trap cells, integrated fluidic circuits that features digital valves that handles cells for analysis, droplet generation which encapsulates cells and a barcoded bead through liquid-in-oil segmentations, static droplets that fractionates liquid using capillary forces, nano(micro)-wells which isolates single cells inside nanolitre sized wells that can be used to isolate cell and Dielectrophoresis (DEP) and Optofluidic devices combine microfluidics with microelectronics and optics, respectively, to precisely manipulate cells of interest. Created with Biorender.

Figure 2.3 – Timeline of Commercial Single-Cell Products. With the advancements in technology, single-cell isolation and analysis platforms have been emerging since early 2006. Different technologies can primarily be categorised based on functionality into: Automated Micromanipulation, Fluorescence-activated Cell Sorting (FACS), Nano-Well systems, Droplet Generators, Dielectrophoresis and Optofluidics. Created with Biorender.

Figure 2.4 – Technical challenges with analysis of CTCs and potential pathways to study the tumour microenvironment. A) Technical barriers for isolation of CTC clusters with the current platforms based on different morphological, size and surface biomarkers of clusters which may lead to inability to capture them. B) Representative images of CTC Clusters. Adapted from ref. [3] with permission under open license CC BY 4.0. C) A potential approach for isolating CTC clusters using static microfluidics [4, 5] and adopting spatial technologies for efficiently studying them. Created with Biorender.

Figure 3.1 - Workflow summarising the main steps in generating a PDMS chip from its design to application. Modelling the chip using CAD and doing simulations are the necessary steps before the actual fabrication. The overall process of chip-making can be time-consuming and requires a great deal of precision. The first phase of fabrication is to etch a mould onto a silicon base. Once this mould is complete, PDMS can be poured on the top and then peeled off to obtain the chip.

Figure 3.2 – Microfabrication Workflows. Rapid fabrication of static droplet microfluidic devices through 3D printing, maskless lithography and laser cutting A4 paper. Each method is developed to minimise the required time for prototyping microfluidic devices.

Figure 3.3 – Microfabrication of static droplet microfluidic device using 3D printed moulds. A) Digital Light Processing (DLP) 3D printing of the mould. B) Ethanol dipping of the mould after cleaning the chip. C) PDMS casting of the static droplet microfluidic devices.

Figure 3.4 – Microfabrication of static droplet microfluidic device using maskless lithography. A) Spin Coating of SU8 on silicon wafer. B) Laser writing the pattern on the spin coated wafer. C) Post-baking and heat treatment of the SU8 device. D) PDMS Casting and baking to fabricate the static droplet microfluidic device.

Figure 3.5 – Microfabrication of static droplet microfluidic device using laser cutting technique. A) Laser cutting the pattern on an A4 paper. B) Casting PDMS on the paper mould for fabrication of the static droplet microfluidic device.

Figure 3.6 – Static Droplet Microfluidics A) Operational Steps and B) Working Principle.

Figure 3.7 – Images of the Actual Static Droplet Microfluidic Devices fabricated via 3D Printing, Maskless Lithography and Laser Cutting.

Figure 4.1 – Single cell capturing and retrieving in SDA (a) Schematic illustration of the workflow developed in this study for single cell retrieval using a static droplet array (SDA) microfluidics. The cells were then retrieved for single cell RT-qPCR in this paper. (b) Picture of actual PDMS device which is filled with the red food dye. The close-up views show the architecture of the device, localisation indices and a single cancer cells which is stained with DAPI and anti-CK antibodies.

Figure 4.2 – The SDA device performance for trapping cells. (a) & (b) Single-cell capturing rate of the device with respect to cell concentration and flow rate to find the optimum capture rate of this device. It was found that at 5k cells/mL the single cell capture rate of the device was the highest, about 88% of cells were captured individually. The flow rate plays a smaller role in single cell capture rate, at 5k/mL concentration the variation of capture rate was trivial and there was no significant difference between handheld pipette injection and syringe pump

injection. (c) Device performance tested with MCF-7 and THP-1 cell lines, in a 1:100 ratio (92 single cell were trapped). The green circles on traps were drawn manually to indicate the position of cells. 5 traps were shown with higher magnification for better illustration of the single and double occupied traps. No cell was found to stick to the main channel, inlet, and outlet of the device.

Figure 4.3 – Illustration of the device throughout the freezing and retrieval process along with simulation of the device during injection and freezing. (a) Frozen droplets of food dye tend to all stick to the glass substrate (more rigid surface compared to PDMS chip) after peeling off the device. If the PDMS device was temporarily bonded to a softer substrate than PDMS (e.g. Parafilm), the droplets tend to stick to the PDMS device. (b) pick up of dextran droplet before and after freezing, showing no liquid remaining in the trap. (c) CFD simulation of the flow across the device indicating the flow fills up the traps before proceeding through the main channel. (d) Heat transfer simulation of the droplet placed in -80°C environment with respect to time, elaborating on the rapidness of this method. Simulation indicates the droplets reach -80°C in 5 minutes and are frozen in about 1 minute.

Figure 4.4 – Illustration of the device with greater spacing along with the effect of freezing on cell viability and molecular analysis of the retrieved droplets. (a) Picture of the spaced SDA design with 88 droplets generated using red food dye. This PDMS device was cast in a 3D printed resin mould. Since the space between traps is bigger, this device allows easier pickup of frozen droplets without a microscope. (b) Cell viability after freezing indicated a positive relationship between DMSO content and viability of cells after freezing. Small droplet size and fast cooling reduce the damage of the cells. (c) Comparison between the cycle of the threshold of GAPDH and HER2 genes across the fresh, frozen, and melted droplet sample. Compared to a melted droplet, the frozen droplet has closer Ct value to the fresh cell control, indicating better preservation of the genetic materials after retrieval.

Figure 5.3 – Metabolomic screening of cancer cells via Static Droplet Microfluidics (SDM). A) Overall workflow of Circulating Tumour Cells (CTCs) enrichment, isolation and detection via monitoring the metabolic activity of cells. B) Microscopic image of the SDM device filled with blue food dye. The close-up image shows the architecture and key features of the PDMS

device. C) Working principle of SDM device within three simple steps of i) sample injection, ii) droplet formation and iii) metabolomic screening via pH sensitive dyes.

Figure 5.2 – Working principle of Static Droplet Microfluidic (SDM) device. A) Detection mechanism relies on the fractionation of liquid down to picolitres, uptake of excess uptake of glucose and secretion of lactate from cancer cells compared to white blood cells, resulting in an acidic droplet environment. B) Computational Fluid Dynamics (CFD) analysis of 3 chambers in a row, showing the chamber filling rates over time. C) Post incubation and imaging the SDM device, to determine the metabolically active cells, the intensity of each droplet was profiled using ImageJ, and subsequently the intensity profiles were denoised using MATLAB and lastly the data is processed and analysed.

Figure 5.3 – Programming workflow for analysing droplets. The program workflow consists of 9 key steps in which the microscopic images of static droplets is analysed. The program starts with user inputting variables including minimum pixel, off threshold and on threshold. It is then followed by an initialisation step which image is converted into a matrix containing a single intensity value for each pixel. Based on the user inputs, the software performs gridding to isolate droplets from background pixels and conducts a denoising step to remove smaller size particles. After detecting the droplets, average intensity of each droplet is recorded, normalised and plotted on a chart where the user can export the on-droplet intensity values from the software.

Figure 5.4 – Analysis of Sample Image. A sample image containing circles with different grayscale intensity was used to optimise the program. The figure illustrates different steps of A) importing raw image, B) gridding rows, C) gridding columns, D) plotting droplet intensities, E) defining on threshold and F) normalisation of on droplets in terms of fold change of intensities compared to the off droplets.

Figure 5.5 – Analysis of a Static Droplet Microfluidic Device Image. An actual microscopic image of a static droplet microfluidic device was taken after analysing cancer cell metabolic activity using pH sensitive dyes. The figure illustrates different steps of A) importing the raw image, B) gridding rows, C) gridding columns, D) denoising and elimination of background noise, E) plotting the droplet intensities and F) illustration of the on droplets based on the threshold defined by the user.

Figure 5.6 – Static Droplet Microfluidics (SDM) device characterisation for trapping and monitoring metabolic activity of cells. A) Characterisation of metabolic activity using SDM device and pH sensitive dye based on different droplet volumes (ranging from 5nL to 125pL) and occupancy. B) Characterisation of metabolic activity using SDM device and pH sensitive dye based on different incubation periods (ranging from 15 to 60 minutes) and occupancy. C) Characterisation of metabolic activity using SDM device and pH sensitive dye based on different cell types and occupancy. D) An actual microscopic image (mCherry and bright field channels overlaid) of DU145 cell line inside the SDM device and corresponding denoised & normalised intensity profile, indicating droplets with metabolically active cells.

Figure 5.7 – Static Droplet Microfluidics (SDM) device applications for screening cancer cells. A) Microscopic images of SDM device used to track metabolic activity of MCF-7 cancer cells under oestrogen deprivation and untreated conditions, B) Quantitative analysis of metabolic activity of oestrogen deprived and normal MCF-7 cells using the SDM device. C) Comparing number of cells spiked in healthy human blood versus numbers of active cells found using the SDM device. D) Microscopic images showing a real case scenario, where one metabolically active DU-145 cancer cell is co-trapped with peripheral blood cells. The close-up picture shows DAPI and brightfield channels overlaid of the active droplet that contains a single cancer cell stained with DAPI antibodies. The corresponding intensity graph indicating only one active droplet.

Figure 5.8 – Pre-clinical validation via detection of circulating cancer cells in the blood of mouse models. A) The workflow used for handling and processing mouse models of 67NR (non-metastatic syngeneic model), 4T1.2 (metastatic syngeneic model) and MMTV-PyMT (transgenic model). B) Metabolomic screening of CTC-enriched samples from 8 different mice.

Figure 6.1 – In Silico Study of Breast Cancer Cell Lines and Patients. A) Comparison of 7 lactate related genes of SLC16A2, SLC16A3, SLC16A4, SLC16A7, SLC16A1, LDHB and LDHA across over 40 breast cancer cell lines along with their epithelial mesenchymal transition (EMT) score. B) Statistical analysis of the 7 lactate related genes and perform a Gene Set Enrichment Score (GSVA Score) across four subtypes of breast cancers. C) Hallmark of oestrogen response across early and late stages of breast cancer compared with the hallmark of epithelial-

mesenchymal transition. D) GSVA score of the lactate associated genes with EMT pathway. E) Single cell genomic data analysed based on different classification of PAM50, cancer type, expression of LDHA and LDHB.

Figure 6.2 – Comparison of mesenchymal/epithelial state of cancer cells in respect to expression of A) LDHA and B) LDHB.

Figure 6.3 – Static Droplet Microfluidic Device for Analysis of EMT Induced MCF-7 Cells. A) Static Droplet Microfluidic (SDM) device working principle. B) Comparison of EMT induced MCF-7 and tracking their metabolic activity through the SDM device. C) Analysis of the effect of EMT induction kit over 3 days on lactate production and relative intensity of the droplets.

Abstract

A biopsy is a medical procedure to remove a small tissue sample from a suspicious area to be examined for a disease or condition such as cancer. The biopsy procedure, although providing valuable and detailed information on a patient's condition at a cellular level, is often invasive and requires surgery, resulting in discomfort and pain for the patient. Additionally, accessing deep-seated tissues in the body (e.g., liver and lungs) may not be possible in certain circumstances which leads to difficulties in the diagnosis and treatment of patients.

Advancements in biotechnologies and the emergence of novel tools for the characterisation of cells at single cell resolution have enabled the potential of disease diagnosis through the detection of circulating rare cells in the body fluids such as blood and lymphatic fluid, known as liquid biopsy. Detection of rare cells has been shown to enable the diagnosis and prognosis of many cancers, prenatal diagnosis, and diagnosis of viral infections. Additionally, liquid biopsy is far less invasive than traditional biopsies that can be taken repeatedly which can enable monitoring of the patient's conditions and treatment outcomes. However, the extreme rarity of these circulating cells among peripheral blood cells has limited their use as a biomarker in clinical settings. Current techniques to identify, isolate and analyse the rare cells are extremely laborious and costly, requiring specialised equipment along with skilled operators.

This thesis presents the development of microfluidic tools for characterization and analysis of circulating rare cells at single-cell resolution, with a focus on clinical implementation. By utilising capillary forces, self-driving static droplet microfluidic devices were developed to be capable of fractionating blood samples and isolating single circulating rare cells. The devices feature sub-nanolitre chambers that allow self-isolation of single-cells where they can be used for multi-modal single-cell analysis in confined liquid volume. Firstly, a workflow was developed to perform single-cell molecular studies on circulating rare cells using common laboratory equipment. Furthermore, a detailed study on cell metabolism was conducted to investigate the potential use of lactate production as a biomarker for distinguishing cancer cells from peripheral blood cells by leveraging the miniaturisation effect of the static droplet microfluidic devices. The tools and methods were validated using healthy human blood and preclinical mammary mouse models, along with a MATLAB-based program that was

developed to automate the droplet analysis process and minimise human error. Lastly, the correlation of lactate production and the epithelial-mesenchymal transition (EMT) state of cells was explored as a potential biomarker for understanding the patient's disease state.

Chapter 1 – Introduction

The introductory chapter of this thesis provides a detailed examination of various aspects critical to the field of rare cell analysis and circulating tumour cells. Initially, it explores the concept of cellular heterogeneity, underscoring its biological importance and the implications of cellular variation within the same tissue or organism on cellular studies. This is followed by an in-depth discussion on cell separation methodologies and their applications across multiple biological disciplines, including immunology, cancer research, and stem cell research. Further, the thesis delves into the significance of rare cells, discussing their defining characteristics and the vital role they play in disease diagnostics, treatment, and the broader understanding of biological processes. An encompassing overview of cancer is then presented, detailing its causes, types, and the underlying cellular mechanisms that lead to its development. The chapter also addresses the complex phenomenon of cancer metastasis, with a particular focus on the role of circulating tumour cells. This section elucidates how these cells contribute to the spread of cancer and their significance in the study of metastatic processes. Overall, this introductory chapter aims to lay a solid foundation of understanding, setting the stage for a more detailed and specific exploration of these topics in the subsequent sections of the thesis.

1.1 Cellular Heterogeneity

The study of cell populations at single-cell resolution and understanding the cellular heterogeneity among them can reveal important information regarding different cell types, functionality, conditions and circuits via genomic, transcriptomic, proteomic and metabolomic analysis [6, 7]. Single-cell analysis can provide insights on healthy and diseased behaviours of individual cells that otherwise would have been masked by bulk averaging which can play a crucial role in precision diagnostics and therapeutics [8]. Among different analysis types, single-cell genomic and transcriptomic analysis, has drawn the most attention in the past decade due to its capabilities in discovering cellular information [9]. Typically, single-cell genomic and transcriptomic analysis involves isolation and lysis of single cells to extract, amplify and barcode the DNA/RNA of each cell individually. For RNA analysis, an additional step of reverse transcribing is needed to create complementary DNA (cDNA) due to the unstable nature of RNAs [10].

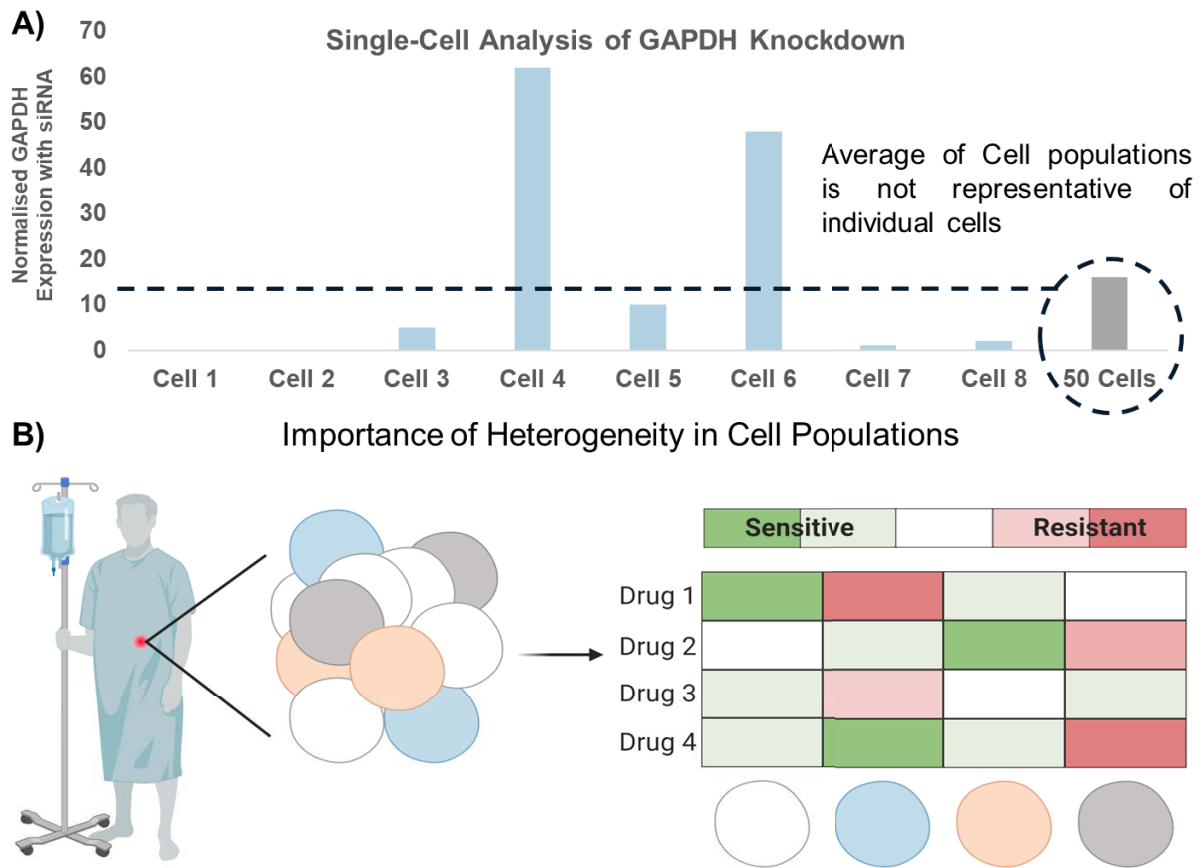


Figure 1.1 – Cellular Heterogeneity and the Importance of it. A) An illustration of how bulk averaging can mask the gene expression of single cells. Inspired from ref. [1]. B) Importance of understanding cellular heterogeneity and sub population of cells for treatment of patients.

1.2 Cell Separation

Cell separation is a powerful technique that allows isolation of subpopulation of cells from a heterogeneous mixture and enables the study of individual cell types individually [11]. Cell separation is extensively used for studying distinct cell types such as immune cells, circulating tumour cells, and stem cells, and provides insight into their function or potential uses in medicine and biotechnology (Figure 1.2). Cell separation is also used in the production of certain therapies such as stem cell therapies and in the diagnosis and treatment of diseases such as cancer [12]. However, in many cases, cell separation requires single cell analysis or purification to achieve the desired results [13]. This technique underpins many discoveries in cell biology and is further enabling research in areas as diverse as regenerative medicine, cancer therapy, and HIV pathogenesis [14].

1.3 Rare Cells and Their Importance

Most of the current single-cell technologies are employed for processing a large population of cells such as tissue biopsies. While there has been a significant development in single-cell analysis platforms for such cases, less attention has been paid to the single-cell analysis of low input samples ($\leq 10^4$ cells) [6]. With advancements in cell enrichments methods, there has been a growing interest in analysing rare cells at a single-cell resolution which can unravel unique insights that are not revealed by bulk molecular analysis [15]. As shown in Figure 1.2, typical examples of rare cell analysis include Circulating Tumour Cells (CTCs), Circulating Foetal Cells (CFCs), immune cells, and stem cells, which are usually found in liquid biopsies (e.g., blood and urine). Rare cells can be defined as a less common cell population with a low occurrence of 1,000 cells or less per milliliter of sample [16]. In the past years, liquid biopsy has gained significant attention due to the critical information that can be obtained from the analysis of rare cells in a non-invasive manner [17-19].

The focus of this thesis is around development of microfluidic devices and workflows that enable low-cost single-cell analysis of rare cells using common laboratory equipment. Despite the ongoing research on different rare cells, CTCs are still among the most studied types of rare cells due to their diagnostic values [20]. Given the accessibility to real human/animal samples for testing the devices, CTCs were mostly used as a perfect use case for the devices developed throughout this thesis.



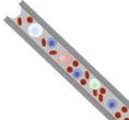

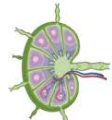


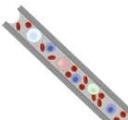

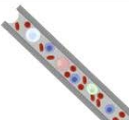
Cell Type	Resident Material			
 CTC	 Bone Marrow	 Peripheral Blood	 Urine	 Lymph
 Stem Cells	 Bone Marrow	 Peripheral Blood		
 Foetal Cells		 Peripheral Blood		

Figure 1.2 – Example of rare cells and resident material. Three typical example of rare cells include circulating tumour cells, stem cells and foetal cells which often can be found in bone marrow, peripheral blood, urine and/or lymph system.

1.4 Overview of Cancer

Cancer is a group of diseases characterized by the uncontrolled growth and spread of abnormal cells that can occur in any organs of the body. The cause of cancer is yet not fully understood, but it is thought to be the result of a combination of genetic and environmental factors [21]. Cancer can be treated using a variety of methods, including surgery, chemotherapy, radiation therapy, and targeted therapies which strongly depend on type/stage of the disease, along with the patient's overall health and preferences [22]. Despite advances in cancer treatment, the disease is still a leading cause of death worldwide [21]. Early detection and prevention are key to reducing the mortality rate from cancer. In addition to the physical and emotional toll of cancer, the disease also has a significant economic impact. According to the World Health Organization, cancer was responsible for nearly 10 million deaths in 2020 [23], with a global economic burden of over 1.16 Trillion Dollars [24]. Overall, cancer is a complex and serious disease that requires ongoing research and efforts to improve prevention and treatment. While progress has been made in understanding and managing cancer, it remains a significant public health challenge.

Early detection and prevention are key to reducing the mortality rate from cancer. Some ways to reduce the risk of developing cancer include avoiding tobacco and other carcinogens, getting vaccinated against certain infectious diseases, practicing safe sex, maintaining a healthy diet and exercise routine, and getting regular screenings for certain types of cancer. Overall, cancer is a complex and serious disease that requires ongoing research and efforts to improve prevention and treatment. While progress has been made in understanding and managing cancer, it remains a significant public health challenge.

1.5 Cancer Metastasis & Role of Circulation Tumour Cells

Among the hallmarks of cancer, the final step of the disease is generally the progression to metastatic cell dissemination and colonisation of distant organs, a process that accounts for

more than 90% of cancer-associated mortality [25]. As shown in Figure 1.1, cancer metastasis occurs through 5 major phases of invasion, intravasation, circulation, extravasation and colonisation. Invasion often begins with cancer cells breaking through the basement membrane, a thin layer of cells that surrounds the primary tumour. Intravasation is followed in which tumour cells enter the bloodstream or lymphatic system and circulate to other parts of the body. The last steps are the extravasation where the tumour cells invade a secondary organ and colonise it to cause cancer to spread.

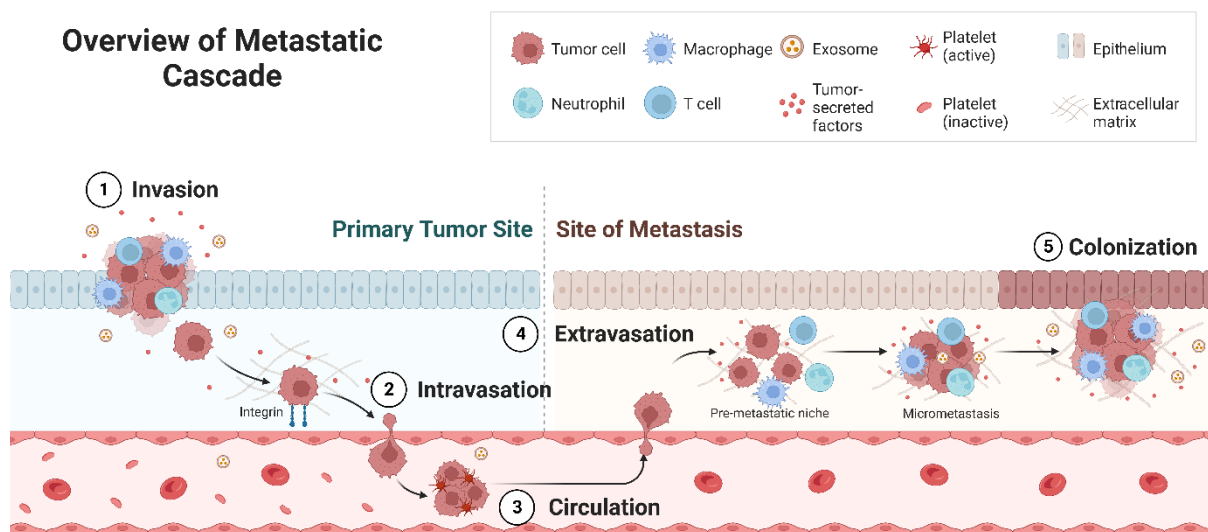


Figure 1.3 – Overview of Metastatic Cascade. The process of cancer metastasis begins from a primary tumour, where a tumour cell spread the cancer through 5 major steps of invasion, intravasation, circulation, extravasation and colonization.

1.6 Role of Circulation Tumour Cells

Circulating tumour cells (CTCs) are the cells that disseminate from a primary tumour and shed into the bloodstream or lymphatic system. These cells are believed to play a key role in cancer metastasis and can survive in the vascular system despite facing challenges such as trauma, oxidative stress, and immune system attacks [26]. CTCs travel in single and cluster formats and must survive from trauma, oxidative stress and immune system attacks in the vascular system to enable metastasis [26-28]. CTCs have a similar genotype and phenotype as the primary tumour and can be used as an alternative strategy for disease diagnosis, prognosis and monitoring treatment efficacy [29]. Besides characterising CTCs, it has been proven that the number of CTCs found in patients' blood correlates directly with the disease progression

and survival rate [30, 31]. Overall, management of cancer via assessment of CTCs in blood samples is far less invasive than taking tissue biopsies, allowing repetitive sampling and monitoring patients' responses to treatments [32]. However, CTCs are exceedingly rare compared to peripheral blood cells, such that one CTC can exist among billions of blood cells [33]. Although erythrocytes can be removed simply by osmotic cell lysis, leukocytes share common physical, chemical and biological properties with CTCs [34]. Hence, isolation and characterisation of enriched CTCs are proven to be a tedious task [35-39].

1.7 Thesis Overview

This thesis has been focused on developing low-cost, versatile and simple tools for isolation and analysis of rare cells. The primary challenge with analysis of rare cells in clinical settings is the reliance on sophisticated technologies that are time consuming and require highly skilled operators. The overall aim of this research project was to provide and suggest simple solutions that would be operated via common laboratory equipment without high level training/skills.

Throughout this thesis, first an in-depth literature review is provided in Chapter 2 with a focus on technologies for enrichment and single cell analysis of CTCs. Major limitations and potential future perspective in the field is discussed in detail. Furthermore, Chapters 3 and 4 focus on development of a static droplet microfluidic device that enables encapsulation of CTCs for molecular analysis at single cell resolution. Chapters 5 and 6 focus on development of a tool for detection and quantifying metabolic activity of CTCs, including a programming approach for rapid quantification of droplets based on their fluorescent intensities. Following to that, in Chapter 7, the correlation between Epithelial-Mesenchymal Transition (EMT) and lactate metabolic activity of cancer cells was studied to explore the potential using single-cell lactate production of cancer cells as a biomarker for diagnosis and prognosis of cancer. Lastly, Chapter 8 provides a conclusion on the key findings of this project along with a perspective on the future works on clinical implication of the proposed devices/workflows.

1.8 Hypothesis and Aims

In this thesis, I propose that integration of microfluidics with current single-cell analysis workflows can lead to development of a low cost and handheld platform for studying rare cells at single cell resolution. Particularly, miniaturisation technologies such as droplet microfluidics can facilitate absolute sample purification, significantly higher effective concentration and consequently lower limit of detection. Additionally, the technology can be used to further validated biological assays and state of cancer cells with their epithelial mesenchymal transition state. As an example, Figure 1.4 illustrates the importance of miniaturisation and its effect on sample purification to lower the limit of detection.

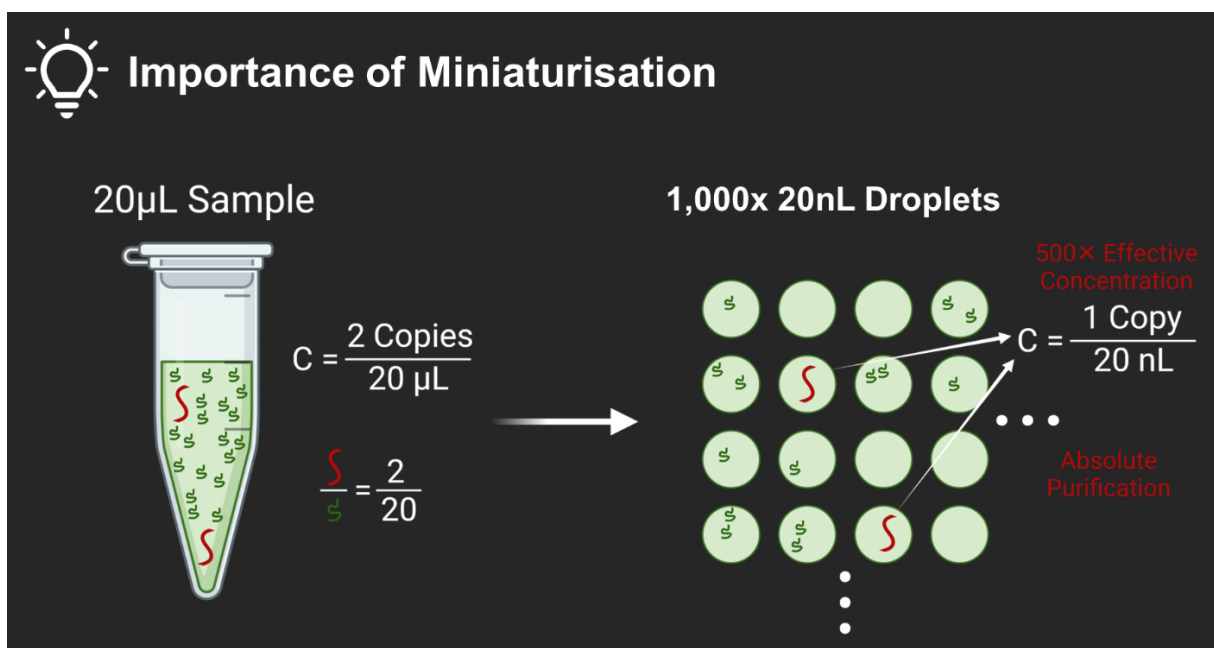


Figure 1.4 – Importance of Miniaturisation. Sample miniaturisation into tiny droplets in contrast to bulk analysis can facilitate a lower limit of detection through sample purification and increasing the effective concentration.

However, majority of current droplet technologies are mainly focused on processing high number of cells with a high throughput; therefore, they are unable to process low input sample such as clinical specimen and rare cells (e.g., CTCs). Also, they are extremely costly and require special equipment which limits their accessibility to general research laboratories. Microfluidics is the science of handling tiny amount of liquid and can be employed to process and isolate individual cells based on their size, deformability, and shape for downstream analysis (Figure 1.5).

✓ **Static Droplet
Microfluidics**



✗ **Conventional Droplet
Generators**

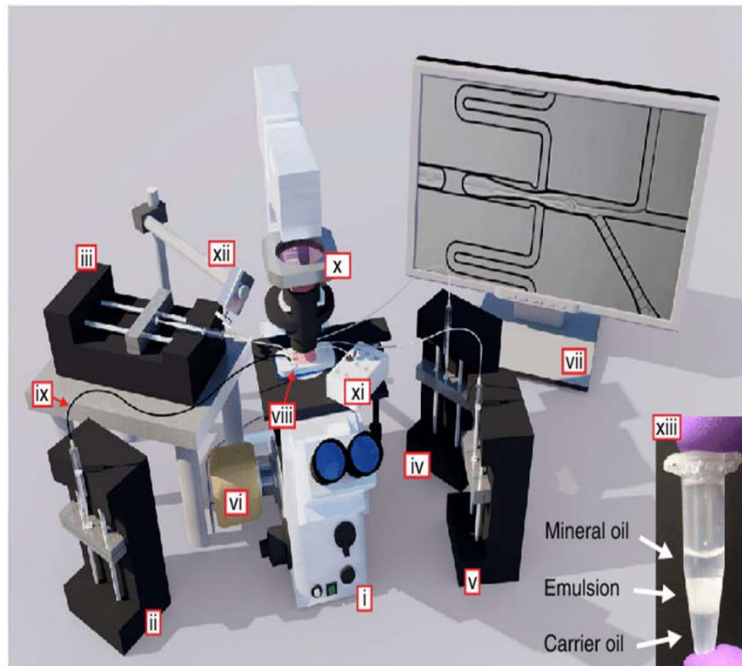


Figure 1.5 – Comparison of Miniaturisation Techniques. Static Droplet Microfluidics only relies on fluid capillary forces to fractionate the sample into sub-nanolitre droplets. In contrast conventional droplet microfluidic that relies on multiple syringe pumps, microscope and complicated setup and operation.

By leveraging on microfluidic science and novel microfabrication techniques, we obtained the following aims throughout this thesis:

Aim 1: Fabrication of Microfluidic Device for Isolation and Retrieval of Single Circulating Tumour Cells. The trapping efficiency is the key factor for effective and efficient isolation of rare cells. Novel Static droplet Microfluidic (SDM) was designed and fabricated to enable capturing of single circulating tumour cells inside individual and confined sub-nanolitre droplets. This eliminates any cross communication between cells that would make it suitable for different analyses. Although wide ranges of devices are proposed for single cell trapping, however, mostly suffer from a retrieval approach. The primary aim of this thesis was to focus on development of a retrieval method of cells using SDM devices. The proposed isolation and retrieval approach can allow handling of cells using a handheld pipette, suitable for transferring cells to PCR tubes or 96-wells for other routine laboratory analyses. This aim was covered throughout chapter 3 and 4.

Aim 2: Single-Cell Molecular Analysis of Single Circulating Tumour Cells. The second aim of this thesis was focused on conducting molecular analysis on single circulating tumour cells. A workflow and a microfluidic device were developed for cell handling, followed by transferring cell to a well for DNA and RNA analysis of single cells in a non-labour-intensive manner, with near no cell loss for using handheld laboratory pipette. Throughout this aim, two approaches for cell lysis and transfer of cell lysate (molecular content) were explored which was followed by quantitative PCR and droplet digital PCR. This aim was covered in Chapter 4.

Aim 3: On-chip Culturing and Metabolomic Screening of Circulating Tumour Cells. Analysis of circulating tumour cells on-chip has been the next challenge addressed in this thesis. The ability to encapsulate single circulating tumour cells inside sub-picolitre individual droplets followed by metabolomic screening. It was successfully shown that excessive lactate production of single cancer cells inside picolitre droplets can result in rapid acidification of the medium and hence was utilised as a label-free biomarker to detect circulating tumour cells. This aim was covered in Chapter 5.

Aim 4: Identifying Lactate Secretion Level of Cancer Cells as a potential biomarker of Epithelial-Mesenchymal Transition state. As the final aim of this thesis, by leveraging the devices and workflows that were developed in the previous aims, the lactate production level of single cancer cells was explored to be used as a potential biomarker for classifying the Epithelial-Mesenchymal Transition (EMT) state of the cells. EMT is a key step in the metastasis of cancers. The potential to classify the EMT state of the cancer cells in a simple and label-free manner can lead to novel approaches for detection and management of cancer patients. This aim was covered in Chapter 6 of this thesis.

Chapter 2 – Literature Review

Summary

This chapter provides an overview on the technologies used for single cell analysis of circulating tumour cells along with a detailed perspective on benefits and shortcomings involved with the use of each technology. Multimodal analysis of circulating tumour cells (CTCs) has the potential to provide remarkable insight for cancer development and metastasis. CTCs and CTC clusters investigation using single-cell analysis, enables researchers to gain crucial information on metastatic mechanisms and the genomic alterations responsible for drug resistance, empowering treatment, and management of cancer. Despite a plethora of CTC isolation technologies, careful attention to the strengths and weaknesses of each method should be considered in order to isolate these rare cells. Here, we provide an overview of cutting-edge technologies used for single-cell isolation and analysis of CTCs. Additionally, we highlight the biological features, clinical application, and the therapeutic potential of CTCs and CTC clusters using single-cell analysis platforms for cancer management. This chapter has been published as a review article in the journal of Trends in Biotechnology (Cell Family) *.

***Radfar, P.**, Es, H. A., Salomon, R., Kulasinghe, A., Ramalingam, N., Sarafraz-Yazdi, E., ... & Warkiani, M. E. (2022). Single-cell analysis of circulating tumour cells: enabling technologies and clinical applications. *Trends in Biotechnology*. DOI: [10.1016/j.tibtech.2022.02.004](https://doi.org/10.1016/j.tibtech.2022.02.004).

2.1 Importance of analysing CTCs

Cancer cells are extremely heterogeneous, and this inherent property appears to be one of the main challenges in shifting the current paradigm towards improving cancer treatment. Among the hallmarks of cancer, metastasis leads to greater than 90% of cancer-related deaths [25]. In recent years, our understanding of the molecular alterations that drive tumour progression and metastasis have improved, which has revolutionized the clinical management of solid tumours towards a more personalized approach. Identifying genomic drivers of cancer initiation and progression has led to the clinical development of a new generation of therapeutic agents, known as targeted therapies. These drugs often target gene products controlling cancer cell proliferation and other survival mechanisms. However, these targeted therapies often lead to therapeutic resistance by the development of mutations in oncogenes or activation of bypass signalling pathways [15]. The longitudinal monitoring of patients' response to a targeted therapy using repeated tissue biopsies is invasive and often impossible due to the size and location of tumours.

An alternative approach involves the analysis of **circulating tumour cells** (CTCs), including single cells and clusters of cells. CTCs refer to the population of cancer cells in the blood circulation, released from primary or metastatic tumours (Figure 2.1) [40]. While it has been proven that CTCs have a short half-lives [41], it is clear that a small number of these can eventually initiate new metastases [27, 42-44]. The genome-wide single-cell RNA-seq and DNA-seq performed on CTCs have provided new insights into CTC heterogeneity and mechanisms of therapeutic resistance to targeted therapies among patients with solid tumours [45]. A significant number of review articles has been published around CTC analysis, discussing the clinical importance and implications of CTCs [46-48]; however, the technical consideration of CTC and CTC cluster analysis have not yet been discussed. In this review, we describe the recent advancements of technologies developed for single-cell analysis, comprehensively discussing the advantages and disadvantages of each approach for analysis of individual and clustered CTCs. Additionally, we highlight the clinical application of single-CTC and CTC cluster analysis in monitoring targeted therapy response in cancer patients towards personalised medicine.

2.2 Cellular and molecular features of CTCs

Phenotypic variation amongst CTCs suggests that specific subpopulations of CTCs exist, and this variation may impart differential metastatic potential [45, 49]. Numerous studies have discovered the link between **epithelial-mesenchymal transition** (EMT) and the acquisition of stemness properties in various cancers [50, 51]. Interestingly, the expression of EMT-related and stem cell markers, including but not limited to CD44 and Vimentin, have been identified in a sub-population of CTCs with the mesenchymal state indicating the existence of cellular heterogeneity among CTCs [49, 52, 53]. For instance, both early- and metastatic-stages of breast carcinoma show an increased number of CTCs with a mesenchymal phenotype [15]. In pancreatic ductal carcinoma (PDAC), single-cell RNA-seq analysis of CTCs identified a loss of epithelial markers E-cadherin and mucin-1 compared to the primary tumour. Remarkably, the expression of pancreatic stem cells markers, ALDH1A1 and ALDH1A2 in CTCs did not correlate with the EMT status, suggesting that EMT and stemness may not be linked in this pancreatic cancer model and thus may follow a tissue-dependent pattern [54]. In addition to these findings, a number of studies have highlighted the role of CTCs in presenting an immune escape mechanism from the body's immune surveillance by the expression of the immune checkpoint protein programmed death-ligand 1 (PD-L1) detected on both single and clustered CTCs from various types of cancer, including lung and head and neck carcinoma [55-58]. These studies highlight how CTC PD-L1 expression may provide a proxy for determining tumour PD-L1 expression, and a measurement for predicting immunotherapy response in these cancer types [58, 59].

The number of CTCs in the blood depends on different factors, such as cancer type and disease status. However, estimates suggest that CTC counts often range between 1 and 100 for every 10^7 white blood cells [33]. While detecting CTCs is challenging due to rarity of them, phenotypic (i.e., size) and biological attributes (i.e., cell surface protein expression) can be utilised to enrich and eventually isolate CTCs among other peripheral blood cells.

Box 2.1 provides further information on CTC enrichment approaches. Although each enrichment technique has its own advantages and shortcomings, high contamination of background cells in the enriched sample and false depletion of target cells remain as the main challenges during the CTC enrichment process [60]. The high contamination of unwanted cells

in the CTC enriched samples leads to challenges for analysis of CTCs [61]. Thus, often an additional step of single-cell isolation is required to study CTCs individually [5].

2.3 Understanding tumour heterogeneity using genomic analysis of CTCs

Whilst CTC enumeration has prognostic value, molecular characterisation and functional testing of captured CTCs can lead to a better understanding of the disease state and potential treatment options [62]. CTCs are often heterogeneous and understanding them at single-cell resolution reveals unique information that is normally masked by bulk/pooled analysis of the samples [47]. Recent studies on single CTCs discovered key insights on the clonal and dynamic evolution of CTCs in response to therapies [63]. For instance, a diagnostic leukapheresis approach identified tumour heterogeneity by analysing CTCs derived from prostate cancer patients [64]. This method allows the analysis of hundreds of CTCs and the identification of sub-clonal copy-number variations (CNVs) that were not easily distinguished in bulk analyses of tumour biopsies [64]. In another example, in multiple myeloma cancer patients, similar clonal profiles were observed between bone-marrow-derived cancer cells and isolated CTCs, with discordances restricted to sub-clonal mutations [17]. It has been found that the mutation spectrum and mutation burden of CTCs and other overt metastases closely resemble regions of the primary tumour known as the metastasis-initiating area [54].

However, the benefit of molecular analysis of CTCs for the study of tumour heterogeneity remains controversial due to the low number of isolated CTCs [47]. Various groups have attempted to address this issue with the use of pooled CTC samples for molecular analysis. Recently, a comprehensive CTC profiling of a panel of 130 genes was performed using individual and pooled CTCs derived from metastatic breast cancer patients [65]. Comparing their metastatic tissue counterparts revealed 85% concordance between individual and pooled samples in at least one or more recurrent somatic mutations and copy number aberration [65]. The presence or absence of CTCs can be further used to unravel the molecular pathways activated or altered during the tumour and metastasis evolution process. For example, distinct gene expression signatures have been found for breast and lung carcinoma from patients with and without CTCs in the blood or disseminated tumour cells in the bone

marrow [66]. Indeed, profiling CTCs from breast cancer patients at the single-cell level showed remarkable intra-patient heterogeneity in the expression of cancer-associated genes [67, 68].

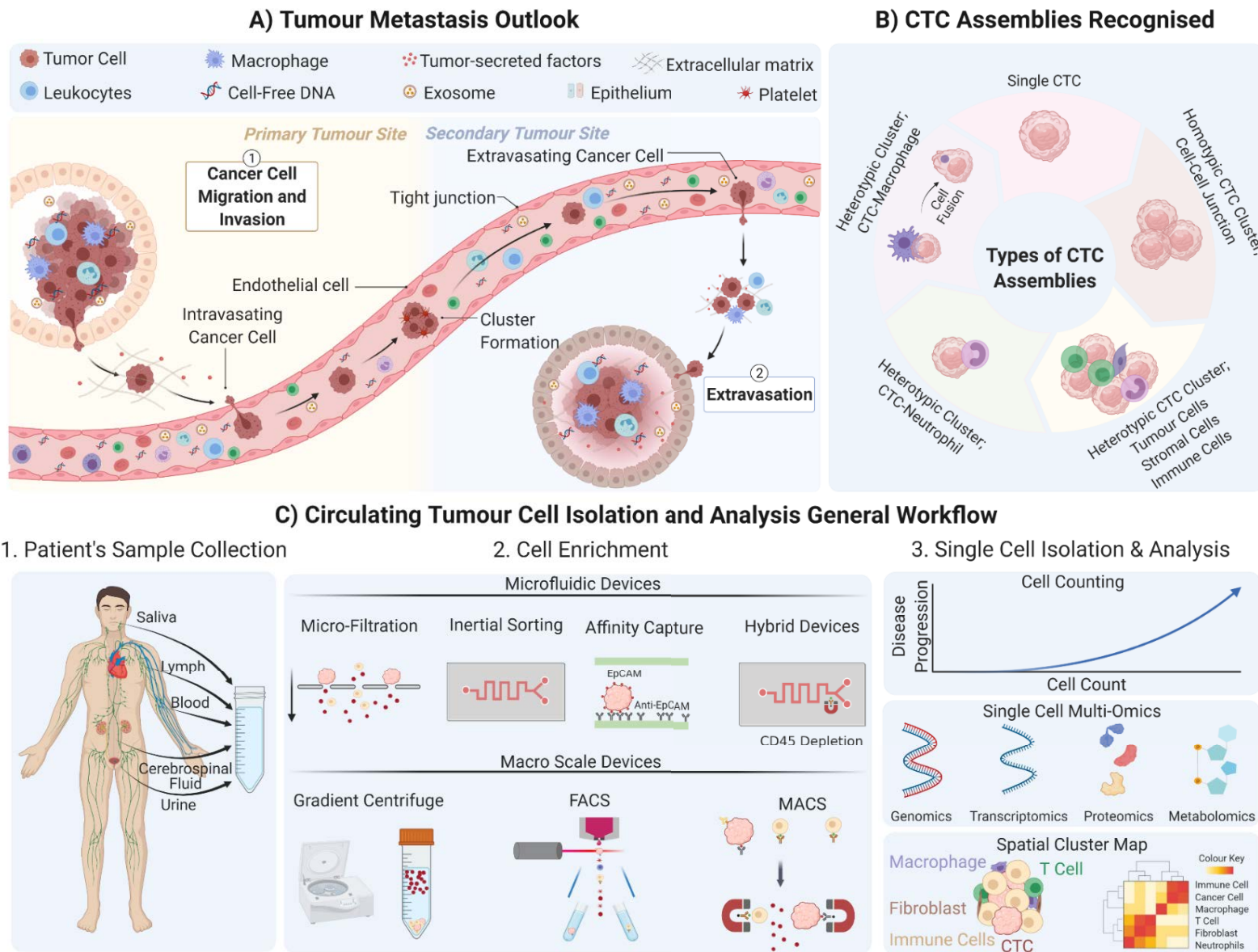


Figure 2.4 - Schematic illustration of the role of CTC in cancer metastasis in various forms and the current workflow for analysis of them. A) Overall outlook of tumour progression with key biological steps of metastasis through intravasation, circulation and extravasation. B) Various CTC assemblies recognised as single cells and clusters [2]. C) Typical workflow for isolation of CTCs including sample collection, CTC enrichment and single-cell characterisation. Created with Biorender.

2.4 CTC single-cell isolation techniques

Whilst CTCs were traditionally analysed through routine imaging that allows for CTC enumeration using a handful of markers, the emergence of enrichment and single-cell isolation technologies have allowed for downstream analysis of CTC with much greater depth of characterisation which provides crucial information of the primary tumour [60]. However, low recovery rate of CTCs and high contamination of background cells in the enriched sample often poses technical difficulties for molecular and functional characterisation of CTCs [4, 47]. Moreover, bulk analysis obscures key information and tends to mask the level of heterogeneity among single CTCs [47, 69]. Thus, use of single-cell analysis technologies can enhance the analysis of CTCs and may identify the potential clinical use of CTCs as a cancer biomarker.

In this section, commonly used single-cell analysis platforms for characterising CTCs are discussed. Figure 2.2 illustrates the conventional and micro-engineered single cell technologies. The commercial implementation of these approaches is shown in Figure 2.3, and a technical comparison of each technique is provided in Table 2.1. Furthermore, Table 2.2 contains detailed information on studies discussed in this section. Lastly, Box 2.2 provides detailed information on types of single-cell analysis often performed post CTC isolation.

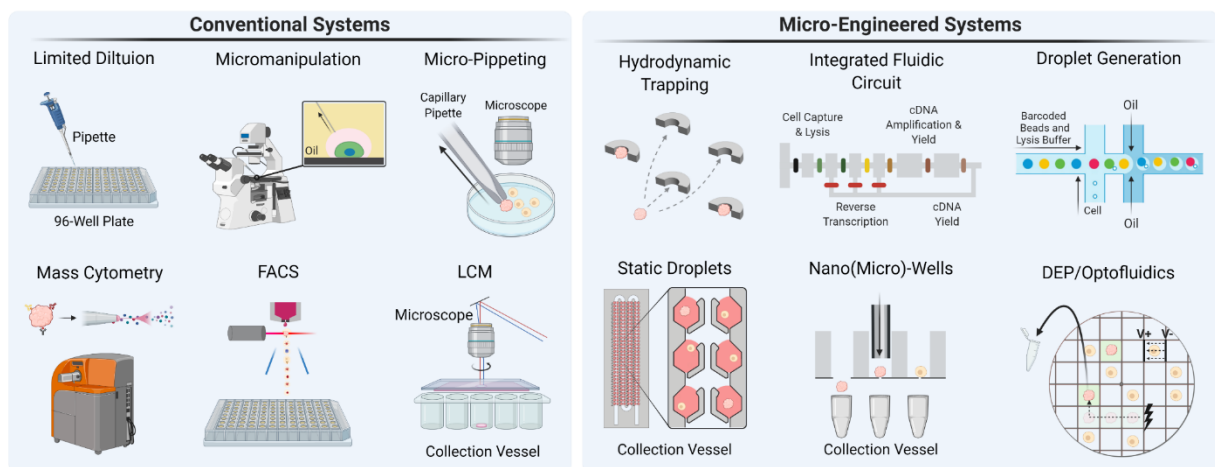


Figure 5.2 - Single-cell Isolation Techniques. Single-cell Isolation techniques discussed in this review are primarily categorised into conventional and micro-engineering devices. The conventional systems include limited dilution using a handheld laboratory pipette, micromanipulation using a micro-pipette on a robotic arm to allow precise manipulation/handling of liquid, micro-pipetting using a thin capillary pipette under a microscope, mass cytometry that determines cellular properties via antibodies labelled with metal ion tags, Fluorescent Activated Cell Sorting (FACS) that uses cell surface biomarkers

to isolate and deposit single-cells into wells, Laser Capture Microdissection (LCM) that takes advantage of the energy of the laser beam to detach the cell of interest from a slide. Micro-engineering devices include; hydrodynamic traps that utilise fluidic resistances to trap cells, integrated fluidic circuits that features digital valves that handles cells for analysis, droplet generation which encapsulates cells and a barcoded bead through liquid-in-oil segmentations, static droplets that fractionates liquid using capillary forces, nano(micro)-wells which isolates single cells inside nanolitre sized wells that can be used to isolate cell and Dielectrophoresis (DEP) and Optofluidic devices combine microfluidics with microelectronics and optics, respectively, to precisely manipulate cells of interest. Created with Biorender.

Table 2.1 Detailed comparison between most commonly used single-cell isolation techniques and how they relate when dealing with CTC analysis.

	<i>Micro-Manipulation</i>	<i>FACS*</i>	<i>Droplet Generators</i>	<i>Nano-Wells</i>	<i>Dielectrophoresis Optofluidics</i>	<i>& Limited Dilution</i>	<i>LCM**</i>
Capture Efficiency	High	Moderate-High	Moderate	Moderate-High	High	Low	High
Doublet Rate	Low <i>Depending on Operator's skills and/or concentration of cells on the imaging slide</i>	Low <i>Related to Sort Mask</i>	Low-Moderate <i>Related to the Loading Concentration</i>	Low-Moderate <i>Related to the Loading Concentration</i>	Low <i>Related to the Loading Concentration</i>	Low <i>Related to the Loading Concentration</i>	Low-Moderate <i>Related to the Loading Concentration</i>
Throughput	Low	High	Moderate	Moderate-High	Moderate	Extremely Low	Low
Upfront Cell Selection	Yes	Yes	No	No	Yes	No	Yes
Starting Amount	Hundreds-thousands	Tens of thousands - millions	Five hundreds - ten thousands	Five hundreds- tens of thousands	Up to tens of thousands	hundreds	hundreds
Laboratory Skills	Moderate	High	Moderate-High	Moderate-High	Moderate-High	Low	Moderate-High
Cell Stress	Low	Moderate-High	Moderate	Low	Moderate	Low	High
Equipment Costs	Moderate-High	High	Moderate-High	Low	Extremely High	Extremely Low	High
Commercial Products	CellCelector (ALS) Eppendorf Micromanipulators SIGHT – Families (Cytexa) cellenONE (Sciencion) iCell8 (Takara)	FACSria (BD Sciences)	GEM Technology (10xGenomics) ddSEQ (Illumina & Bio-Rad) Tapestri Platform (Mission Bio) Nadia (Dolomite Bio) InDrop (1CellBio)	Rhapsody (BD Sciences) C1 (Fluidigm) Easy Puncher (VyCAP) Celsec	DEPArray (Menarini Silicon Biosystems) Lightning Optofluidic (Berkeley Lights) Beacon Optofluidic (Berkeley Lights)	Standard laboratory pipettes.	Arcturus XT (Thermo Fisher) LMD6&7 (Leica Microsystems) CellCut (MMI)
Recommendations	Often suitable after an initial enrichment with a great flexibility for different downstream analysis. Higher throughput is achieved via automated systems. Ability to select individual cells that can significantly lower the analysis costs.	Suitable for second purification and samples with high contamination. Using FACS for single-cell isolation often becomes challenging when dealing with low sample input such as CTC case.	Not recommended for pure low load CTC samples. Not flexible with different analysis types. For CTC analysis, sample pooling is required which will increase the analysis costs.	Vary in range from simple to complex systems and are mostly cost-effective. They are more flexible with downstream analyses. Each nano-well can be used for isolation and/or reaction chamber for different analysis.	High control in cell handling and great choice for single CTC isolation in an automated way. However, they are complex and have an extremely high setup and operational costs.	Limited dilution and LCM approaches are less commonly used for CTC isolation due to their technological limitations including, low-throughput and labour-intensiveness.	

*FACS: Fluorescent Activated Cell Sorting

** LCM = Laser Capture Microdissection

2.4.1 Limited Dilution

Limited dilution, also known as serial dilution, is a simple and cost-effective method for isolation of single cells by dispensing between 0.3-0.5 cells per dispense volume. As the distribution follows Poisson distribution probability, this approach results in a high number of empty wells but critically minimises the multi-occupancy rate [70]. This method can be achieved using a common handheld pipette or pipetting robots and hence is a low-cost approach. Despite the accessibility, this approach is less favourable for isolation of CTCs at the single cell level given the rarity of these cells and large number of wells that would be required [71]. It should also be noted that modern high-throughput single cell genomics instruments such as droplet and nano-well systems use limiting dilution to minimise doublet rates during cell encapsulation.

2.4.2 Micro-pipetting & Micromanipulation

Another approach for the manual isolation of single CTCs from an enriched sample is using a micropipette made from an ultrathin glass capillary. In this approach, the enriched sample is analysed under a microscope, and the cells of interest are identified often based on fluorescent labelling and morphology. Then, an ultrathin glass micropipette approaches the cell of interest and manually gets aspirated (e.g., mouth pipetting), which then is deposited into a collection tube [70]. The major drawbacks of single-cell isolation through manual micro-pipetting are the low throughput, labour intensiveness and reliance on operator's skills [72]. For instance in a study by Xu and co-workers, micro-pipetting has been used to isolate and analyse CTCs in blood samples from 20 early-stage lung cancer patients before and after one cycle of treatment to reveal detailed genetic variations of the CTCs [73].

Micromanipulators, as opposed to micro-pipettes, are typically semi-automated single-cell isolation platforms which consist of an inverted microscope paired with micro-pipettes that are controlled by a mechanical interface. Micro-pipettes are ultra-thin capillary glasses, connected to an aspiration and dispensation unit with capability of handling liquid down to nanolitre scale [70].

In this technique, the CTC enriched sample is often provided as a suspension in a dish or centrifuged on a slide, where the operator identifies the cell of interest using typical CTC

surface biomarkers – e.g., EpCAM. The micropipette is driven to the proximity of the cell and is aspirated via a suction force for consequent transfer of the cells to a collection vessel [74]. As an example, using this approach, Lohr and colleagues reported an integrated process to isolate, qualify and sequence whole exomes of individual CTCs where they identified ~70% mutation similarity of CTCs with the original tissue in prostate cancer patients [54]. Despite the advantages of this approach, including high precision liquid handling and low sample loss, micromanipulation of single cells is a time-consuming, labour-intensive method and can cause damage to the cells which limits the applicability of this approach in clinical settings [72].

To overcome these limitations, commercial products have been developed to automate the cell detection and isolation process within a short time frame (Figure 2.3). In a study by Gkoutela and co-workers, DNA methylation profiles of single CTC and CTC clusters from 43 breast cancer patients and 13 mouse models were analysed to understand the link between CTC clustering and specific DNA methylation changes which can promote stemness and metastasis [26]. In a similar study, Reinhardt and colleagues combined a microfluidic enrichment method named Diagnostic Leukapheresis with an automated micromanipulator followed by a subsequent single-cell transcriptome profiling of CTCs from 7 breast cancer patients [75]. Despite the advantages of automated micromanipulators for identifying, isolating and transferring cells based on their morphology and biomarkers in a labour-free and non-intensive way, this method still suffers from high setup costs, system complexity and low transfer efficiency while handling adhesive cells.

2.4.3 Laser-Capture Microdissection

Laser-capture microdissection (LCM) is a tissue capture technique to isolate single cells from mostly solid tissue slices [76]. Alternatively, this technique has been adopted for isolation of CTCs from enriched sample via fixation/immobilisation of target cells on a slide. Cells are isolated using a highly accurate target recovery and is then transferred to a tube or well for various downstream analysis including genomics and transcriptomics analysis. LCM is traditionally labour-intensive, time consuming and requires fixation/immobilisation of samples when dealing with suspended cells [77]. In a study conducted by Park and colleagues, a single-cell sample preparation and genome sequencing analysis was performed on enriched CTCs using hydrogel encapsulation, followed by LCM to isolate the target cells [78].

Furthermore, Zhu and colleagues performed proteomic analysis of spiked CTCs in whole blood using an immune-density method, followed by single cell isolation using LCM, nanodroplet sample processing and ultrasensitive nanoLC-MS [79].

2.4.4 Fluorescence Activated Cell Sorting

Fluorescence-Activated Cell Sorting (FACS) is a high throughput flow cytometry technique that is capable of characterising, detecting and separating cells via fluorescent tags and allows for sorting of cells by passing an electrostatic charged droplet (containing a cell) through a high voltage electric field [80]. Most commonly, fluorescently conjugated antibodies are used for measuring and sorting cells based on different protein expression on cell surface. Intracellular detection is also possible, but requires fixation and permeabilisation of cells which compromises some downstream assays including single-cell RNA sequencing [81].

In a study by Wang and colleagues, FACS was deployed to use CD45⁻ and hTERT⁺ markers to isolate CTCs from 8 breast cancer patients for measuring SNVs and matched 22 co-occurring mutated genes among CTCs and their primary tumours [82]. Furthermore, Lambros and colleagues, used FACS to isolate single CTCs from 14 advanced prostate cancer patients and studied them through whole genome amplification and copy-number aberration (CNA) which identified complex inter patient, inter cell, genomic heterogeneity that were missed on bulk biopsy analyses [64].

FACS technologies allow isolation and deposition of nanolitre droplets containing a single cell into a well plate. However, FACS can be limited when dealing with low sample volumes (e.g., enriched CTC samples) due to inherent difficulties including system stabilisation and insufficient sample for cell staining and inability to isolate cells with low expression of target proteins [83].

2.4.5 Droplet Generators

Droplet generators leverage the ability of microfluidics to precisely handle tiny volume of liquid (down to pico-litres), and are specifically designed to create water-in-oil droplets by mixing these two immiscible fluids (Figure 2.2) [84, 85]. To allow for massively parallel single-cell DNA/RNA analysis, a barcoded bead in lysis buffer is paired with a single cell inside a droplet. Each droplet is used as a reaction chamber where cell lysis occurs, and the DNA/RNA

of the cell are tagged with the barcode. In the case of RNA analysis, complementary DNA is made by reverse transcription and then amplified, followed by pooling all droplets together to construct a library for DNA/RNA sequencing [84]. In a study conducted by Brechbuhl and colleagues, single-cell analysis of CTCs from 11 breast cancer patient were conducted through an initial filtration enrichment followed by single-cell RNA sequencing using a commercial and automated droplet generation package [86]. Similarly, D'Avola and co-workers studied CTCs from 6 hepatocellular carcinoma patients using a commercial single-cell droplet microfluidic package, indicating the potential of droplet microfluidics for CTC studies for cancer types with limited access to the tissue samples [87].

In addition to high-throughput genomic analysis, droplets can be manipulated by merging, sorting and splitting to test droplet sizes, pH, deformation and behaviour [88, 89]. Droplet-based isolation has allowed a potential application in the study of metabolic activity of CTCs. In line with this, in a study conducted by Del Ben and colleagues, CTCs were isolated inside picolitre droplets and detected via their excessive metabolomic activity (lactate production) and showed potential to detect as little as 10 CTCs among 200,000 white blood cells by using pH level measurement of droplets as an alternative to conventional CTC biomarkers [90]. Consequently, Rivello and colleagues further explored this concept and used the pH level measurement of droplets to separate highly metabolomic active cancer cells from blood of cancer patients and conducted a single-cell RNA sequencing [84].

Despite their high-throughput, droplet generators face difficulties when dealing with low sample input due to system stabilisation times and lowish capture rates and may result in high-cell loss. To overcome the droplet instability with low sample input, CTCs can be pooled with background cells. However, the analysis cost per CTC would increase due to inability to select droplets of interest for downstream analysis and there is a risk of cell loss resulting from the inability to completely deconvolute CTCs from mixed pools. In addition, droplet generators have high setup and operational costs, can be complex and require expertise to operate them which may limit the accessibility of these devices.

2.4.6 Nano (Micro)-Wells

Recently, nanolitre sized wells have been designed and deployed as a simple method for isolation of single cells. Similar to droplet systems, nano-wells are operated by pairing a single-

cell with a barcoded capture bead for downstream analysis. Cell loading occurs according to a Poisson distribution, and the sample must be diluted to allow the desired single-cell occupancy rate. Both cell and beads are passively loaded through settlement of sample due to gravity, which greatly reduces the need for specialised equipment. Using barcoded beads that are matched to the well size, bead occupancy rates can reach close to 100%. This approach results in many wells that contains no cells, therefore the risk of having wells with multiple cells is lowered, but as each well contains a bead, high cell capture rates are retained [83]. Nano-wells are well known as a simple method to analyse single cells for different applications including RNA sequencing [71] and secretion studies [91].

In a study by Park and colleagues, molecular profiling was performed on single CTCs from 55 non-small-cell lung cancer patients, using massively parallel nano-well arrays combined with an on-chip Real-Time PCR (RT-PCR) [92]. Furthermore, Tamminga and co-workers have shown the potential of using a self-seeding nano-wells to isolate and assess released CTCs during surgery for non-small cell lung cancer [93].

Generally, nano-wells are simple to operate, low-cost, and allow for parallelisation, however, these techniques often suffer from cross contamination and not perfectly suitable for running limited sample including CTCs and other rare cells [71]. It is also worth mentioning that nano-wells can be used to enhance the micromanipulation process of single-cells by easier detection and retrieval of cells [81].

2.4.7 Integrated Fluidic Circuits

Integrated fluidic circuits utilise pneumatic membrane valves, pressurised via air, to deflect an elastomer and control fluid movement inside micron-sized channels. In this technique, cells are often encapsulated inside micro-chambers where multi-modal analysis takes place (Figure 2.2). However, these systems are typically limited in throughput and suffer from high complexity [70]. Iyer and colleagues used the Polaris system (Fluidigm Inc, United States) to analyse the transcriptome of 57 single CTCs collected from 3 different breast cancer patients and compared them to 558 single CTC data available publicly, showing inverse gene expression pattern between PD-L1 and MHC that is implicated in immunotherapy [94].

2.4.8 Dielectrophoresis & Optofluidics

Dielectrophoresis (DEP) is a phenomenon that exerts forces on dielectric particles as result of a non-uniform electric field. DEP has been deployed to manipulate single cells by utilising electro-kinetic principles via combination of microfluidics and microelectronics [95]. Similarly, optofluidic-based isolation approaches combine optics and microfluidics to accurately manipulate particles and cells. These devices provide a high level of control on cell-handling which is effectively used in arrays to isolate single cells and have shown to be applicable for CTC studies [96, 97].

Despite their complexity, DEP and optofluidic arrays have been widely adopted and used to analyse CTCs at single cell resolution. Tucci and colleagues used DEPArray technology to isolate and analyse CTCs from 17 stage IV cutaneous melanoma patients based on their cell morphology and immunophenotype features which enabled matching mutational status of CTCs with primary tumours [98]. Furthermore, Cappelletti and colleagues analysed 21 blood samples from 10 patients with metastatic renal cell carcinoma using the same DEPArray technology and identified two subpopulations of epithelial and non-conventional CTCs that lacked epithelial and leukocyte markers [62].

Advancements in microfluidic technologies and adoption of Dielectrophoresis and Optofluidics for cell handling has led to great abilities to precisely manipulate single cells for downstream analysis. However, the high complexity and consequently high cost of these devices just for cell manipulation/isolation is a major drawback for clinical applicability of DEP and optofluidic isolation-based devices.

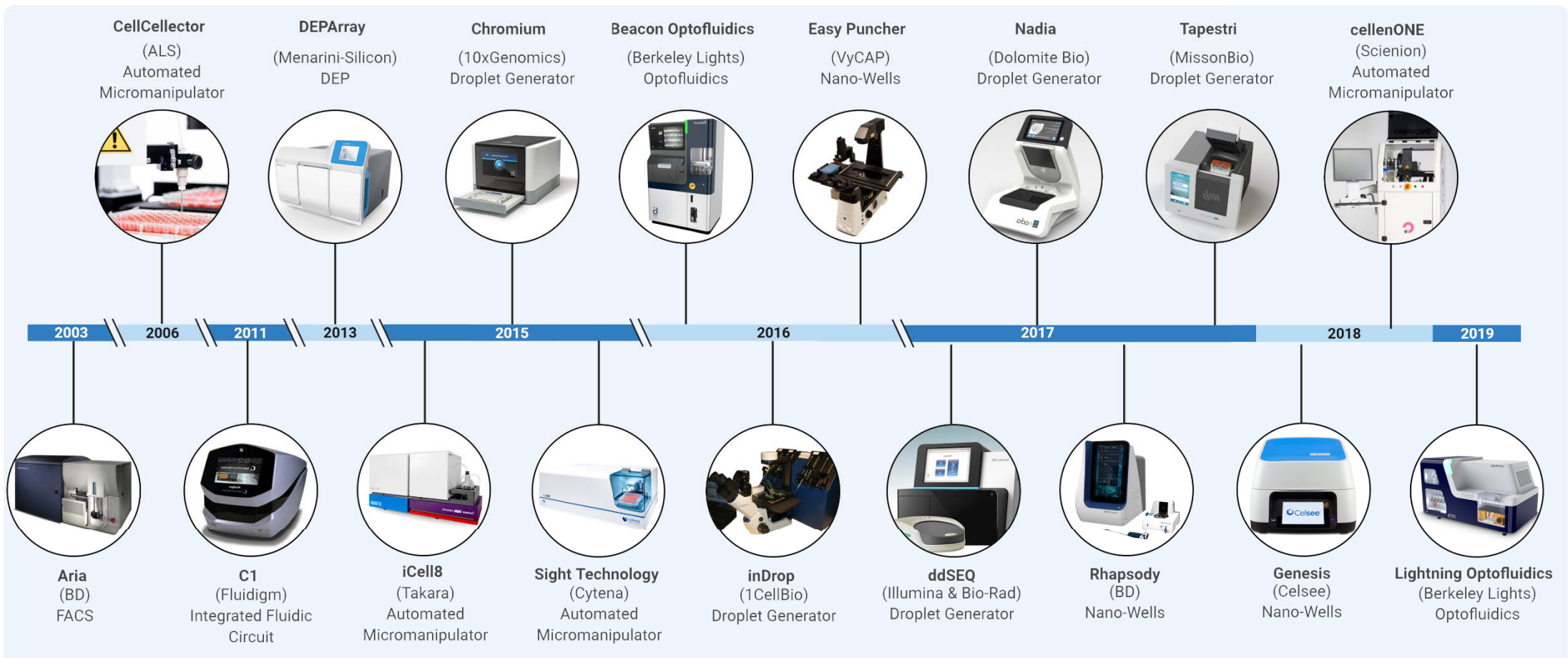


Figure 2.3 - Timeline of Commercial Single-Cell Products. With the advancements in technology, single-cell isolation and analysis platforms have been emerging since early 2006. Different technologies can primarily be categorised based on functionality into: Automated Micromanipulation, Fluorescence-activated Cell Sorting (FACS), Nano-Well systems, Droplet Generators, Dielectrophoresis and Optofluidics. Created with Biorender.

2.5 Current obstacles in single-cell isolation of CTCs

Whilst it is possible to leverage the difference in physical and biological characteristics of CTCs to isolate them from the blood, there is currently no single method that would ensure all CTCs from various cancer types are captured within the one device. For example, not all CTC will be larger than their non-cancerous counterparts and not all CTCs will express a cell surface marker that is unique from cells normally found in the blood. This issue is compounded in the case of CTC clusters due to the wider range of cluster size, different morphologies of cells and the fact that CTC clusters might be composed of non-cancer cells (Figure 2.4A and 2.4B).

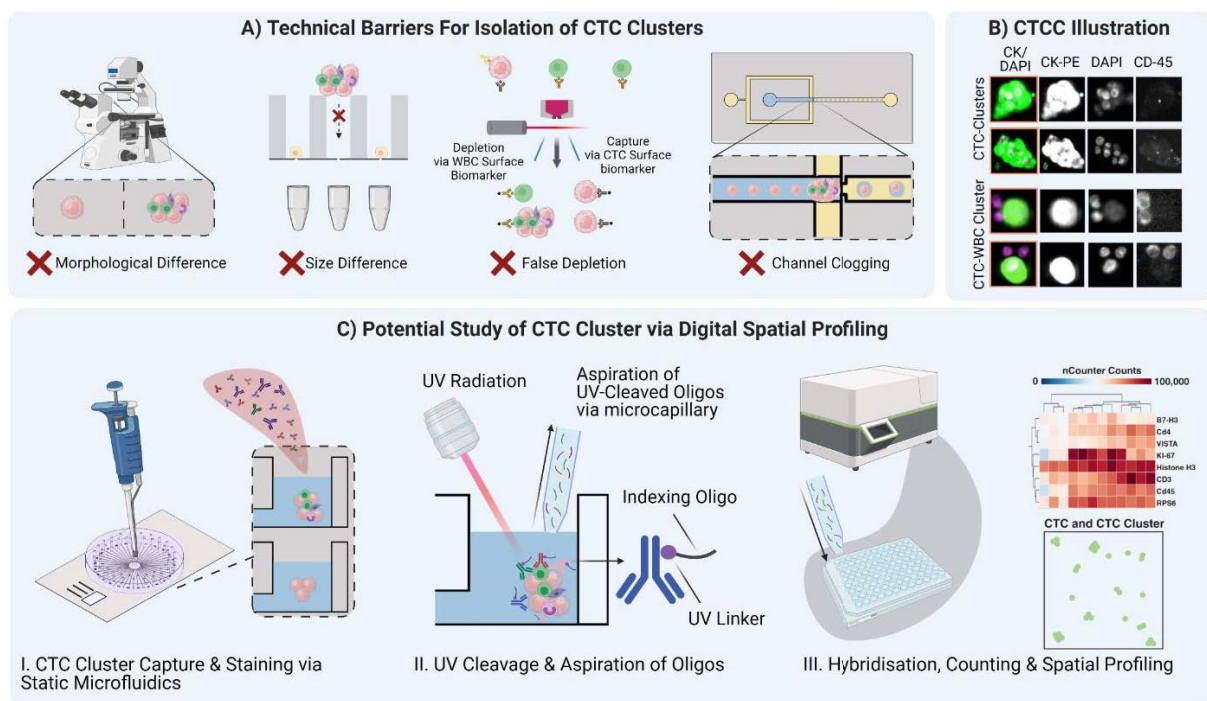


Figure 2.4 - Technical challenges with analysis of CTCs and potential pathways to study the tumour microenvironment. A) Technical barriers for isolation of CTC clusters with the current platforms based on different morphological, size and surface biomarkers of clusters which may lead to inability to capture them. B) Representative images of CTC Clusters. Adapted from ref. [3] with permission under open license CC BY 4.0. C) A potential approach for isolating CTC clusters using static microfluidics [4, 5] and adopting spatial technologies for efficiently studying them. Created with Biorender.

2.6 Clinical application of single-cell analysis of single/cluster CTCs in cancer targeted therapies

Personalised cancer therapy aims to treat patients according to individualised genomic profiles in tumours [99]. Studies have reported major resistance mechanisms to targeted

therapies across a range of cancer types using genomic analysis of CTCs [45, 47]. It is well known that mutations are one of the leading causes of intrinsic and acquired resistance to targeted therapy agents. Considering tumour clonal evolution studies through single-cell analysis, identifying these mutations can be used to monitor tumour evolution trajectories upon therapy pressure and allow the administration of appropriate treatment regimens [100, 101]. The molecular characterization of CTCs at the single-cell resolution could help to identify and analyse drug-tolerant clones within the TME, which are clinically defined as a minimal residual disease (MRD) [102].

To date, the majority of clinical studies evaluating CTC genomic abnormalities have highlighted the presence of gene alterations that can alter the efficacy of target therapies, including but not limited to mutations, rearrangements, or amplifications in *EGFR*, *KRAS*, *HER2*, *PIK3CA*, *ALK*, and *ROS1*, among others [45, 47]. For instance, targeting mutated EGFR using an EGFR tyrosine kinase inhibitor (TKI) improved survival rates among patients with non-small cell lung cancer (NSCLC). Numerous studies reported mutations that can also be detected in captured CTCs [103, 104].

Maheswaran and colleagues isolated CTCs from NSCLC patients identified an in-frame deletion in exon-19, a drug-sensitive-related mutations *EGFR*^{L858R}, and drug-resistance mutation *EGFR*^{T790M} [104]. In agreement with these results, an NGS-based analysis of isolated CTCs detected matched *EGFR* mutations between isolated CTCs and the corresponding primary tumour [103]. The presence of genomic re-arrangements, particularly rearrangements in the *ALK* or *ROS1* have been detected through CTCs analyses [105-107], and a high concordance has been reported for *ALK* rearrangements in CTCs and tumour biopsies in NSCLC [72]. In colorectal cancer (CRC), mutations in codon 12 (G12X) of *KRAS* have been identified in isolated CTCs and positively associated with cancer progression [108]. Since *KRAS*-mutated CTCs can evade EGFR-TKI therapies, continuous monitoring of *KRAS* mutations status using CTCs may facilitate the early detection of developed resistance to EGFR-TKI.

In primary and metastatic breast carcinoma, mutations in *PIK3CA* have been introduced as one of the major molecular resistance mechanisms to HER2-targeted therapy. *PIK3CA* mutations in CTCs have been found in 15.9% of metastatic breast cancer patients [109], with higher rates of *PIK3CA* mutations among CTCs in patients with a HER2-positive status in

comparison with HER2-negative status primary tumours [110, 111]. Additionally, a positive association between the development of drug resistance and the expression of mesenchymal markers in CTCs has been reported in patients with breast and prostate cancer [112, 113]. Taken together, these pre-clinical and clinical findings highlight both the predictive power of genetic alteration analysis of CTCs at the single-cell and the benefit of such analysis in longitudinal studies of those CTCs that display stemness phenotypes during targeted therapy.

Besides gene mutations and rearrangements, CNVs can also be analysed in CTC samples. The analysis of CTCs before the course of treatment can be used to identify distinct CNV signatures in patients with chemo-sensitive and -resistant small-cell lung cancer (SCLC) and thus highlight molecular mechanisms of disease progression [114]. In contrast to ctDNA, the detection of mutations and CNVs in CTCs can provide additional information and correlations when is coupled with specific transcriptomics, proteomics or morphological analysis [45]. In castration-resistant prostate cancer, gene expression changes to androgen receptor-splice variant seven have been widely investigated in CTCs to explore its role in developing treatment resistance to androgen inhibitors [26, 72, 115]. Moreover, RNA-seq analysis of single CTCs from patients with resistance to androgen receptor inhibitors also displayed the activation of the glucocorticoid receptor and non-canonical WNT signalling pathways as possible resistance mechanisms [116]. The phenotypic transformation and cellular plasticity are among the main mechanisms of drug resistance across various tumour types, including NSCLC, prostate cancers, and melanoma [101, 115, 117-119]. Genomic and proteomic analysis of CTCs at the single-cell resolution could provide new insight into the molecular mechanisms behind this phenomenon and aid in identifying appropriate therapies for certain patients experiencing drug resistance. In the neuroendocrine type of prostate cancer, isolated CTCs showed a phenotypic switch associated with endocrine therapy resistance [120]. Additionally, phenotypic transformation to a poorly differentiated phenotype has been observed in CTCs from patients with melanoma who developed relapse in response to BRAF inhibitor (PLX4720) [117].

Interestingly, in the case of breast carcinoma, CTCs from patients with ER+ /HER2- tumour represented a transformation to a HER2+ status-related phenotype under cytotoxic treatment without acquiring additional genetic aberrations [101]. In support of this finding, a recent study evidenced 73% concordance in ER status and 77% concordance in HER2 status

between CTCs and matched primary tumours [121]. To validate these findings in larger cohorts, recently two clinical trials in breast cancer (DETECT-IV (NCT02035813)) and prostate cancer (CABA-V7 (NCT03050866)) launched where therapy decisions are based on the cellular and molecular features of CTCs in a personalized manner.

2.7 Concluding remarks and future perspectives

CTC enumeration studies have consistently shown a link between CTC numbers and disease outcome. Whilst CTC enumeration has been considered as a powerful prognostic tool, single-cell characterisation technologies that allow a deep characterisation of CTCs are now beginning to provide high resolution molecular details about the mechanisms involved with metastasis and therapeutic resistance. These tools are giving us a unique insight into CTC heterogeneity and potentially the primary tumour. The characterisation offered by modern single-cell genomics approaches are providing details of patients' tumour beyond the traditional image-based CTC enumeration. They also supply information in addition to what is covered by ctDNA analysis, namely which genes are actually being expressed or which mutations are being co-expressed within the same cell. Despite this potential, there are still a number of technological barriers that must be addressed before CTC and CTC clusters can routinely and accurately be assessed using high dimensional, single-cell molecular assays (Outstanding Question).

As cancer is a complex disease, often caused by multiple factors involving more than one gene alteration, gaining a true understanding of the clinical relevance of CTCs and CTC clusters across the spectrum of cancer is a non-trivial task. It would involve a wide spectrum of studies across many patients with various stages of their disease under different treatment conditions. One approach to expedite the process is to develop high efficiency isolation approaches that can be coupled to high resolution molecular profiling tools. Although these assays are becoming increasingly available, they are still prone to biases such as strong stochastic variation, low (and/or uneven) coverage, and high dropout and error rates [122]. Despite the demerits, there is no doubt that genomic analysis can, and has provided a deeper characterisation of CTCs. Clinical studies showed that it might lead to an improved ability to patient stratification for personalised targeted therapies.

An alternative method to further our understanding on how CTCs and CTC-clusters relate to cancer progression and treatment selection is to generate CTC cell lines and CTC-derived xenografts (CDX) for molecular analysis and drug screening [122]. In-vitro results along with in-vivo validation using CDX enable the identification of anti-cancer therapeutic agents with increased tumour-killing activity, highlighting the suitability of this approach in principle. However, in-vitro expansion of the cell line or generation of CDX from CTCs is expected to put selective pressures on the isolated CTCs resulting in potential changes. Additionally, it is impossible to create a platform that allows long-term study of the immune component of the CTC clusters which plays a critical role in the increased metastatic potential of them. Therefore, while CTC expansion might be a suitable solution upon the identification of an appropriate growth medium for CTCs, these drug screen assays often require a significant time/cost and CTC expansion may not be performed for every patient.

By combining the results from high resolution single-cell molecular characterisation of CTCs together with drug screening, it may be possible to connect the phenotypic and genomic profiles of CTCs and CTC clusters to determine inherent drug sensitivities. If drug sensitivity can be strongly linked to the molecular and phenotypic characteristics of the CTCs and CTC clusters, it might be possible to figure out the most proper treatment for individual patients and to further alter treatments as the disease progresses.

Thus, to enable integration of CTC analysis in clinical settings, enrichment platforms are required to be: 1) simple and cost-effective to operate, 2) applicable across a wide range of cancers, 3) allow CTC and CTC clusters to be isolated rapidly prior to any biological changes are induced and, 4) highly efficient in capturing viable CTCs and CTC clusters in a format and elution volume that are compatible with current and emerging downstream high dimensional molecular assays. Together, we envision that, technological improvements in CTCs isolation, functional profiling of enriched CTCs using state-of-art technologies such as spatial transcriptomic and proteomic profiling, and ex-vivo expansion of CTCs for drug susceptibility testing are now key to highlight the CTCs analysis as a potential cancer diagnostic and prognostic biomarker for clinical practice.

In line with that, this thesis advocates for the integration of microfluidics with existing single-cell analysis workflows, aspiring to forge a cost-effective, portable platform for analysing rare

cells at a single-cell level. Central to this proposition are advanced miniaturisation technologies like droplet microfluidics, which significantly enhance sample purification and effective concentration, thereby markedly lowering the detection limit. This novel approach is not only instrumental in refining detection capabilities for rare cells but also pivotal in advancing the validation of biological assays, particularly in scrutinizing the epithelial mesenchymal transition state in cancer cells. To provide a lucid, quantitative demonstration of these advancements, this section will feature comparative metrics and illustrative examples, like Figure 1.4, which visually encapsulates the impact of miniaturisation on sample purification and detection thresholds. This structured presentation, possibly in bullet points or tabulated form, aims to concisely yet comprehensively underscore the technological strides and potential applications of this research in the realm of single-cell analysis.

Table 2.2 - Summary of key studies on circulating tumour cells via different single-cell isolation platforms.

Study #	Single-Cell Isolation Technology	Single-Cell Isolation Feature	CTC Enrichment Technique	Cancer Type/Organ	Significance & Outcomes	Ref.
1	Micro-pipetting	Surface biomarkers	Deterministic lateral displacement & immunomagnetic - WBC depletion	Signet ring cell carcinoma & adenocarcinoma	Xu and colleagues developed an integrated system consisting of two enrichment stages, i.e., a deterministic lateral displacement step for depletion of erythrocytes and an immunoaffinity part for leukocytes removal. The putative CTCs were picked up using in-mouth pipette technology followed by single-cell analysis. The authors showed successful detection and isolation of CTCs from 15 out of 20 patient samples tested, and consequently conducted single-cell DNA sequencing to show copy number variations, single nucleotide variants and insertion or deletion (InDel).	[73]
2	Micromanipulation	Surface biomarkers & sub-nanolitre wells used as a guide	Magnetic cell sorting	Prostate cancer	Lohr and colleagues reported an integrated process to isolate, qualify and sequence whole exomes of isolated single CTCs. They matched 70% mutation similarity of CTCs with the original tissue in prostate cancer patients. In this work, magnetic cell sorting was deployed to enrich CTCs from peripheral blood of patients, stained and loaded the enriched CTCs onto an array of 84,672 sub-nanolitre wells and used a micromanipulator to transfer the single CTCs to a PCR plate after identification of target cells.	[54]
3	Automated micromanipulation	Size based selection & surface biomarkers	Parsortix	Breast cancer	Gkountela and co-workers reported a study in which DNA methylation profiles of single CTCs and CTC clusters from 43 breast cancer patients and 13 mouse models were analysed to understand the link between CTC clustering and specific DNA methylation changes that promotes stemness and metastasis. The blood samples were enriched for CTCs using Parsortix system (size-based filtration) prior to transfer to individual PCR tubes using a commercial and automated micromanipulator. A total of 188 single CTCs and 149 CTC clusters were detected and analysed through whole-genome bisulfite sequencing or RNA-sequencing.	[26]
4	Automated micromanipulation	Size based selection & surface biomarkers	Parsortix	Breast cancer	Reinhardt and colleagues performed single-cell transcriptomic profiling of 33 single CTCs from seven breast cancer patients for characterisation of inter-cellular heterogeneity in terms of endocrine resistance. They revealed CTC subpopulations with different expression of transcripts regarding the differential phenotypes involved in endocrine signalling pathways and response or resistance to endocrine therapy. In this work authors used the Parsortix system	[75]

and an automated micromanipulator for isolation and Real-Time quantitative PCR (RT-qPCR) analysis of individual cells.

5	Laser-capture microdissection	Surface biomarkers	Microfluidic-Ratchet (deformability based)	Prostate cancer	Park and colleagues performed single-cell genome sequencing on 8 single CTCs using a panel of 73 cancer-related genes. The authors initially enriched the sample for CTCs using a deterministic lateral displacement microfluidic device, followed by a hydrogel encapsulation and LCM to isolate the target cells, showing a 93% single-cell transfer efficiency.	[78]	
6	Laser-capture microdissection	Surface biomarkers	Immune density	Cancer cell line	Zhu and colleagues demonstrated the potential of carrying out proteomic profiling of 5 spiked CTCs enriched from whole blood using immune-density method, followed by single cell isolation using LCM, nanodroplet sample processing and ultrasensitive nanoLC-MS. Their workflow could identify an average of 164 protein groups from samples comprising a single LNCaP cells (a prostate adenocarcinoma cell line).	[79]	
7	Fluorescence Activated Cell Sorting (FACS)	Surface biomarkers	FACS	Breast cancer	Wang and colleagues deployed FACS to separate and isolate single CTCs using CD45 ⁻ and hTERT ⁺ detection scheme. They isolated 11 CTCs from 8 breast cancer patients for measuring SNVs and matched 22 co-occurring mutated genes among CTCs and their primary tumours. The authors proposed CTC-shared SNVs as a potential signature for identifying the origin of the primary tumour in a liquid biopsy.	[82]	
8	Fluorescence Activated Cell Sorting (FACS)	Surface biomarkers	Apheresis followed by immunomagnetic capture via CellSearch	Prostate cancer	Lambros and colleagues used FACS to isolate 185 single CTCs from 14 advanced prostate cancer patients and studied through whole genome amplification and copy-number aberration (CNA) which identified complex inter patient, inter cell, genomic heterogeneity missed on bulk biopsy analyses. This was the first scientific evidence of using apheresis technique to process large blood volumes (mean volume of 59.5mL) to enrich CTCs in a sample.	[64]	
9	Droplet generation	Single-cell sequencing	RNA	Size-based filtration	Breast Cancer	Brechbuhl and colleagues investigated intravascular interactions between circulating breast cancer cells and other peripheral blood mononuclear cells via single-cell RNA sequencing. They predicted an enhanced immune evasion in the CTC population with EMT characteristics. The authors in this work used a commercial and automated single-cell droplet generation package and a total of 93 CTCs from 11 breast cancer patients were detected throughout their analysis.	[86]
10	Droplet generation	Single-Cell Sequencing	RNA	CD45 negative enrichment	Hepatocellular carcinoma	D'Avola and co-workers performed single-cell RNA sequencing on CTCs from 6 hepatocellular carcinoma patients which there is a limited access to the tissue sample. They showed genome wide expression profiling of CTCs demonstrate CTC heterogeneity which helps detecting known oncogenic drivers in hepatocellular carcinoma such as IGF2. They developed a method that combines image flow cytometry and high density single-cell mRNA sequencing.	[87]
11	Droplet generation	Metabolomic activity – lactate production	immunomagnetic - WBC Depletion	Colorectal cancer	Del Ben and colleagues isolated CTCs through the monitoring of their metabolic activities in droplets. They highlighted a limit of detection as little as 10 CTCs among 200,000 white blood cells from four patients by leveraging advantage of pH measurement or lactate concentration changes in the extracellular compartment of individual cells without surface antigen labelling.	[90]	

12	Droplet generation	Metabolomic activity – lactate production	Immunomagnetic - WBC depletion	Prostate cancer	Rivello and co-workers proposed a metabolic assay chip as a label-free and droplet-based microfluidic device for single-cell extracellular pH measurement for detection and isolation of highly metabolic CTCs. The study was conducted on 56 patients and suggested that the level of metabolic activity of cancer cells can be a prognostic and promising biomarker to study tumour progression and metastasis. [84]	
13	Nano(micro)-wells	Size-based nanolitre molecular (RT-PCR)	sub-wells & analysis	Immunomagnetic – EpCAM positive selection via MagSifter	Non-small-cell lung cancer	Park and colleagues performed single-cell mutation profiling on single CTCs from 55 non-small-cell lung cancer patients, using massively parallel nano-well arrays. First, CTCs were enriched from the whole blood samples using MagSifter (using anti-EpCAM antibodies for positive selection), and then the sample was diluted and seeded by direct pipetting and centrifuging on an array of 25,600 wells where cells were isolated individually. Consequently, multigene profiling of individual CTCs was performed through RT-PCR in a high-throughput and multiplexed fashion for single-cell mutation profiling. [92]
14	Nano (micro)-wells	Size-based nanolitre wells	Sub-capture	Immunomagnetic via CellSearch	Non-small-cell lung cancer	Tamminga and co-workers have shown the potential of using a self-seeding nano-wells to isolate and assess released CTCs during surgery for non-small cell lung cancer. The authors isolated over 267 CTCs from 10 different non-small cell lung cancer patients without undergoing surgical resection. Initially, the authors used CellSearch platform for CTC enrichment from peripheral blood and performed copy number analysis through single-cell whole genome sequencing. The single-cell isolation device operates similar to a filtration system in which the sample is passed through wells with a 5µm pore. Larger cells, such as CTCs, clog the wells but allow the remaining sample to flow through the device. Once the well containing the cell of interest is identified, an automated puncher needle approaches and ejects the cell by punching the well and transferring the cell into a collection vessel. The authors concluded that CTCs defined by CellSearch were identified in higher numbers in the pulmonary vein compared with radial artery and suggested that release of CTCs were not influenced by surgical approach. [93]
15	Integrated fluidic circuits	Fluidic chambers & Single-Cell Sequencing	RNA	Size based inertial microfluidics via ClearCell FX	Breast cancer	Iyer and colleagues used the Polaris system to analyse the transcriptome of 57 single CTCs collected from 3 different breast cancer patients and compared to 558 single CTC data from publicly available single-cell transcriptome expression profiles of CTCs. They showed CTCs of different cancer types lie on a nearly perfect continuum of EMT values. Additionally, by using full length transcriptomic analysis they identified a number of new cell surface biomarkers (ITGB5, TACSTD2, SLC39A) in addition to the standard EpCAM. [94]
16	Dielectrophoresis (DEP)	Surface size and molecular (ddPCR)	biomarkers, shape & analysis	Immunomagnetic - WBC depletion	Melanoma cancer	Tucci and colleagues studied a total of 661 single CTCs from 17 late-stage melanoma patients for the expression of melanoma stem cell markers such as CD271, ABCB5, RANK, and the BRAF mutational status by droplet digital PCR. They used an immune-magnetic negative depletion approach to eliminate CD45-, CD31- or CD34-positive cells, followed by isolation of individual CTCs using a commercial DEPArray machine. [98]
17	Dielectrophoresis (DEP)	Single-cell sequencing	RNA	Parsortix	Renal cell carcinoma cancer	Cappelletti and colleagues studied 21 blood samples from 10 patients with metastatic renal cell carcinoma and showed an eightfold amplification of MET in CTCs and a sevenfold increase in cfDNA which was correlated with resistance to Crizotinib and Alectinib . Authors used Parsortix enrichment technology for enumeration of CTCs, followed by isolation of 37 single CTCs using a DEPArray technology. The isolated CTCs were analysed through next generation sequencing to identify two subpopulations of epithelial CTC and non-conventional CTC that lack epithelial and leukocyte markers. DEPArray was also used to isolate CTCs from a patient with stage IV non-small cell lung cancer who experienced development of resistance to Crizotinib and primary resistance to Alectinib . Analysis showed a progressive increase in CTC numbers and cell free DNA during treatment. [62]

Chapter 3 – Rapid Fabrication of Static Droplet Microfluidic Devices for Isolation of Circulating Tumour Cells

Summary

This chapter explores three microfabrication approaches of 3D printing, maskless lithography and laser cutting for creating static droplet microfluidic devices. The microfluidic devices are used to encapsulate circulating tumour cells in confined and controlled droplets for various studies that are explored throughout this thesis. Currently, complex fabrication methodologies to create microfluidic devices remain as one of the key barriers for innovative solutions. Most fabrication methodologies suffer from high-cost, time consuming processes, reliance on specialised equipment/facilities and labour-intensive approaches. To provide alternatives, in this work, we propose simple, yet effective, fabrication methods for rapid prototyping of microfluidic devices using three separate approaches of 3D printing, maskless lithography and laser cutting. We discussed the benefits and shortcomings of each approach for prototyping and creating static droplet microfluidic devices and showcased the potential of encapsulating and studying single cells.

This chapter is under preparation for submission to the journal of Analyst as a communication journal*.

*Radfar P, Rahnama R, Ding L, Warkiani ME. Rapid Fabrication of Static Droplet Microfluidic Devices.

3.1 Introduction

Cancer metastasis is the leading cause of death among cancer patients [21]. Metastasis is spreading process through which primary tumours cells travel through vascular system to a secondary sight where new tumours are formed [25]. Given the important role of Circulating Tumour Cells (CTCs) in cancer metastasis, they carry valuable information on the tumour conditions and patients' disease state [26]. Thus, in the past few decades CTCs have been clinically used as a non-invasive diagnostic and prognostic tool. However, CTCs are extremely rare in the circulation and isolation of them among billions of peripheral cells are often a challenging task [33]. Various enrichment techniques have been developed in the past to remove background blood cells from cancer patients' blood (see ref. [123] for further information). However, despite all the potential benefits, high contamination of leucocytes and high sample loss during enrichment are considered as the major clinical challenges of CTCs [35-39]. In the past few years, researchers have been developing complementary tools and platforms to alleviate the limitations involved with CTC enrichment platforms [124-127]. Among all options, droplet microfluidics has been one of the most promising approaches for purification and analysis of the post-enrichment samples [123]. The idea relies on fractionating the sample into tiny droplets and based on statistical probabilities, cells are individually encapsulated and analysed over different biological assays [5, 128]. However, majority of droplet microfluidic systems rely on costly setups and specialised equipment. While static droplet microfluidics have been suggested as a simpler approach to encapsulate and analyse cells, fabricating the complex structures are difficult, requires advanced micro-fabrication skills and often is time-consuming [4]. Figure 3.1 illustrates the conventional approach for fabricating microfluidic devices using soft lithography.

Conventional Soft Lithography for Microfluidic Chip Fabrication

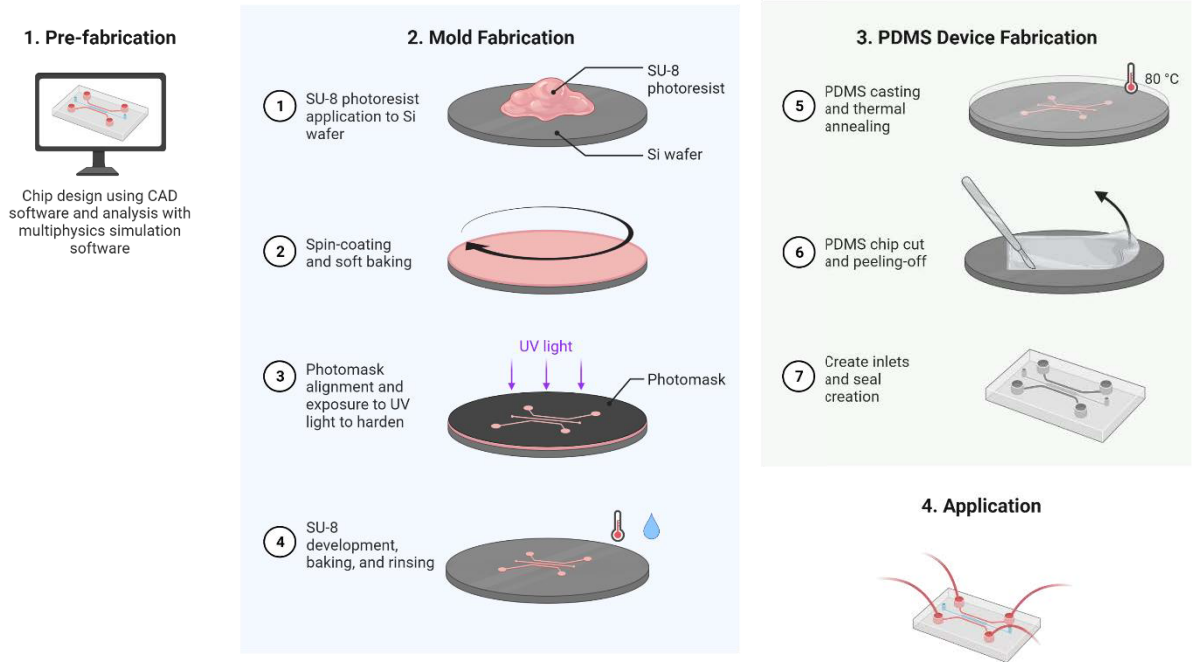


Figure 3.1 - Workflow summarising the main steps in generating a PDMS chip from its design to application. Modelling the chip using CAD and doing simulations are the necessary steps before the actual fabrication. The overall process of chip-making can be time-consuming and requires a great deal of precision. The first phase of fabrication is to etch a mould onto a silicon base. Once this mould is complete, PDMS can be poured on the top and then peeled off to obtain the chip.

To overcome the limitations, in this work we showcase three different approaches for rapid and low-cost fabrication of static droplet microfluidic devices using 3D-printing, laser cutting and maskless lithography. The aim of this work is to represent the latest state of the art technologies that can be utilised for rapid prototyping and use of microfluidic devices for single-cell analysis purposes.

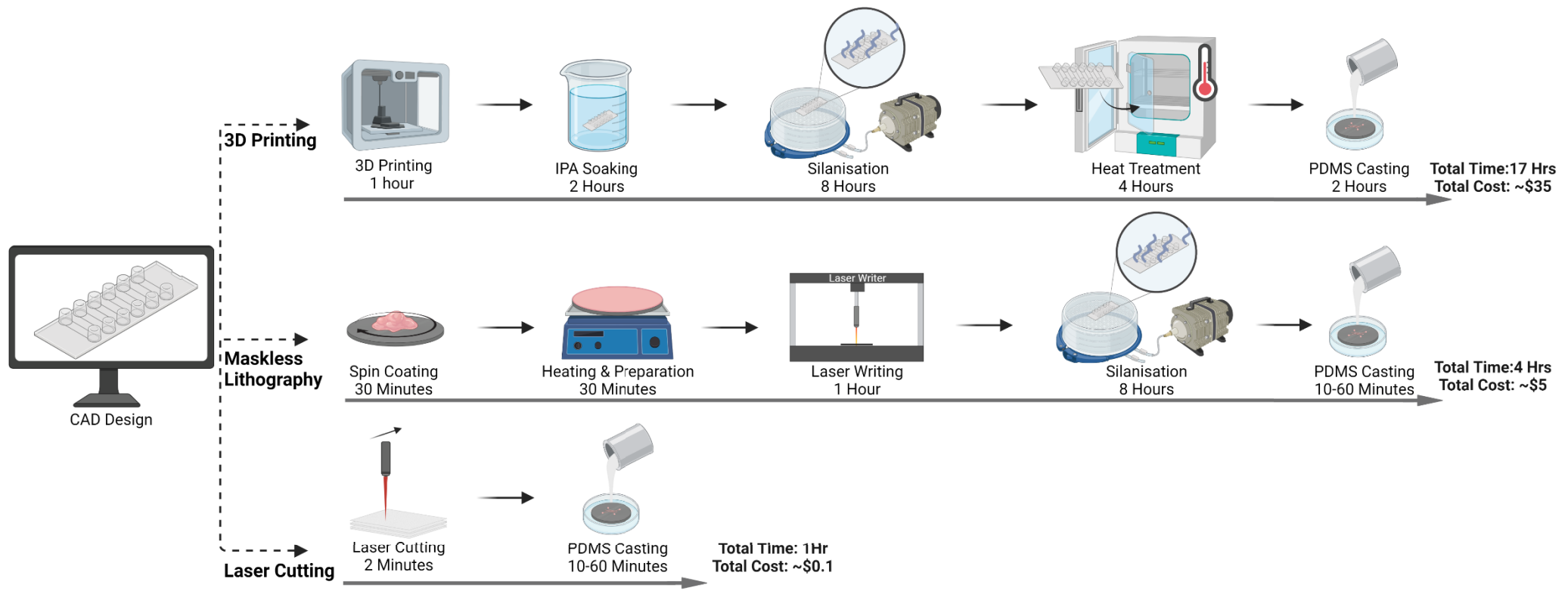


Figure 3.2 – Microfabrication Workflows. Rapid fabrication of static droplet microfluidic devices through 3D printing, maskless lithography and laser cutting A4 paper. Each method is developed to minimise the required time for prototyping microfluidic devices. 3D printing of microfluidic moulds involves the printing of the structure using a 3D micro-printer, soaking in ethanol or IPA, salinisation, heat treatment and PDMS casting. Additionally, maskless lithography involves spin coating of a photoresist on a wafer, heating the wafer, laser writing, salinisation and PDMS casting. Lastly, laser cutting is the shortest process that only involves laser cutting a paper and directly casting PDMS.

3.2 Result and Discussion

3.2.1 Working Principles and Device Design

Static Droplet Microfluidic (SDM) devices proposed in this manuscript leverage the capillary forces of the liquid/sample for fractionation and generation of droplets. Each device consists of a main channel with chambers on the sides that are interconnected via tiny air vents. As the liquid travels through the main channel, side chambers are filled owing to the existence of the air vent that allows the air to escape but stops the liquid due to the hydrophobicity of the device (refer to ref. [5] for detailed discussion on the SDM device working principle).

The SDM devices were designed using a bottom-up approach based on the minimum resolution of the fabrication method to design the smallest possible air vent at end of each pocket. The air vent dimensions were used to calculate the maximum capillary pressure barrier that could be applied. Finally, the chambers, middle channel and length of the device was designed accordingly. Please refer to [5] for detailed guide on design of the static droplet devices.

3.2.2 Fabrication Approaches

In this work, three methods of 3D microprinting, maskless lithography and laser cutting were utilised to rapidly prototype the master for fabrication of SDM devices using polydimethylsiloxane (PDMS). Table 3.1 provides an overall comparison of the three fabrication approaches used in this work.

3D Microprinting. The advancements 3D printing technology has enabled the possibility for rapid development of micron-scale structures suitable for the use as microfluidic devices [129]. The SDM devices in this work were developed using MiiCraft Ultra 50 3D printer. The design was made using computer-aided design modelling software, SolidWorks 2018 (Dassault Systems, France), and the file was exported to the MiiCraft software to as an STL file to process. The 3D design model was sliced by the MiiCraft's software using 50 μ m slicing in z-axis with curing time of 1.2 seconds along with 2 base layers and 4 buffer layers. The 3D printing was completed within an hour and the part was collected from the printer for 5 rounds of Isopropanol Alcohol (IPA) washing. After removing any residual resin, the part was post-cured using a UV box to enhance the surface properties. Then the post-processed part was dipped inside IPA for 2 hours to eliminate uncured monomers and oligomers. Next, to

avoid permanent sticking of PDMS to the master mould, a salinisation was done using trichloro (1H, 1H, 2H, 2Hperfluoro-octyl) silane (Sigma-Aldrich, Australia) in a pressure desiccator for 8 hours under vacuum. In the final stage, the moulds were heat treated for 4 hours in 44 degrees oven before casting PDMS and placing it 65°C oven.

The entire process from design to production of the PDMS SDM device took around 17 hours and estimated to cost ~A\$5. The lowest possible resolution achieved was down to 50µm in the x-y axis and 10µm in the z-axis which in this case we designed and tested devices down to 20nL droplet sizes with an 50µm air vent at the end of each pocket. It is also worth mentioning that lower droplet volumes are also possible to be fabricated using this approach by adjusting the design. The major benefit of this approach is the ability to create 3-dimensional structures with variable heights in z-axis. Additionally, 3D printers are reasonably accessible, affordable, do not require special training and can be installed in most laboratory/workshop settings.

Laser Cutting A4 Paper to Fabricate Static Droplet Microfluidics Devices

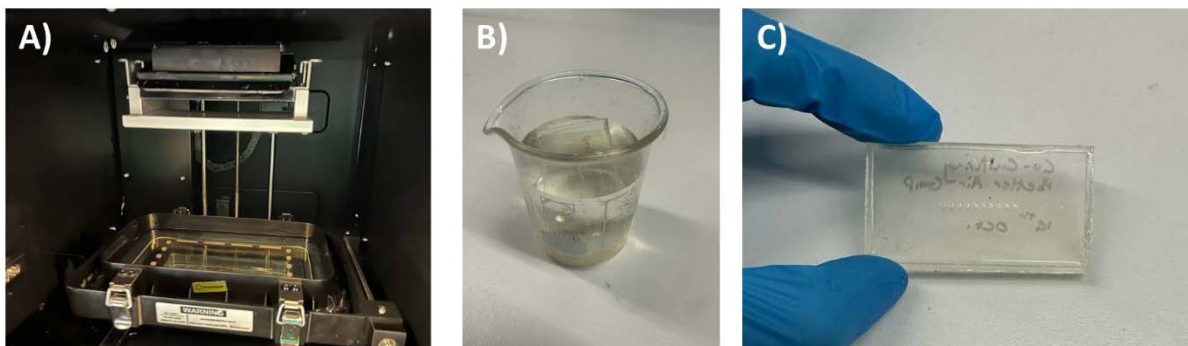


Figure 3.3 – Microfabrication of static droplet microfluidic device using 3D printed moulds. A) Digital Light Processing (DLP) 3D printing of the mould. B) Ethanol dipping of the mould after cleaning the chip. C) PDMS casting of the static droplet microfluidic devices.

Maskless Lithography. The second approach proposed in this manuscript was based on maskless lithography using photoresist chemicals to fabricate the master moulds of the SDM. The process involved preparation of a silicon wafer as a substrate for spin-coating a 50µm layer of SU8-2050 photoresists (MicroChem Co., USA). The spin-coated wafer was then soft-baked according to manufacturer’s guidelines, followed by pattern printing using the µPG101 laser-writer machine (Heidelberg, Germany) with 5mW laser power and 0µm focus. Prior to this step, the design was made using computer-aided design modelling software,

AutoCAD 2017 (Autodesk, United States), and the file was exported as a DXF drawing to the Heidelberg software. After completion of the laser-writing step, the part was post-baked, developed using SU8 developed (MicroChem Co., USA) and hard-baked as per manufacturer's guidelines. Finally, the prepared mould was silanised under vacuum using trichloro (1H, 1H, 2H, 2Hperfluoro-octyl) silane (Sigma-Aldrich, Australia) for 2 hours to achieve an easier release of PDMS upon casting. Finally, PDMS was casted, degassed and baked in the 65°C oven.

The entire process from design to production of the PDMS SDM device took around 4 hours with an estimated cost of ~A\$3. The lowest resolution achieved by this approach was down to half of the height of the channels – i.e., 25µm minimum resolution with 50µm channel height. In this study, 1nL droplets were designed and tested successfully. Lower droplet volumes may also be achieved via altering the design. In contrast to 3D printing, laser writers are often expensive, inaccessible, require high-end training and often are installed in cleanroom facilities. The major benefits of this approach include faster turnaround time, high quality and durability of the finished moulds and the ability to create larger models.

Maskless Lithography of Microfluidic Devices

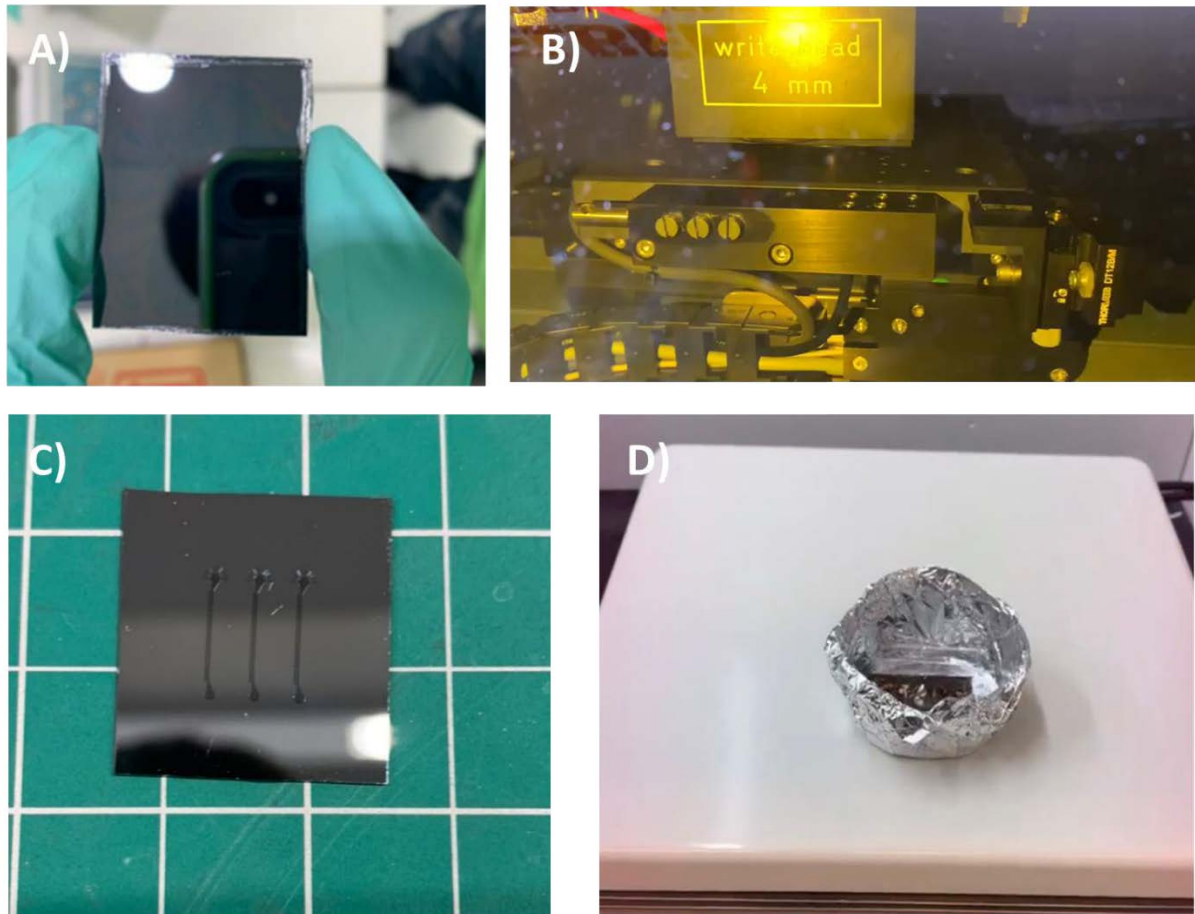


Figure 3.4 – Microfabrication of static droplet microfluidic device using maskless lithography. A) Spin Coating of SU8 on silicon wafer. B) Laser writing the pattern on the spin coated wafer. C) Post-baking and heat treatment of the SU8 device. D) PDMS Casting and baking to fabricate the static droplet microfluidic device.

Laser Cutting. The last approach proposed in this manuscript is based on fabrication of the master mould by laser cutting A4 paper as the simplest and most accessible approach. In this approach, simply the A4 paper was placed inside the laser cutting machine (Universal Laser Systems, Australia) and the designed file was imported from AutoCAD 2017 (Autodesk, United States) to the machine's software. The machine rapidly cuts the pattern out of the paper and the model was then transferred to a petri-dish. Owing to the advantages of this approach, no further salinisation, alcohol dipping or other post processing is required. Thus, PDMS was then directly poured onto the mould, degassed and placed in the oven.

Laser cutting A4 paper and using it as a mould for fabricating microfluidic devices is among the quickest, most affordable and simplest approaches. The cutting process often takes less

than two minutes depending on the number of features, followed by a 10-minute PDMS casting using 125°C oven. Thus, the entire process from design to fabrication can take place in less than 15 minutes while costing less than \$0.1. However, the minimum resolution is constrained to 150-200µm in the x-y direction. The height of the device was dependent on the thickness of the paper used (i.e., 100µm thick paper was used in this work). In contrast to the 3D printing and lithography approaches, laser cutting is accessible, low-cost, and simple to use without requiring cleanroom or high-end fabrication facilities/laboratories.

Laser Cutting A4 Paper to Fabricate Static Droplet Microfluidics Devices

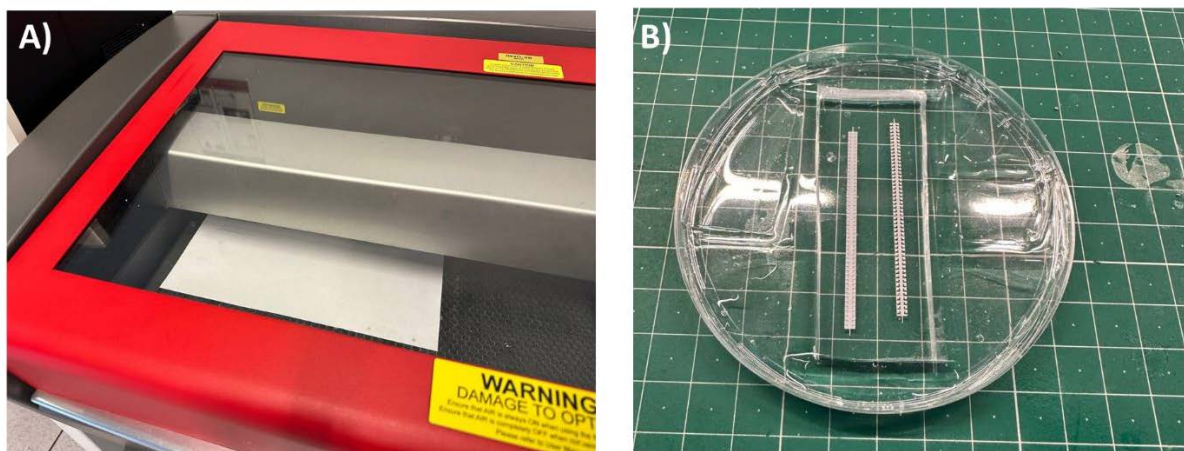


Figure 3.5 – Microfabrication of static droplet microfluidic device using laser cutting technique. A) Laser cutting the pattern on an A4 paper. B) Casting PDMS on the paper mould for fabrication of the static droplet microfluidic device.

Fabrication Method	Production Cost	Production Time	Equipment Cost	Accessibility	Skills/ Training	Resolution	Design Complexity
3D Printing	Highest	Longest	Medium	Accessible	Minor Training	30µm	Highly Complex Designs - 3 Dimensional
Maskless Lithography	Medium	Medium	Highest	Inaccessible	High Level of Training & Skills	1µm	Low Complexitiy - Planar Designs
Laser Cutting	Lowest	Lowest	Lowest	Accessible	Minor Training	50-100µm	Low Complexitiy - Planar Designs

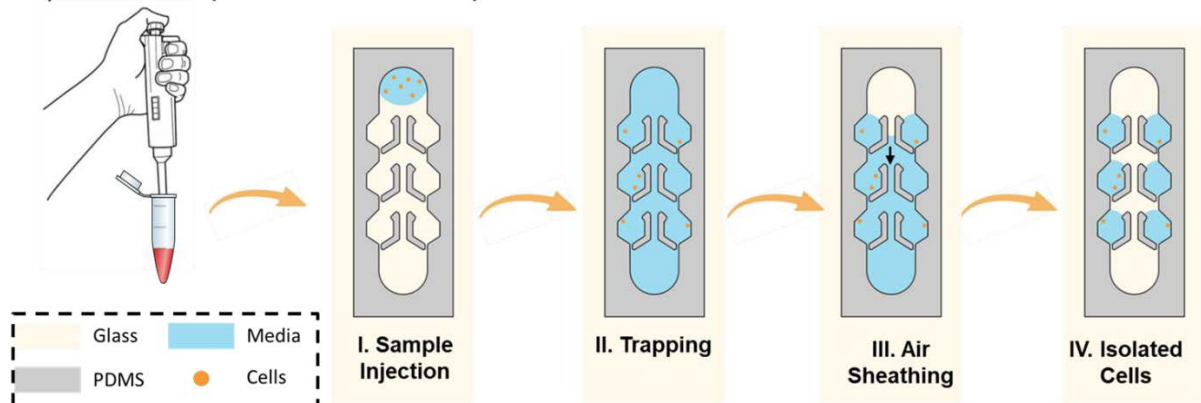
Table 3.1 – Qualitative Comparison of Microfabrication Approach. Rapid fabrication of

microfluidic devices are compared in terms of production cost, production time, equipment cost, accessibility, skills/training, resolutions and design complexity. Each fabrication methodology comes with a range of benefits and limitations.

3.3 Experimental Results

To further demonstrate the potential of using the SDM devices fabricated using the three proposed approaches, each device was used to encapsulate and analyse single cells. Figure 3.6 illustrates the working principle of SDM devices.

A) Static Droplet Microfluidic Operations



B) Static Droplet Microfluidic Working Principle

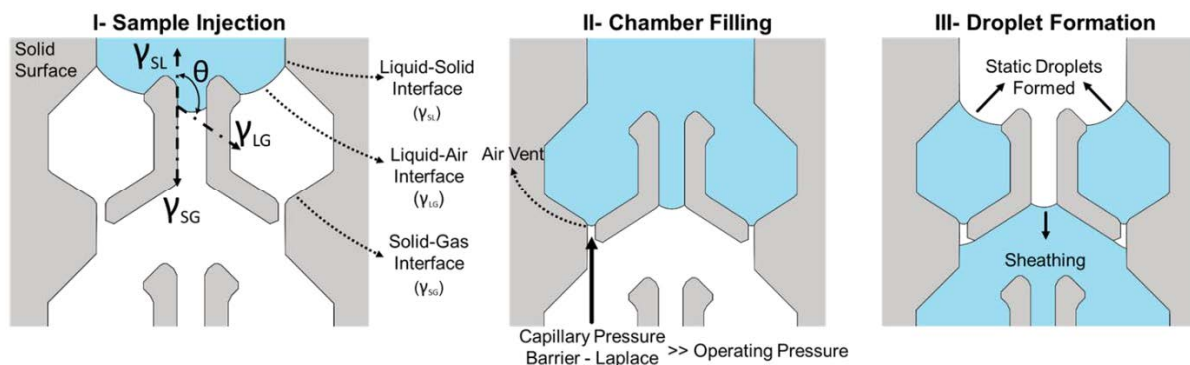


Figure 3.6 – Static Droplet Microfluidics A) Operational Steps and B) Working Principle.

As shown in Figure 3.7, range of SDM devices were fabricated with various geometrical and volumetric variations. The devices were used to encapsulate single cell cells and shown in the following chapters in this thesis. It is worth mentioning that number of cell occupancy in each droplet follows Poisson distribution in respect to the injected sample. It is worth mentioning that core focus of this work is on the fabrication approaches. However, application and use cases of the SDM device fabricated is to study molecular, protein and metabolomic aspect of the cell populations at single cell resolution in a confined and miniaturised environment.

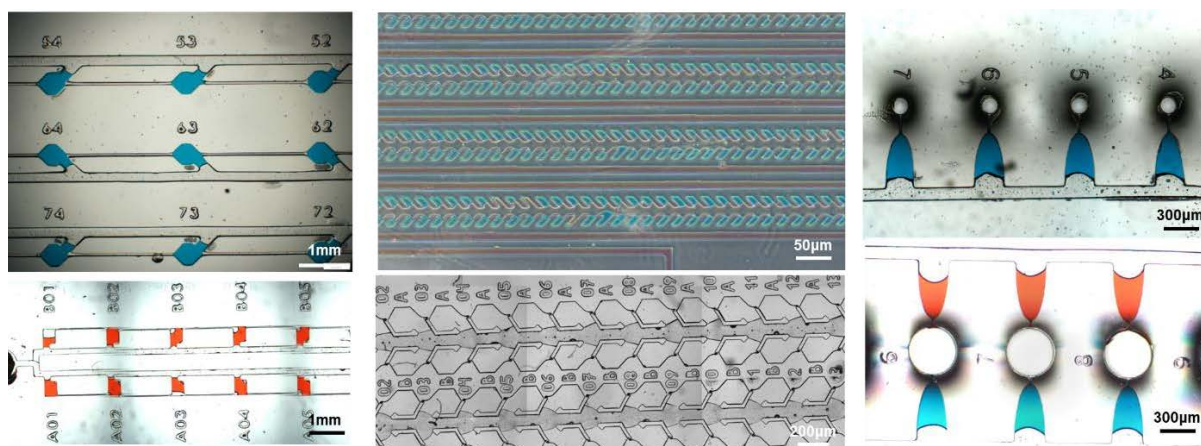


Figure 3.7 – Images of the Actual Static Droplet Microfluidic Devices fabricated via 3D Printing, Maskless Lithography and Laser Cutting.

3.4 Summary and Conclusion

In this paper, three simple and robust fabrication approaches for rapid prototyping and creating microfluidic devices were reported. 3D micro-printing, maskless lithography and laser cutting was utilised to fabricate static droplet microfluidic devices. Lastly, each device was used to encapsulate and analyse single cells. Furthermore, advantages and disadvantages of each approach was thoroughly discussed to provide readers with insight on the potential use cases of fabrication methodologies. This work can provide an overall understanding on the new emerging fabrication tools in the microfluidic industry. Based on the requirements, often single cell devices require finer fabrication resolution thus maskless lithography was mainly adopted as the fabrication approach for this thesis.

Chapter 4 – An Easy-to-Operate Method for Isolation and Molecular Analysis of Single Rare Cells

Summary

This chapter focuses on a novel microfluidic device for encapsulation of circulating tumour cells and retrieval of them using common laboratory equipment such as handheld pipette for single cell molecular studies. In-depth study of cellular heterogeneity of rare cells (e.g. circulating tumour cells (CTCs) and circulating foetal cells (CFCs)) is greatly needed in disease management, but has never been completely explored due to the current technological limitations. Herein, we developed a retrieval method for single-cell analysis using a Static Droplet Array (SDA) device through liquid segmentation with almost no sample loss. We explored the potential of using SDA for low sample input and retrieving the cells of interest using everyday laboratory equipment for downstream molecular analysis. This single-cell isolation and retrieval method is low-cost, rapid and provides a solution to the remaining challenge for single rare cell analysis. The entire process takes less than 15 minutes, is easy to fabricate and allows for on-chip analysis of cells in nano-litre droplets and retrieval of desired droplets. To validate the applicability of our device and method, we mimicked analysis of single CTCs by isolation, retrieval, and mRNA real-time PCR analysis. This chapter has been published in 2 journals of *Microchimica Acta** and *Analytical Chemistry*^x.

*Ding, L.[#], **Radfar, P.**[#], Rezaei, M., & Warkiani, M. E. (2021). An easy-to-operate method for single-cell isolation and retrieval using a microfluidic static droplet array. *Microchimica Acta*, 188(8), 1-11. DOI: [10.1007/s00604-021-04897-9](https://doi.org/10.1007/s00604-021-04897-9)

^xRezaei, M., **Radfar, P.**, Winter, M., McClements, L., Thierry, B., & Warkiani, M. E. (2021). Simple-to-operate approach for single cell analysis using a hydrophobic surface and nanosized droplets. *Analytical chemistry*, 93(10), 4584-4592. DOI: [10.1021/acs.analchem.0c05026](https://doi.org/10.1021/acs.analchem.0c05026)

4.1 Introduction

The study of cell populations at single-cell resolution and understanding the cellular heterogeneity among them can reveal important information regarding different cell types, functionality, conditions and circuits via genomic, transcriptomic, proteomic and metabolomic analysis [6, 7]. Single-cell analysis can provide insights on healthy and diseased behaviours of individual cells and can play a crucial role in precision diagnostics and therapeutics [8]. Among different analysis types, single-cell genomic and transcriptomic analysis, have drawn the most attention in the past decade due to its capabilities in discovering cellular information [9]. Typically, single-cell genomic and transcriptomic analysis involves isolation and lysis of single cells to extract, amplify and barcode the DNA/RNA of each cell individually. For RNA analysis, an additional step of reverse transcription is needed to create complementary DNA (cDNA) due to the unstable nature of RNAs [10]. Conventionally, single-cell isolation and analysis were possible through limited dilution [130], micromanipulation [131], Fluorescence-Activated Cell Sorting (FACS) [80], Laser-Capture Microdissection (LCM) and complex integrated microfluidic platforms (e.g. Fluidigm C1) [9], which are constrained by cost, minimum sample input, sample loss, time and labour [6]. Recently, multiple products have been developed to allow massively parallel single-cell isolation and barcoding of individual cells genomic material which is then followed by cDNA synthesis. Currently, most commonly used single-cell isolation methods are microfluidic droplet generators that encapsulate single cells with a uniquely barcoded RNA capture beads in a tiny water-in-oil droplet. However, droplet-based techniques often face challenges when dealing with low sample input (i.e., due to initial stabilisation time of the system), while requiring specialised equipment and high setup and operational costs [132]. An alternative approach to droplets is the use of nanolitre wells that sample gets loaded and settles down by gravity which reduces the need for specialised equipment and operating dead volume (e.g., BD Rhapsody system). Wells are designed with specific dimensions to allow for single cell and bead occupancy at the right sample concentration. Although nanolitre wells overcome some of the issues associated with droplet generators; the lack of a mechanism to encapsulate/isolate the cells in the wells leads to lower capture efficiency and a significant cross-contamination [6].

Most of the current single-cell technologies are employed for processing a large population of cells such as tissue biopsies. While there has been a significant development in single-cell analysis platforms for such cases, less attention has been paid to the single-cell analysis of low input samples ($\leq 10^4$ cells) [6]. With advancements in cell enrichment methods, there has been a growing interest in analysing rare cells at a single-cell resolution which can unravel unique insights that are not revealed by bulk molecular analysis [15]. Typical examples of rare cell analysis include Circulating Tumour Cells (CTCs), Circulating Foetal Cells (CFCs), immune cells, and stem cells. These cells are usually found in liquid biopsies (e.g. blood, urine), are processed through an enrichment step to remove the majority of unwanted cells. In the past years, liquid biopsy has gained significant attention due to the critical information that can be obtained from the analysis of rare cells in a non-invasive manner [17-19]. In most of the enrichment cases, a low number of rare cells is found among thousands of undesired background cells (e.g. in CTC cases usually 1-10 CTCs among thousands of white blood cells (WBCs) are found in one millilitre of a cancer patient blood sample) [74]. Single-cell analysis of such rare cells is not easily possible through droplet or nanolitre well systems due to abovementioned limitations associated with these approaches, especially cells losses. The majority of the current single-cell studies on rare cells are done via conventional approaches including limiting dilution, micromanipulation, and LCM, despite their disadvantages [47]. Besides, there has been multiple single-cell capturing and analysis methods reported in literature based on hydrodynamic or active trapping of cells [133-137]. However, these methods suffer from high complexity, reliant on specialised equipment, inability to process low number of cells (e.g., high cell loss) and lack of a simple retrieval method. Thus, there is a critical need for the development of a low-cost, rapid, and simple single-cell analysis platform that is capable of processing a low number of input cells and does not require special equipment. In Table S2 (supplementary file), different single-cell isolation techniques are compared for isolation and analysis of rare cells.

To overcome these challenges, we have developed a simple and low-cost method for single-cell trapping, isolation and retrieval using a microfluidic Static Droplet Array (SDA). The volume of SDA traps is 20 nanolitre, and the whole process is designed to be operated using a handheld pipette and fluorescent microscope, making the method more accessible to general laboratories. Our novel retrieval method is based on temporary bonding of the chip

on a substrate during the injection, followed by freezing and peeling off the chip. The freezing step allows the droplets to stick to the substrate after chip peel off, which can be picked and transferred to a PCR tube, without losing any molecular content. We demonstrated a proof-of-concept study for single-cell analysis of rare cells by injecting 300 cells and analysing them via quantitative reverse transcription PCR (RT-qPCR) to validate our protocol.

4.2 Material and Methods

4.2.1 Device design and fabrication

The proposed devices have pocket volumes of 20 nanolitres designed with a hexagonal cross-section, optimised to trap single cells, and sized accordingly to allow for pickup of the droplets with a 10 μ L pipette tip after freezing the chip. Also, pocket sizes were designed to ensure enough nutrient is provided for on-chip culturing of the cells. The main channel and trap entrance dimensions are 170 μ m and 220 μ m, respectively, which allows the fluid to fill the traps first. Height of the channel was designed at 100 μ m to allow cell movements and avoid clogging of the channel.

In this work, we used two different strategies to fabricate master moulds of our devices. The first master mould was made using standard photolithography as follows. Initially, the SDA pattern was designed using AutoCAD software (AutoDesk, United States of America) and printed out on a glass mask. Then, photolithography was performed using nLOF2020 photoresist and Karl Suss MA6 mask aligner (SUSS Microtec, Germany) on a silicon on insulator (SOI) wafer with 100mm diameter. Eventually, Deep Reactive Ion Etching (DRIE) was deployed to transfer the pattern into the wafer with an aspect ratio of 1:10.

To explore the possibility of an alternative approach for master mould fabrication, we have utilised high resolution SLA printing technology to make devices with bigger spacings between the traps. The 3D printed mould was fabricated using MiiCraft Ultra 50 (MiiCraft, Taiwan) with a printing area of 57 \times 32 \times 120mm and XY resolution of 30 μ m as per previous works of our research group [138]. The 3D-printer used in this work utilises a 385-405nm UV wavelength to cure resin (BV-007) on a printing platform. Given the lower resolution of 3D printing compared to soft lithography, we adjusted the design parameters to accommodate for that. The design was made using computer-aided design modelling software, SolidWorks 2018

(Dassault Systemes, France), and the file was exported as an STL file to MiiCraft printing software (MiiCraft 125, version 4.01, MiiCraft Inc). Slicing of 50 μ m in z-axis was used with a curing time of 1.2 seconds, 2 base layers and 4 buffer layers, to ensure the part is adhered to the picker during printing. After the printing was over, the mould was washed thoroughly using isopropanol alcohol to remove any residual resin and post-cured for enhancing the surface properties of the mould. Then to eliminate any uncured monomers and oligomers on the surface, the mould was dipped in isopropanol alcohol for 2 hours.

Once the fabrication and preparation of both soft lithography and 3D printed moulds were completed, to avoid any Polydimethylsiloxane (PDMS) sticking to the surfaces of the moulds, salinisation was done using trichloro (1H, 1H, 2H, 2H-perfluoro-octyl) silane (Sigma-Aldrich, Australia) in a pressure desiccator under vacuum for 2 hours to produce a hydrophobic coating layer for easier release of cured PDMS. PDMS (Sylgard 184, Dow Corning, USA) was prepared by mixing elastomer and curing agent in a standard ratio of 10:1, followed by degassing in a vacuum chamber until all air bubbles are removed. The mixture was then poured onto the moulds and cured at 65°C for one hour before peeling. The PDMS device was then cut from the mould and inlet and outlet access holes were made using 1mm biopsy punch. The device was then pressed on Glass slide (Corning, Australia), which was pre-coated with 1% BSA (Sigma Aldrich) for one hour, to create a temporary binding.

4.2.2 Cell culture

Breast cancer cell line, MCF-7, and monocyte cell line, THP-1, were cultured in complete media made of RPMI media (Gibco, Australia) with 10% foetal bovine serum (Gibco, Australia) and 1% Penicillin-streptomycin antibiotics (Gibco, Australia) in T-25 flasks (Corning, Australia). The cells were passaged at 80% confluency, and the seeding density was about 0.7×10^6 cells.

4.2.3 Cells/beads loading and capture rate counting

Once cells reached 80% confluency in the flask, the cells were detached by TrypLE (Gibco, Australia) and cells were resuspended in 1mL culture media after centrifugation. Cells were then counted using a haemocytometer (Sigma-Aldrich, Australia) and cell viability of >90% was ensured by 0.4% Trypan blue solution (Gibco, Australia). A range of different cell concentration solutions (5-50cells/ μ L) was prepared by diluting the cells in DPBS (Gibco, Australia) and after injection of the solutions, a fluorescent microscope was used to compare single cell capture rates. Different injection speeds, between 10-90 μ L/min, were tested by

using a syringe pump as well as a handheld micropipette. Before injecting 5 μ L of the sample into the microfluidic chips, the cell suspension was remixed by pipetting for 5 seconds. After injection, the device was imaged under a microscope, and cell occupancy in each chamber was identified.

The workflow of our method includes 5 steps (Figure 4.): 1) cells were harvested, diluted to the appropriate concentration and injected by a handheld pipette into the device; 2) the remaining liquid in the main channel (if any) of the device was aspirated to create individual droplets; 3) the device was frozen by placing it in -80 $^{\circ}$ C fridge for 5 minutes; 4) the device was taken out, and the PDMS chip was peeled off; 5) the droplets of interest were picked up by a hand-pipette for further studies.

4.2.4 Cell viability assay

The effect of different dimethyl sulfoxide (DMSO, Sigma-Adrich, Australia) concentrations on the cellular viability post-freezing were examined. Firstly, MCF-7 cells were centrifuged and suspended in 1mL fresh media in 1.5mL microtubes. 2 μ L of live and dead stain (Abcam, Australia) was added into each tube. Then the cells were allocated into 5 different tubes to make 1, 3, 5, 7, 10% DMSO content in the cell solutions, and the cells were injected into the device, sheathed with air and the number of live and dead cells were counted under the microscope. After that, the chips were frozen in -80 $^{\circ}$ C freezer and taken out after 10 minutes. The device was thawed in 37 $^{\circ}$ C incubator for 5 minutes and imaged under the microscope to calculate the number of live cells post freezing.

4.2.5 Immunofluorescence staining and imaging

MCF-7 cells and THP-1 cells were harvested, centrifuged at 400g for 5 minutes and resuspended in 100 μ L methanol (Sigma-Aldrich, Australia) in two 1.5mL Eppendorf tubes. The tubes were then incubated at -20 $^{\circ}$ C for 5 minutes for permeabilization and fixation. After two times washing by DPBS, the cells were resuspended in a cocktail of 96 μ L DPBS, 2 μ L DAPI solution and 2 μ L anti-cytokeratin antibody or anti-CD45 (Miltenyi Biotech, Australia). The tubes were incubated in 4 $^{\circ}$ C fridge for one hour. To wash-off unbounded antibodies, the cells were then centrifuged and washed with 1mL DPBS for two times. Then, the mixed cells solution was diluted to 60cells/ μ L and injected into the microfluidic device. The device was imaged using an Olympus IX 73 inverted fluorescent microscope (Olympus, Japan). Panorama

bright field and fluorescence images were taken by defining the imaging starting point and endpoint.

4.2.6 Single-cell RT-qPCR

To verify the preservation of genetic material in our proposed method, known number of MCF-7 cells were injected to the chip using a handheld pipette and then frozen quickly as mentioned above. The chip was peeled off from the substrate and the droplets were retrieved and transferred into a 200 μ L PCR tube under two conditions; 1) frozen droplet (by placing the chip on an ice block), 2) melted droplet. As a control, individual MCF-7 cells were isolated with serial dilution and assessed using the same PCR protocol. The cells were lysed, extracted, reverse-transcribed, and pre-amplified by NEBNext[®] Single Cell/Low Input complementary DNA (cDNA) Synthesis & Amplification Module (New England Biolab, Australia). Briefly, the cells were mixed with 0.5 μ L 10 \times lysis buffer, 0.25 μ L RNase inhibitor and 4.25 μ L nuclease-free water and incubated at room temperature for 5 minutes. Then, 1 μ L of Single Cell RT Primer Mix and 3 μ L of nuclease-free water was added into the lysed cells and was incubated at 70 $^{\circ}$ C for 5 minutes to synthesise first-strand cDNA. To make cDNA strands for PCR, reverse transcription was carried out by adding 5 μ L Single Cell RT Buffer, 1 μ L Template Switching Oligo, 2 μ L Single Cell RT Enzyme Mix and 3 μ L nuclease-free water into the lysed cells. The solution was then incubated at 42 $^{\circ}$ C for 90 minutes and 70 $^{\circ}$ C for 10 minutes. Lastly, in order to increase the amount of cDNA for detection with RT-qPCR, cDNA pre-amplification was performed with adding 50 μ L Single-Cell cDNA PCR Master Mix, 2 μ L of Single Cell cDNA PCR Primer and 28 μ L of nuclease-free water to reach a final volume of 100 μ L. The sample was then incubated in thermal cycler.

Then, RT-qPCR was performed with HER2 and GAPDH (Life Technologies, Australia) primers to confirm the loss of genetic material of cells. Briefly, PCR was performed with SuperScript[®] III Platinum[®] SYBR[®] Green One-Step qRT-PCR Kit (Invitrogen, Australia). 25 μ L of Master mix, 1 μ L of *Taq* Mix, 1 μ L of forward and reverse primers, 2 μ L of samples and 20 μ L of nuclease-free water was added into the PCR well plate (Biorad clear well PCR plate; HSL9601) to make a final volume of 50 μ L. The CFX96 Touch (Biorad, Australia) thermocycler was set following the manufacturer's guideline. Enzymes were activated at 95 $^{\circ}$ C for 5 minutes, and the following cycle was repeated for 40 times: 15 seconds at 95 $^{\circ}$ C, 30 seconds at 60 $^{\circ}$ C, and 40 $^{\circ}$ C

for 1 minute (Table S1). The results were then analysed with CFX Maestro software (Biorad, Australia).

4.2.7 Numerical simulation

To better understand the flow behaviour of the fluid in our device as well as the heat transfer during the freezing and thawing process, numerical simulations were performed using ANSYS Fluent 2020R2 (ANSYS, United States of America) [139, 140]. The fluid flow was performed using a 2D and 3D laminar single-phase solver to understand the flow rate through the trap opening compared to the main channel. Boundary conditions, including inlet velocity, were assigned similar to the real-case scenario, as mentioned in the result and discussion section. Furthermore, for the heat transfer, a 3D dimensional transient analysis was performed on a single droplet with the size and shapes of our chip with a 1.5mm glass base and PDMS on the 3 other sides. The bottom face of the glass was set at a constant temperature of -80°C , and the droplet was initially set at 23°C . Phase transitions were not taken into account as the main focus of this study was to understand the rate of heat transfer during the freezing process [141]. Fluid properties of the water were set as water density = $998\text{kg}/\text{m}^3$, dynamic viscosity = 1.002×10^{-3} thermal conductivity = $0.5\text{W}/\text{m.K}$, heat capacity at constant pressure = $4218\text{J}/\text{kg.K}$.

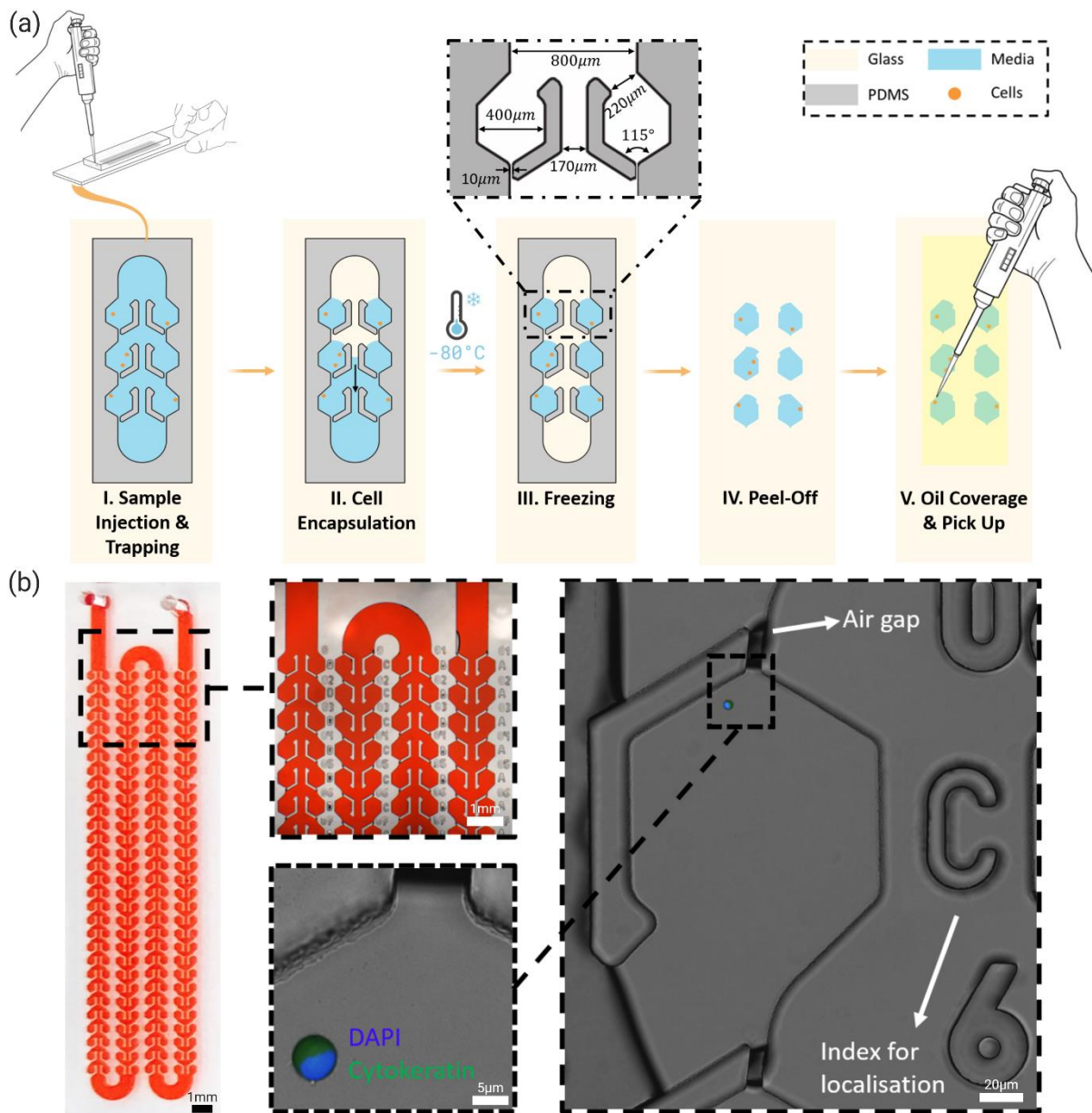


Figure 4.1 – Single cell capturing and retrieving in SDA (a) Schematic illustration of the workflow developed in this study for single cell retrieval using a static droplet array (SDA) microfluidics. The cells were then retrieved for single cell RT-qPCR in this paper. (b) Picture of actual PDMS device which is filled with the red food dye. The close-up views show the architecture of the device, localisation indices and a single cancer cells which is stained with DAPI and anti-CK antibodies.

4.3 Theory of static droplet array

The channel dimensions (170-800µm) and operating flow rates (10-90µL/min) results in a laminar flow regime across the device, which is a key operating parameter for effective cell trapping. A Reynold's number of 2.9 was calculated for this chip, which refers to a laminar

flow by $Re = \rho u D_h / \mu$, where ρ is density of the fluid, u is the mean velocity of the fluid (calculated by flow rate/cross section area), D_h is the hydraulic diameter of the channel, and μ is the dynamic viscosity of the fluid. In this case, the fluid density and viscosity were estimated with the values of PBS. The larger inlet dimension of side chambers forces majority of the fluid to fill the chambers first due to the lower resistance of this pathway. Injection flow rate plays an essential role in the behaviour of fluid and performance of this device. The subsequent pressure drop (due to resistance) across a pathway is caused by friction and fitting losses. Friction losses are dependent on the flow regime and length of the channel, and fitting losses can be described by $P_{drop} = \frac{1}{2} \rho V^2 C$; where ρ is the density, V is the fluid mean velocity, and C is the pressure drop coefficient obtained experimentally and is dependent on geometrical features of the channel (not the flow velocity) [142]. In parallel fluidic networks, the flow rate across each pathway is adjusted based on their resistances, in a way that total energy loss over each of the pathways is equal. Therefore, lower resistance of the side chambers compared to the main channel allows the liquid to fill the pockets first, and once the pockets are full, the liquid flows through the main channel to the next pair of pockets. However, at higher velocities (flow rates), the bending resistance (pathway to side chambers) increases that might result in all the fluid travelling through the main channel (i.e., side chambers remain empty). The 10 μ m air gap designed at the end of each chamber allows air to escape but stops the liquid from proceeding by utilising surface tension properties of the media-air interface on a hydrophobic channel [143]. This phenomenon is often referred to as bursting pressure which provides a large enough pressure barrier for the chamber pathway that the rest of fluid would favour moving along the main channel, to the next empty pockets and hence, no other cells would enter the filled chambers. The bursting pressure is highly dependent on the fluid viscosity, fluid surface tension, channel material and dimensions. Bursting pressure in a channel can simply be found using $P_{Capillary} = \frac{Surface\ Tension\ Force}{Area} = \frac{\sigma \cos\theta \times perimeter}{Area}$, where σ is the surface tension constant of the liquid-air and θ is the contact angle which is 107° for PDMS [142, 143]. In this case, the air gap provides a minimum of 4600 Pa pressure barrier. Once the chambers are filled, other cells in the fluid do not enter the chambers. Considering that cells only enter while the chambers are being filled, the trapping rate across device remains unchanged as the fluid flows through the device. The particle-particle interaction was ignored in this experiment for two reasons: firstly, the particle to

particle interaction created by Brownian effect is negligible when the diameter of the cells and beads is bigger than 1-2 μm . Secondly, the concentration of cells and beads are too low to create an influential interaction [144].

4.4 Results and Discussion

4.4.1 Device performance - trapping

In order to characterise the device performance, we first used 15 μm fluorescent polystyrene beads during the design process to mimic the trapping behaviour of cancer cells. Once the design was finalised, the device performance was optimised using MCF-7 cells. The effect of different flow rates and cell concentration on the trapping efficiency of the device was investigated. As shown in Figure 4.2 (a), the experimental results have shown the single cell occupation follows Poisson distribution trend line, for instance at the sample concentration of 50cells/ μL (1cell/20nL) the single cell encapsulation rate was recorded at 32% (average of 80 single cells trapped out of 250 injected cells). Furthermore, the single cell encapsulation can be increased up to 88% by lowering the sample cell concentration to 5cells/ μL (average of 22 single cells trapped out of 25 cells injected). The single-cell encapsulation results were repeated a minimum of 5 times to minimise the potential experimental errors and the associated variability of the results are shown in the figures based on the standard deviation. Generally, lowering the injection concentration would significantly increase the single cell encapsulation rate; however, it would result in greater number of empty chambers. Also, it is noteworthy that greater number of cells could be processed by increasing the number of traps and/or running multiple devices in parallel, especially for potential integration of the proposed workflow for clinical pipelines.

Besides, as shown in Figure 4.2 (b), no major difference was found on the capturing rate by adjusting the flow rate, given the flow rate stays within the operational limit (up to 90 $\mu\text{L}/\text{min}$) of the device and does not cause leakage in the system (considering the temporary binding). Also, the injection via a handheld pipette showed similar capturing rate which indicates the independency of this device on specialised equipment for sample injection, such as syringe pumps. Furthermore, To lower systematic losses during operation of our SDA, a minimum of 5 μL of the solution was injected, just to cover volume of the pockets (4.8 μL). The 5 μL injected

sample would fill more than half of the chip, which then air was injected to push the remaining of the sample from the main channel to fill the remaining pockets. Once all chambers are filled, any excess solution (if more than 4.8 μ L) could be collected from the outlet.

To further explore the potential of using this device for single-cell analysis of rare cells, we injected MCF-7 and THP-1 cell lines in a ratio of 1:100 to mimic the scenario of CTC isolation post enrichment from peripheral blood, based on previously published works of our research group [35, 145-147]. First, the harvested cells were stained using DAPI, anti-cytokeratin and CD-45 and then a mixture of both cell types was made at the optimum concentration. Then 5 μ L of the sample was injected to our device (consisting of ~297 THP-1 cells and 3 MCF-7 cells), and we observed average of 92 cells were captured individually ($38.3\% \pm 2.0\%$, N = 3). Generally, the washing steps involved in CTC enrichment is highly optimised to remove most debris and soluble proteins to a level which cells are well identifiable from background noise under fluorescent microscope. As shown in figure 4.2 (c), two traps were found to contain MCF-7 cells, which one was a singlet, and the other two were trapped in a double-occupancy chamber (with a THP-1 cells). This illustrated the potential of using our proposed workflow to analyse rare cells at single-cell resolution. It is also worth mentioning that increasing the number of pockets and consequently lowering the cell concentration would allow for a more efficient analysis (increasing the single-cell trapping rate) within a single device.

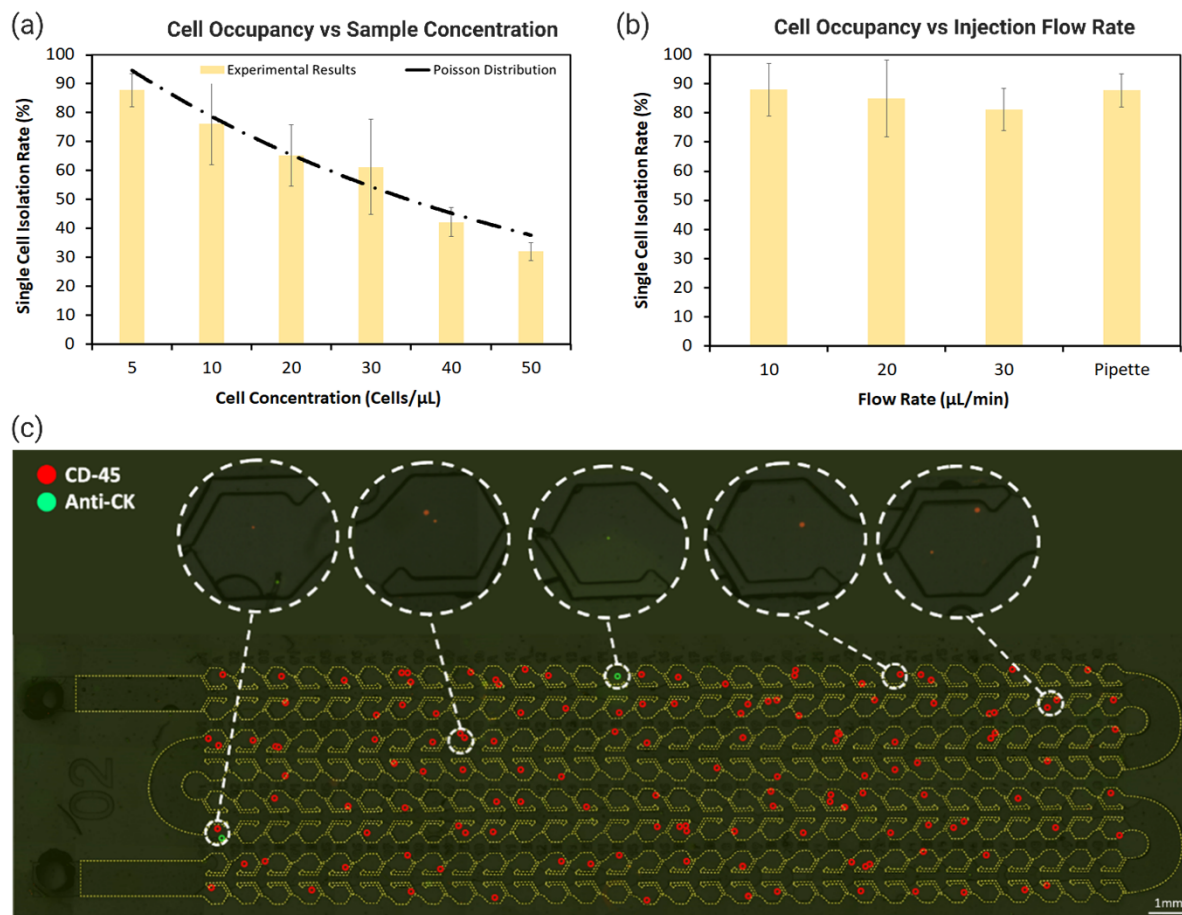


Figure 4.2 – The SDA device performance for trapping cells. (a) & (b) Single-cell capturing rate of the device with respect to cell concentration and flow rate to find the optimum capture rate of this device. It was found that at 5k cells/mL the single cell capture rate of the device was the highest, about 88% of cells were captured individually. The flow rate plays a smaller role in single cell capture rate, at 5k/mL concentration the variation of capture rate was trivial and there was no significant difference between handheld pipette injection and syringe pump injection. (c) Device performance tested with MCF-7 and THP-1 cell lines, in a 1:100 ratio (92 single cells were trapped). The green circles on traps were drawn manually to indicate the position of cells. 5 traps were shown with higher magnification for better illustration of the single and double occupied traps. No cell was found to stick to the main channel, inlet, and outlet of the device.

4.4.2 Retrieval through quick freezing

When analysing rare cells (including CTCs), current single cell isolation methods (e.g., micromanipulation, FACS, LCM and droplet barcoding) are constrained by the low input cell number processing and hence suffer from low yield, high cost, damage to cells, poor repeatability, and over-reliance on operator skills. Besides, these platforms do not allow for collection and monitoring of live single cells for on-chip studies. To overcome

abovementioned challenges of single-cell devices, we developed a simple and stand-alone approach for retrieval of single-cells based on a low-cost SDA microfluidic device that is capable of isolation and on-chip analysis of single cells.

The retrieval is done through freezing the temporary bonded SDA device against a glass or parafilm substrate, followed by a peel-off step. The freezing step allows all frozen droplets to stick to the surface with a greater hardness – i.e., using glass as substrate results in frozen droplets to stick to the glass while parafilm substrate allows the droplets to stick to the PDMS chip. Once the chip is peeled off, we covered the surface with oil to avoid merging or evaporation of droplets during the retrieval process. Then droplet of interest would be picked up using a handheld pipette and transferred to a PCR tube for downstream analysis. The entire process can take less than 15 minutes from injection to retrieval of the cell of interest. For a better illustration, food dye and dextran were used in Figure 4.3 (a) and (b) to show the freezing process and droplet retrieval using this method. -80°C freezer could be used for rapid freezing (~ 5 minutes) or long-term storage of the chip. Furthermore, Figure 4.3 (c) and (d) show the fluid flow and heat transfer of the proposed approach during the injection and freezing process through computational fluid dynamic simulation. An average cooling rate of $0.3^{\circ}\text{C}/\text{s}$ was obtained with most of the heat transfer occurring through conduction of the 1.5mm glass substrate.

In terms of user-friendliness during retrieval, glass substrate allows easier handling of the chip throughout the injection process due to its rigidity, while parafilm substrate allows an easier pick up since the droplets stay on the chip and geometrical features of the trap (arms) assists with keeping the droplet in its original space even if melting occurs. To further enhance this method, we designed an SDA device with the same trap shape and size, but with 2mm spacing between each trap to avoid droplet merging during the pickup process. The new device was fabricated using a 3D printer, as explained in materials and methods section, and consisted of 88 traps in total in a 15mm by 35mm moulding area (figure 4.4(a)). The droplets generation process was recorded in Movie S4, showing the same droplets formation theory in this spaced chip.

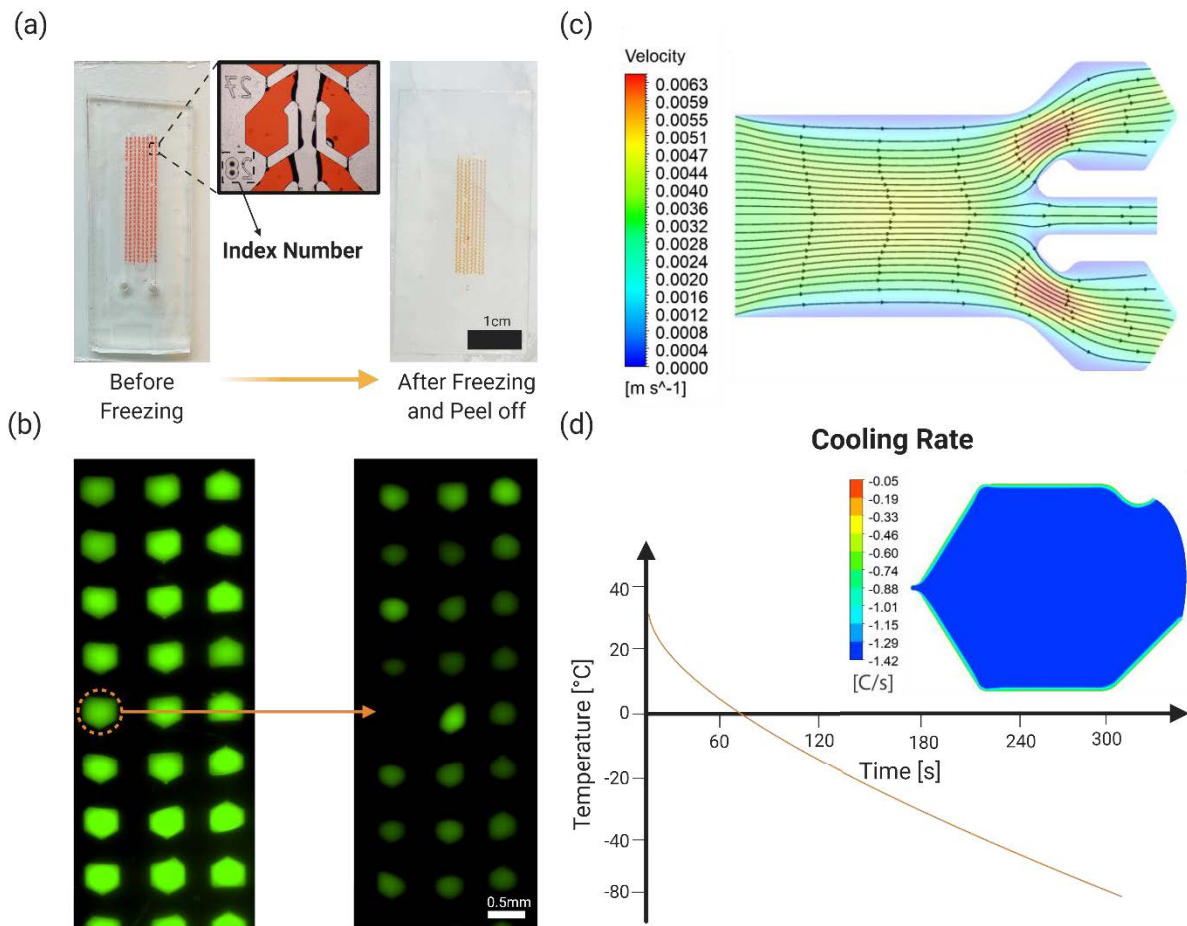


Figure 4.3 – Illustration of the device throughout the freezing and retrieval process along with simulation of the device during injection and freezing. (a) Frozen droplets of food dye tend to all stick to the glass substrate (more rigid surface compared to PDMS chip) after peeling off the device. If the PDMS device was temporarily bonded to a softer substrate than PDMS (e.g. Parafilm), the droplets tend to stick to the PDMS device. (b) pick up of dextran droplet before and after freezing, showing no liquid remaining in the trap. (c) CFD simulation of the flow across the device indicating the flow fills up the traps before proceeding through the main channel. (d) Heat transfer simulation of the droplet placed in -80°C environment with respect to time, elaborating on the rapidness of this method. Simulation indicates the droplets reach -80°C in 5 minutes and are frozen in about 1 minute.

The ice crystals formed during freezing and thawing of cells cause the cell membrane to burst [148]. For Applications where cells need to be retrieved after freezing, e.g. on-chip preservation and/or culturing, viability of cells post-freezing becomes crucial. Therefore, DMSO could be employed as one of the most commonly used cells cryoprotectant, which prevents water crystallisation during the freezing. We investigated the viability of cells after freezing and thawing the chip with different DMSO content (1%, 3%, 5%, 7%, and 10%) in -

80°C freezer. The viability was investigated by imaging the chip before freezing and after thawing, using live and dead cells staining. As shown in figure 4.4 (b), all cells frozen without DMSO were dead after thawing, and no cells could maintain the shape. In the 1% DMSO groups, none of the cells exploded due to water crystal formation, but the viability of the cells was low compared to the other DMSO groups. It was shown that the post-thawing viability is directly proportional to the DMSO concentration and a maximum viability of 86% (N = 5) was recorded when 10% DMSO was used. It is worth mentioning that in our previous works, we have shown the cell viability is not affected during the injection and trapping due to the low operational pressure of the device and minimal stress being applied through hand injection of cell solution via a handheld pipette. Also, the potentials of culturing cells in the device over 48 hours period with less than 5% drop in cell viability were shown [143, 149].

4.4.3 RNA analysis through RT-qPCR

To show the applicability of our method for single-cell molecular analysis, we performed single-cell RT-qPCR of some major genes such as GAPDH (housekeeping gene) and HER2 (epithelial marker). Although through the freezing process the cells would naturally burst, but the RNA content will be preserved in the frozen droplets which can be retrieved. Therefore, we investigated the amount of RNA retrieved from (1) frozen and peeled-off chip placed on ice block where the frozen droplets were picked before melting occurs, (2) frozen and peeled-off chip placed on bench and picked up after melting occurred. We compared the retrieved RNA content of both cases to a fresh cell in a tube. Figure 4.4 (c) and S4 show the RT-qPCR results and the Cycle of Threshold (Ct) value of GAPDH and HER2 in the fresh single-cell were 26.16 and 31.06 (N = 3), in comparison with a single cell of the frozen droplet sample that were 27.28 and 32.43 (N = 3). The single cell of the melted droplet sample showed a Ct value of 33.23 and 39.06 (N = 3), respectively, while there was no Ct value for the negative controls. By comparing the (Ct) values across both genes, we observed a similar amount of RNA detected in the frozen and fresh sample, while a significant loss occurred when the droplets were melted. Once the droplet melts, some of the RNA content would attach to the surface of the chip which would not be recovered. The ice block allows extra time for handling and pick up of the cell without causing the droplets to melt. While the Ct values do not indicate the actual concentration or copy number of the genetic material content (i.e. RNA), but the

minor difference between the Ct values of the fresh and frozen sample shows a high recovery of the RNA throughout our retrieval approach.

4.4.4 Cell loss during retrieval

To quantify the cell loss throughout the retrieval process, we tested the entire method for retrieval and transfer of 10 single cells (frozen and thawed with 10% DMSO content) to a 96-well plate by using a handheld pipette. The pickup was repeated for 5 times, and an average of 80% cell transfer (8 out of 10 cells) was recorded. The cell loss was mainly due to the manual handling of the 20 nanolitre droplet using a conventional 2 μ L pipette, which can be improved by using more accurate equipment. As mentioned above, spacing out the droplets can significantly improve the handling of the chip during thawing and picking up, since droplets have almost no chance of merging during the pickup, as they are separated apart.

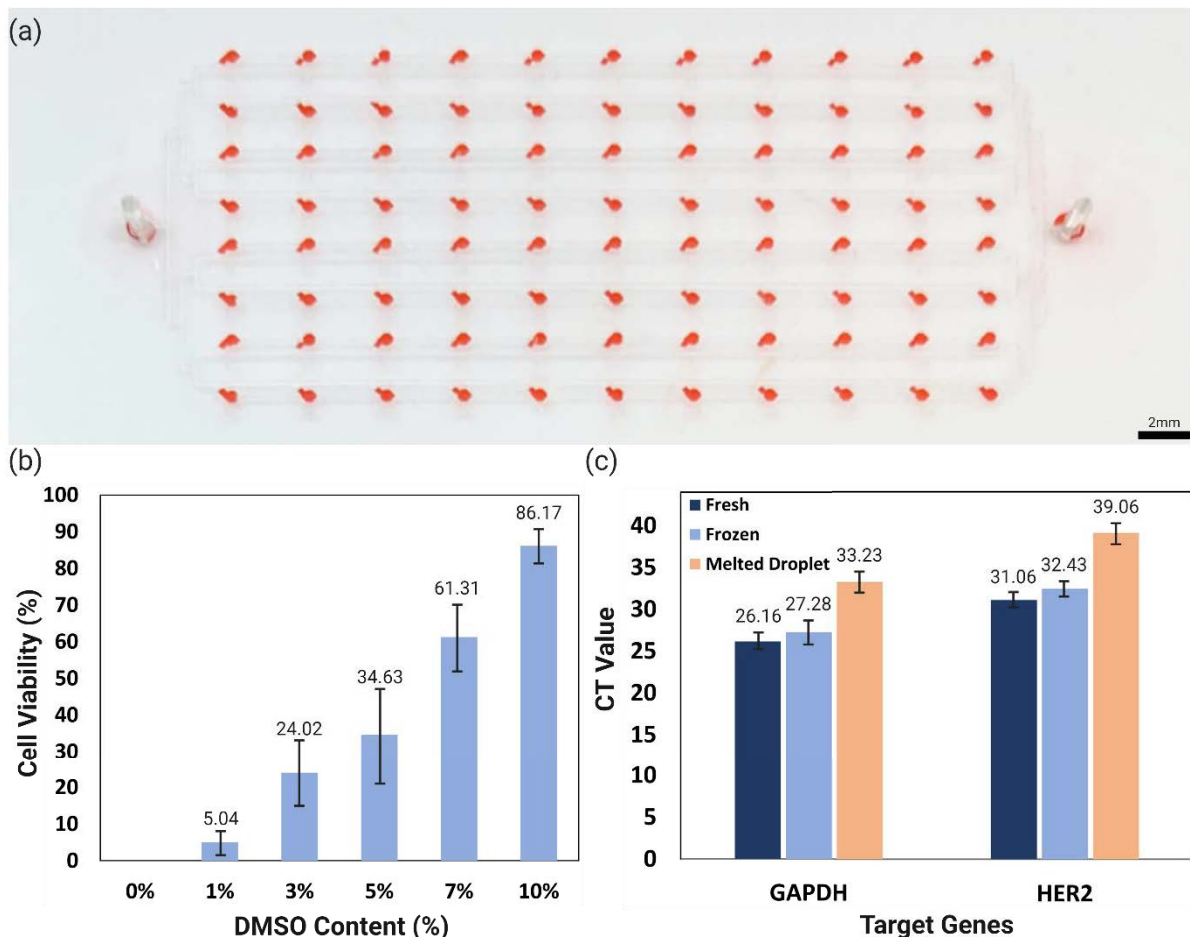


Figure 4.4 – Illustration of the device with greater spacing along with the effect of freezing on cell viability and molecular analysis of the retrieved droplets. (a) Picture of the spaced SDA design with 88 droplets generated using red food dye. This PDMS device was cast in a 3D printed resin mould. Since the space between traps is bigger, this device allows easier pickup of frozen droplets without a

microscope. (b) Cell viability after freezing indicated a positive relationship between DMSO content and viability of cells after freezing. Small droplet size and fast cooling reduce the damage of the cells. (c) Comparison between the cycle of the threshold of GAPDH and HER2 genes across the fresh, frozen, and melted droplet sample. Compared to a melted droplet, the frozen droplet has closer Ct value to the fresh cell control, indicating better preservation of the genetic materials after retrieval.

4.4.5 – Alternative Retrieval Approach via Highly Hydrophobic Surface

As an alternative approach to rapid freezing the chip a highly hydrophobic substrate was used to enable on-chip lysis of cells and retrieval of the cell lysate using a handheld pipette. The use of SDA device allows us to undertake the whole process only by using a hand-held pipette and microscope. A highly hydrophobic coating was used on the substrate to enable efficient recovery of cell lysate. The proposed workflow is shown in Figure 4.5.

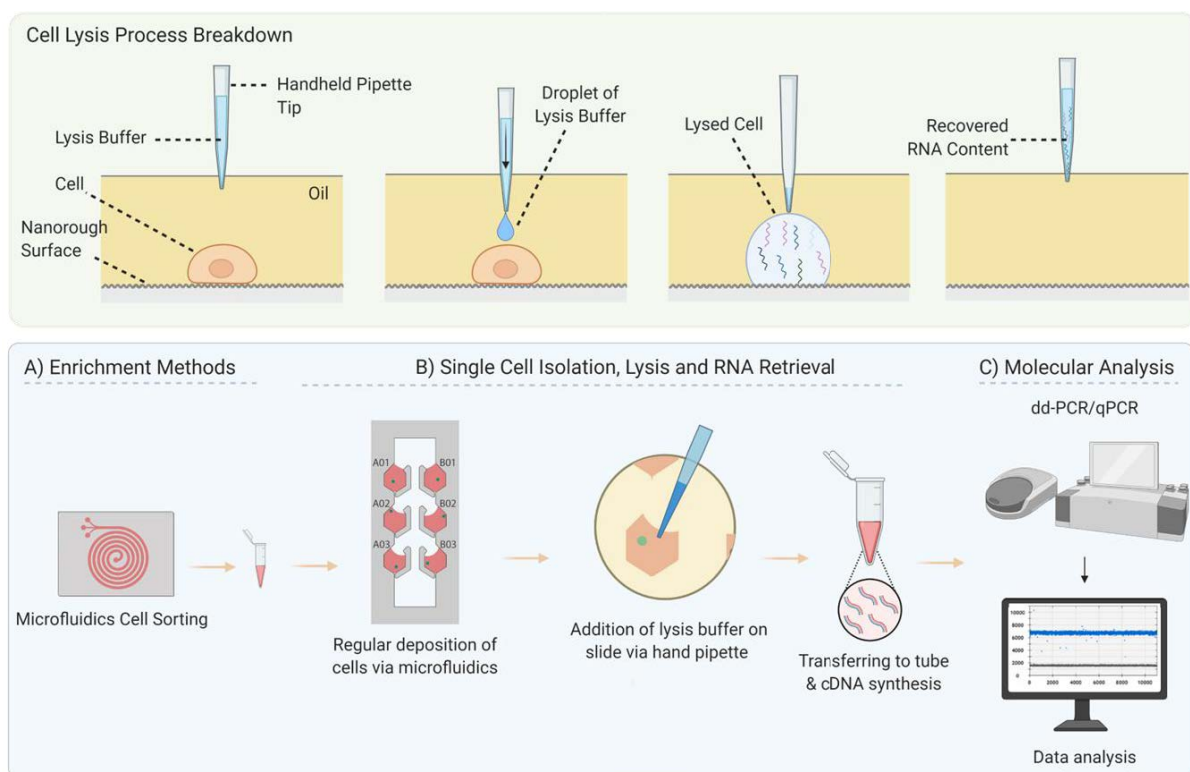


Figure 4.5 – Schematic of adding a droplet of lysis buffer on a cell attached to the highly hydrophobic surface following by genetic material retrieval. A) The manual approach uses a static droplet generator to encapsulate cells on the highly hydrophobic slide. The encapsulated cells are scanned under the microscope and then the chip is peeled off leaving the droplets on the slide following by adding oil to cover the slide. Given the size and spacing of the droplets, lysis buffer can be added with a hand-held pipette. C) Following the addition of the lysis buffer in each of the methods, the droplet is then

transferred to a tube for the synthesis of cDNA and downstream molecular analysis of the sample at a single cell resolution.

As a proof of concept, we designed a 20×20 nL and a higher throughput version of 336×20 nL pocket/trap devices (Figure 4.6 A, B and C) incorporating SDA on a hydrophobic surface. It is noteworthy that SDA devices with greater numbers of traps and different trap volumes can be fabricated, as shown in previous sections (500×2.5 nL and 600×14 nL traps).[150] This flexibility in manufacturing of SDA devices with different trap quantity and volume that can be easily operated with standard laboratory pipette provides us with a robust manual single-cell isolation method with no loss for rare cells analysis. The volume of each droplet generated by the chip is 20 nL, while can still be visualised without using a microscope. The pockets were designed 2 mm apart allowing for manual lysis of cells without mixing with adjacent droplets. Also, a micromanipulator could be combined with the SDA system as a method of cell lysing when an automated platform is required, which can allow for lower spacing between traps. It is important to note after allowing 5 minutes' sedimentation time and the peeling-off the SDA device, the droplets tended to attach to the SDA chip due to the higher hydrophobicity of the substrate. To overcome that issue, we used a thin layer of superhydrophobic material on SDA channel, which ensure to keep droplets on the substrate surface after the peeling-off.

After lysing single cells (ACH-3P), RNA extraction and cDNA synthesis, real-time PCR for KRT-7-FAM, GAPDH-HEX for single cells with two negative controls (PCR clean water, RNA template) were performed. Although ddPCR and pre-amplification are compatible with our SDA approach, we used an ultra-sensitive probe-based real-time PCR kit (QuantiNova; Qiagen) that is able to accurately detect rare targets down to one copy without applying pre-amplification step to simplify our analysis method. In our proof-of-principle study, we demonstrated the ability to recover the cell lysate using SDA chip and 2 µL pipette as well as performing real-time PCR for the detection of single-cell RNA expression without pre-amplification step.

As shown in Figure 4.6 (D and E) the Ct values of KRT-7 and GAPDH in the lysed single cell were 35.53 ± 0.6 and 29.78 ± 0.7 compared to collected single cell that were 34.31 ± 0.2 and 28.68 ± 0.3 , respectively; Ct values were not detected in both negative controls. Although the Ct values do not reflect the absolute concentration and copy number of these mRNAs, these slight differences between Ct values (5 independent replicates) indicate a comparable

recovery of genetic materials from a single-cell lysed on our highly hydrophobic surface using SDA chip and 2 μ L pipette to a single cell collected and lysed in a tube.

Finally, to further demonstrate the ability of our SDA chip on a highly hydrophobic surface in capturing and isolation of rare cells for downstream analysis, we mimicked a rare cell sample post enrichment and injected into our high throughput SDA device (336 pocket device). As per our previous research findings for CTC[151] and CFC[152] isolation using inertial microfluidic device, about 1-10 cells of interest are enriched among 1000-2000 WBCs in 1 mL of patient's blood. Using the similar ratio, we mixed stained THP-1 cell line (anti-CD45) to represent WBCs with stained BeWo cell line (Anti-Pan-Cytokeratin) as rare cells in a ratio of 1:100. We first injected 7 μ L of cells mixture at the concentration of approximately 60,000 cells/mL (total of \sim 400 cells, 4 BeWo cells among 396 THP-1 Cells) into our device, and observed an average single cell capturing rate of 38% (over 5 injections). Among the captured single cells, 1.4 ± 0.55 BeWo were successfully isolated individually (Figure S2). Furthermore, given the scarcity, importance of rare cells and in order to improve the single cell capturing rate of the device, we lowered the concentration of the injected sample to 30,000 and 15,000 cell/mL which significantly increases the average single capturing rate to 62% and 81%, respectively. It is worth mentioning, the lower concentration results in lower total cell injected in the system and hence requires more devices to process given number of cells. To overcome this, the device design can be further optimised to increase the total number of pockets, which can be achieved by lowering the spacing between pockets (e.g. 2 mm to 1 mm) and adjusting the height to width ratio of pockets. Overall, in the context of rare cells isolation and analysis (CFCs or CTC), after an initial enrichment, using our SDA chip on a hydrophobic surface not only compartments cells in a single cell droplet but also provides the opportunity to detect, lyse and analyse our desired single cells in rapid and simple way.

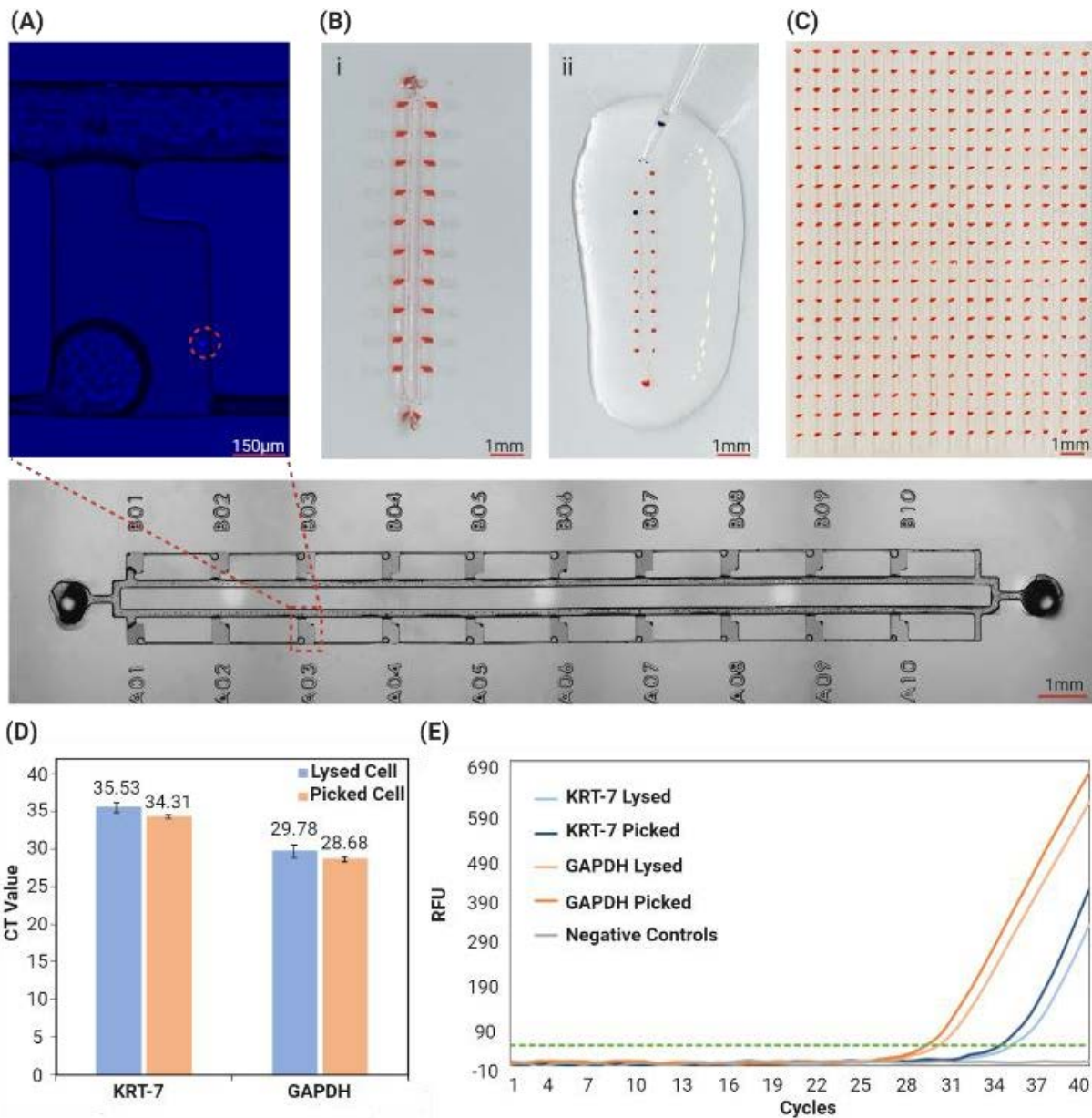


Figure 4.6 - A) Shows the microscopic image of the device injected with a cell solution at a concentration of $60 \times 10^3/\text{mL}$ (bright field and DAPI channels). B) The SDA device shown with red food dye injected for visualisation purposes (i) and addition of blue food dye to the droplet to mimic lysis buffer and uptake of the chosen droplet using a $2 \mu\text{L}$ pipette (ii). C) Image of 336 pocket SDA device with red food dye injected for visualisation purposes. D) Ct value of mRNAs of a lysed single cell on a 90 second nano rough PDMS as well as collected single cells (N=5). E) Real-time qPCR reaction performed using KRT-7 and GAPDH assays for lysed single cell on a 90 second nano rough PDMS as well as collected single cells (ACH-3P).

4.5 Conclusion

Single cell analysis provides novel insights to answer comprehensive biological questions that fail to be solved by bulk sample analysis and reveals the heterogeneity among a subpopulation of cells. The number of techniques and instruments for single-cell analysis have been soaring in recent years and data generated from single-cell studies show significant potentials in revealing heterogeneity among the various biological system. However, the high cost and technical expertise required have hugely limited the use of single-cell devices, especially in clinical settings. Besides, current single-cell technologies are incapable of analysing rare cells (e.g., CTCs) at single-cell resolution in an efficient and cost-effective manner. We have demonstrated a simple, highly efficient, and cost-effective method for single-cell isolation, followed by fluorescence microscopy and molecular analysis using RT-qPCR with minimal cell loss throughout the process by only using common laboratory tools. Nonetheless, the application of the proposed workflow is not limited only to molecular studies, and it enables the users to undertake various studies including cell secretion, drug testing, cloning, and culturing studies. Lastly, this methodology is applicable to all SDA devices and overcomes the challenge of cell retrieval after injection [143, 153, 154]. The method we reported here provides a simple and effective procedure for obtaining multiplexed visual and molecular analysis in the single-cell level by using common laboratory tools. Although our droplet retrieval method is simple and overcomes shortcomings of previously proposed methods, the total number of static droplets in the device should be maximised before it can be integrated in real-case applications, including clinical settings. Besides, automation of this process, e.g. use of automated micromanipulators for labour-free transfer of cells, could provide significant advantages for the use of this workflow in clinical or research settings by lowering the human-error, minimising cell loss and/or increasing the throughput.

Chapter 5 – Rapid Metabolomic Screening of Cancer Cells via High-Throughput Static Droplet Microfluidics

Summary

Effective isolation and in-depth analysis of Circulating Tumour Cells (CTCs) are greatly needed in diagnostic, prognosis and monitoring therapeutic response of cancer patients but has not been completely fulfilled by conventional approaches. The rarity of CTCs and lack of reliable biomarkers to distinguish them from peripheral blood cells have remained as outstanding challenges for their clinical implementation. Herein, we developed a high throughput Static Droplet Microfluidic (SDM) device that is capable of isolating and classifying the number of metabolically active CTCs in peripheral blood at single-cell resolution. Owing to the miniaturisation and compartmentalisation capability of our device, we demonstrated the ability to precisely measure lactate production of different types of cancer cells. The SDM device is a simple and robust technology that can eliminate the need for specialised equipment and expertise required for single-cell analysis of CTCs and facilitate on-site metabolic screening of cancer cells. This chapter is under preparation for submission to the journal of Analyst as a communication journal*.

* **Radfar, P.**, Ding, L., de la Fuente, L. R., Aboulkheyr, H., Gallego-Ortega, D., & Warkiani, M. E. (2023). Rapid metabolomic screening of cancer cells via high-throughput static droplet microfluidics. *Biosensors and Bioelectronics*, 223, 114966. DOI: [10.1016/j.bios.2022.114966](https://doi.org/10.1016/j.bios.2022.114966) - Impact Factor = 12.54

5.1 Introduction

Cancer is a broad term for a group of complex diseases that involve abnormal and uncontrollable growth of a cell population with the potential to invade other body organs. Cancer's rising prominence as the second major cause of death globally has demanded vital worldwide research to lessen the health and socioeconomic burden of this disease [21]. Research over the past several decades has shown that cancer arises from the transformation of normal cells into tumour cells via a complex multi-stage process as a result of the interaction between a person's genetic factors with external agents [155, 156]. Among the hallmarks of cancer, the final step of the disease is generally the progression to metastatic cell dissemination and colonisation of distant organs, a process that accounts for more than 90% of cancer-associated mortality [25]. During metastasis, cancer cells of the primary tumour locally invade surrounding tissues, enter lymph and blood microvasculature (intravasation), translocate mainly via the bloodstream to microvessels of the distant tissue and lastly exit the bloodstream (extravasation) to penetrate and facilitate proliferation for the formation of a secondary tumour (colonisation) [157]. Thus, early diagnosis and treatment play a vital role in the effective management of cancer. However, cancer is difficult to diagnose at early stages, and choosing the right treatment often requires invasive collection of tissue biopsies from cancer patients. Obtaining tissue biopsies is associated with many difficulties including discomfort for the patient, clinical risks, surgical complications, and economic considerations [158, 159]. Additionally, some tumours are not accessible which complicates or disallows the chance of taking biopsies from the patients. Therefore, alternative approaches for the diagnosis, monitoring and prediction of cancer, such as liquid biopsy, have attracted significant attention lately [160, 161].

Circulating tumour cells (CTCs) are the cells that disseminate from a primary tumour and shed into the bloodstream. CTCs are known to be the major precursors of cancer metastasis [26]. CTCs travel in single and cluster formats and must survive from trauma, oxidative stress and immune system attacks in the vascular system to enable metastasis [26-28]. CTCs have a similar genotype and phenotype as the primary tumour and can be used as an alternative strategy for disease diagnosis, prognosis and monitoring treatment efficacy [29]. Besides characterising CTCs, it has been proven that the number of CTCs found in patients' blood correlates directly with the disease progression and survival rate [30, 31]. Overall,

management of cancer via assessment of CTCs in blood samples is far less invasive than taking tissue biopsies, allowing repetitive sampling and monitoring patients' responses to treatments [32]. However, CTCs are exceedingly rare compared to peripheral blood cells, such that one CTC can exist among billions of blood cells [33]. Although erythrocytes can be removed simply by osmotic cell lysis, leukocytes share common physical, chemical and biological properties with CTCs [34]. Hence, isolation and characterisation of enriched CTCs are proven to be a tedious task [35-39].

CTC enrichment methods are mainly categorised into immunoaffinity- and physical property-based approaches [124-127]. Briefly, immunoaffinity methods utilise the surface markers of CTCs to separate them from peripheral blood cells, and physical-based approaches use differences in size, shape, deformability and density of CTCs to separate them [162]. While both approaches have their own advantages and shortcomings, they all rely on immunostaining to confirm the identity of CTCs or utilisation of sophisticated single-cell omics technologies to assess the molecular and functional characteristics of CTCs [47, 163]. However, enrichment approaches are often incapable of capturing all CTCs which have no/low level of specific surface biomarkers or those that share similar physical characteristics to white blood cells [42, 164]. Despite the enrichment method, isolation and identification of CTCs are usually labour-intensive, time-consuming and costly [4].

In the 1920s, Otto Warburg first discovered the increased lactate production as the result of increased glycolysis in cancer cells which results in acidification of tumour environment [165, 166]. Additionally, acidification of the cancer environment has been observed in tumorigenesis and increasing acquisition of more metastatic phenotypes [34, 167]. While acidification of the tumour microenvironment has been well reported in the past decades, few studies have shown the potential of monitoring metabolic activity and lactate production of single cells for detection of CTCs and cancer-associated stromal cells [34, 168]. The concept relies on fractionation of liquid down to picolitre droplets for encapsulation of single cells, where the glucose uptake and excessive lactate production of the tumour cells result in rapid acidification of the tiny droplet environment which may be monitored via pH sensitive fluorescent dyes. Furthermore, the study by Rivello et al. has shown the importance of capturing and quantifying the number of circulating stromal cells, given their crucial role in cancer metastasis [168]. In fact, the authors showed the inability to capture these cells via

conventional immunoaffinity-based approaches, and yet emphasized the importance of studying single-cell metabolism of cancer patients.

To effectively fractionate liquid into tiny segments, droplet microfluidic devices are commonly used. These rely on their unique ability to precisely handle tiny volumes of liquid and create mono-sized water-in-oil droplets by mixing two immiscible fluids [83]. Although droplet microfluidics provides a unique opportunity for the detection of CTC without relying on specific biomarkers, they suffer from high sample loss, expensive setup costs and operational complexity, which limits the clinical applicability of these devices [5]. Additionally, besides the technical expertise required, droplet generators require expensive instruments (e.g., syringe/pressure pumps) and reagents (e.g., synthetic surfactant in fluorinated oils). Ultimately, droplet generators face difficulties in fractionating small sample volumes due to the initial stabilisation time needed to operate the system [4]. In summary, despite the benefits of using droplet microfluidics for monitoring the metabolic activity of cancer cells in peripheral blood, its drawbacks limit the accessibility of this approach for general laboratories and clinics.

To overcome the abovementioned challenges, in this work we developed a simple and robust workflow for enrichment, isolation and detection of highly metabolomic active cancer cells from blood within 40 minutes of sample collection. Our workflow includes a size-based enrichment of cancer cells from peripheral blood cells using inertial microfluidics, previously developed by our research group [146], followed by isolation of single cells using a novel arrow-shaped Static Droplet Microfluidics (SDM) capable of fractionating liquid into 125pL droplets (Figure 5.1A). The SDM device was used to monitor the metabolic activity of each cell using a pH-sensitive fluorescent dye which is an ideal candidate for robust detection of highly metabolic cancer cells. Our SDM device is simply operated via a standard handheld pipette, eliminating the need for costly equipment/reagents or skilled operators. In this work, we characterised the functionality of the SDM device to monitor and quantify metabolic activity down to a single-cell level using different cancer types, showing their excessive production of lactate compared to human leukocytes. We show the clinical applicability of the proposed workflow for detection of spiked cancer cells in human healthy blood, and lastly, and we demonstrate its diagnostic potential using pre-clinical blood samples from mouse models of cancer with differential metastatic properties.

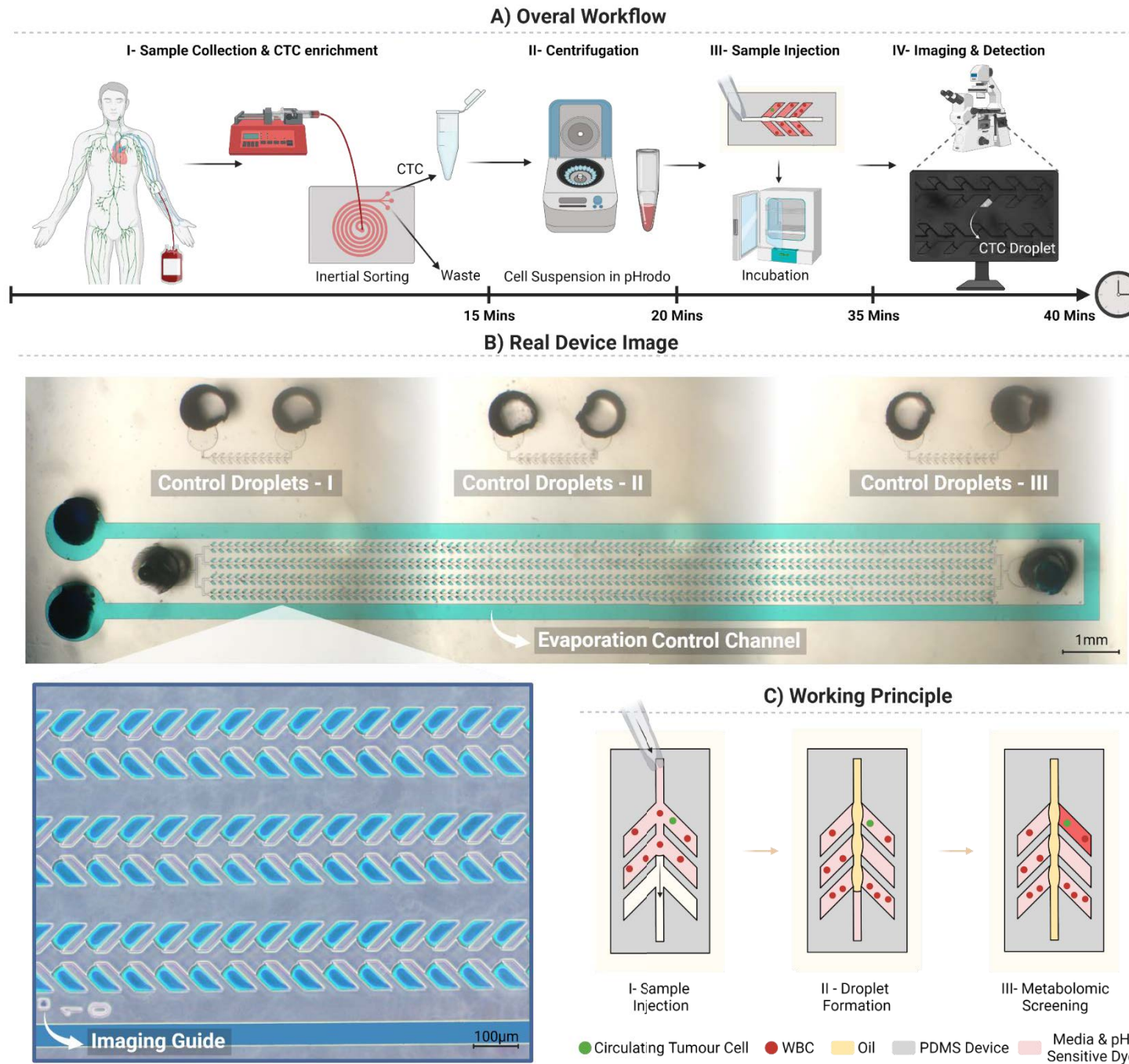


Figure 5.6 – Metabolomic screening of cancer cells via Static Droplet Microfluidics (SDM). A) Overall workflow of Circulating Tumour Cells (CTCs) enrichment, isolation and detection via monitoring the metabolic activity of cells. B) Microscopic image of the SDM device filled with blue food dye. The close-up image

shows the architecture and key features of the PDMS device. C) Working principle of SDM device within three simple steps of i) sample injection, ii) droplet formation and iii) metabolomic screening via pH sensitive dyes.

5.2 Materials and Methods

5.2.1 Device Design and Fabrication

The SDM devices were produced via photo and soft lithography. Firstly, the microfluidic patterns were designed using AutoCAD software (AutoDesk, USA). The lower throughput SDM devices were fabricated via a mask-less lithography approach using μ PG101 machine (Heidelberg, Germany). Briefly, silicon wafers were prepared and spin-coated with a uniform layer of 35 μ m thickness of SU8-2050 (MicroCehm Co., USA), soft-baked, and ultraviolet exposed, baked post-exposure, developed and hard-baked according to the manufacturer's guidelines. Lastly, salinisation was done using trichloro (1H, 1H, 2H, 2Hperfluoro-octyl) silane (Sigma-Aldrich, Australia) in a pressure desiccator for 2 hours under vacuum to produce a hydrophobic coating layer on the master mould. It is noteworthy that exposure settings of μ PG101 machine, including power and focus of the laser writer, were optimised to achieve the desired quality of final master mould.

Once the mould preparation was completed, fresh polydimethylsiloxane (PDMS, Sylgard 184, Dow Corning, USA) was prepared by mixing elastomer and curing agent in a ratio of 10:1 and then degassed inside a vacuum desiccator to remove air bubbles. Then the degassed PDMS was slowly poured on the master moulds and cured for 1-2 hours at 65°C. Finally, the PDMS devices were cut from the mould and designed inlets and outlets holes were made using a 0.75mm biopsy punch, and permanently bonded against a glass substrate using by plasma treatment and activation of both surfaces.

In this work, two SDM devices were proposed as the final working prototype. First, a smaller device was designed containing 800 chambers with 125pL volume each, suitable for low-throughput applications (Figure 5.1B). Similarly, second SDM device was a higher throughput version of the first one, containing 38,400 chambers with total working volume of 4.8 μ L, suitable for rare cell analysis.

5.2.2 Device Loading and Operation

Prior to sample loading, the inlet and outlet ports were covered with a scotch tape (3M, Australia) and the device was pre-vacuumed inside a desiccator for at least 30 minutes to remove air from the chip. In the lower throughput device, cell sample was suspended in pHrodo solution (Catalogue number: P35372, Thermo Fisher, US) at a concentration of 2000

cells per μL of liquid, and then $1\mu\text{L}$ of sample gets injected into the device via a handheld pipette. For the injection of the sample, simply the inlet tape is pierced via the pipette tip which allows the liquid to be aspirated automatically into the device, due to the negative pressure inside the channels. This eliminates any potential operator error in the injection step. After removing the inlet and outlet tape, the excess liquid is then removed from the outlet port and replaced by mineral oil for incubation (Figure 5.1C).

Similarly, the higher throughput device is used to process entire CTC enriched sample. As shown in Figure 5.1A, the blood sample is first enriched for CTC based on size, using our previously developed slanted spiral microfluidic device operated at 1.7mL per minute [146]. The enriched sample is collected and centrifuged at $400\times g$ for 5 minutes. The supernatant was replaced by $5\mu\text{L}$ of pHrodo dye. The sample is then resuspended thoroughly. To simplify the process and minimise any potential sample loss, first about $4\text{--}5\mu\text{L}$ of mineral oil is aspirated using a $10\mu\text{L}$ pipette and then the entire $5\mu\text{L}$ of pHrodo solution is aspirated inside the same tip. The oil plug inside the tip and above the sample eliminates the need for the sheathing step. Prior to injection and piercing the inlet tape, it is recommended to avoid having any air bubble underneath the sample, inside the pipette tip. Following this allows the device to automatically remove the interconnecting liquid in the main channel and generate the droplets in one step. If required, extra oil can be injected to fully cover inlet and all 16 outlet ports. As shown in Figure 5.1C, we have designed an evaporation control channel along with 3 control SDM units used as blank PDMS, DPBS control and pHrodo without cells. The controls were used for image analysis and normalisation purposes. Lastly, the evaporation control channel is filled with DPBS (Gibco, Australia) to avoid any undesired evaporation of droplets. After 15 minutes of incubation at 37°C , the device is imaged using a fluorescent microscope and the image is then analysed as described in the “SDM Imaging and Analysis” section. A detailed operational video of low- and high-throughput devices are provided in the Supplementary Movie S1 and S2.

5.2.3 Cell Culture and generation of syngeneic mouse models of breast cancer

Human prostate cancer cell line, DU145, breast cancer cell line, MCF-7 and MDA-MB-231, were cultured in complete media made of RPMI media (Gibco, Australia) with 10% foetal bovine serum (FBS) (Gibco, Australia) and 1% Penicillin-streptomycin antibiotics (Gibco, Australia) in T-25 flasks (Corning, Australia). The cells were passaged at 80% confluency, and

the seeding density was about 0.7×10^6 cells. The 67NR and 4T1.2 mouse cell lines were culture in RPMI media supplemented with 5% of FBS at 37°C with 5% CO₂. Cells were split when 70-80% confluence was reached. After one week of culturing, both cell lines were trypsinized and resuspended in DPBS (Gibco, Australia) for the generation of the syngeneic mouse models of 67NR and 4T1.2. Briefly, 50,000 cells for the 4T1.2 model, or 20K cells for the 67NR, were injected into the mammary gland ducts of Balb/c mice. The surgery was carried out on anaesthetized mice (2.5-4% Isoflurane at 1L/minute oxygen rate) by cutting the inguinal nipple and injecting the cells directly into the mammary ducts in a volume of 4µl with 0.1% Trypan blue dye (Gibco, Australia).

5.2.4 Healthy Human Blood

Blood samples were obtained from healthy volunteers through Australian Red Cross (Material Supply Agreement no: 21-01NSW-04). A total of 20 blood samples from healthy volunteers were used. All blood specimens were collected in EDTA-contained vacutainer tubes (BD, Franklin Lakes, NJ, USA) and lysed via the RBC lysis buffer (BioLegend) prior to processing on chip. For each experiment, a known number of cancer cells were spiked in the fresh blood samples of the healthy donors and procedure described in “Device Loading and Operation” section was followed.

5.2.5 Immunofluorescence Staining

In order to confirm the cell content inside droplets, cancer cells were stained with Hoechst (16.23 mM) (Sigma-Aldrich, USA). Briefly, harvested cells were centrifuged at 400×g for 5 minutes inside a 1.5mL Eppendorf tube (Eppendorf, Germany). The supernatant was removed and cells were suspended in 2µL of Hoechst and 98µL DPBS per 10⁴ cells. After 10 minutes of incubation at 37°C, the sample was washed twice with DPBS prior to suspension inside pHrodo solution (Figure 5.2A).

5.2.6 Numerical Simulation

To better understand the flow behaviour inside our SDM device, numerical simulation was carried out using ANSYS Fluent 2020R2 (ANSYS, US). To lower the computational load, the device was simulated using a 2-dimensional k-ε turbulence model (Figure 5.2B). A transient and multi-phase solver was used to observe the filling of the device. Boundary conditions were assigned similar to real-case scenario where the inlet was defined as a pressure inlet,

set at atmospheric pressure, the fluid domain and PDMS boundaries were set at -100kPA to simulate the vacuumed device. The primary fluid phase was set as water with default properties, including density = 998 kg/m³ and dynamic viscosity = 1.002×10⁻³. Similarly, the secondary phase was set as air with density = 1.225 kg/m³ and dynamic viscosity = 1.7894×10⁻⁵.

5.2.7 SDM Imaging and Analysis

After incubation the SDM device was imaged using an Olympus IX 73 inverted fluorescent microscope (Olympus, Japan) and 10x magnification lens. The bright field and fluorescence images of the whole SDM device were taken automatically by defining the required setting, imaging starting point and endpoint.

The image analysis workflow is shown in Figure 5.2C. The fluorescent intensity of the droplets was obtained through ImageJ software. Horizontal rectangular sections were drawn across the droplets of each row to plot the average intensity of each pixel. The intensity profile was then exported and denoised using MATLAB software where the local maxima and minima were identified. Each local minima point is representing the PDMS boundary between pockets, while the local maxima represented the intensity of each droplet. Finally, intensity data were normalised against the PDMS control and plotted as folds of difference between droplet intensities. During device characterisation, to fully understand the metabolic activity of cells, the fluorescent intensity was matched with the cell occupancy of each droplet which was confirmed using Hoechst staining.

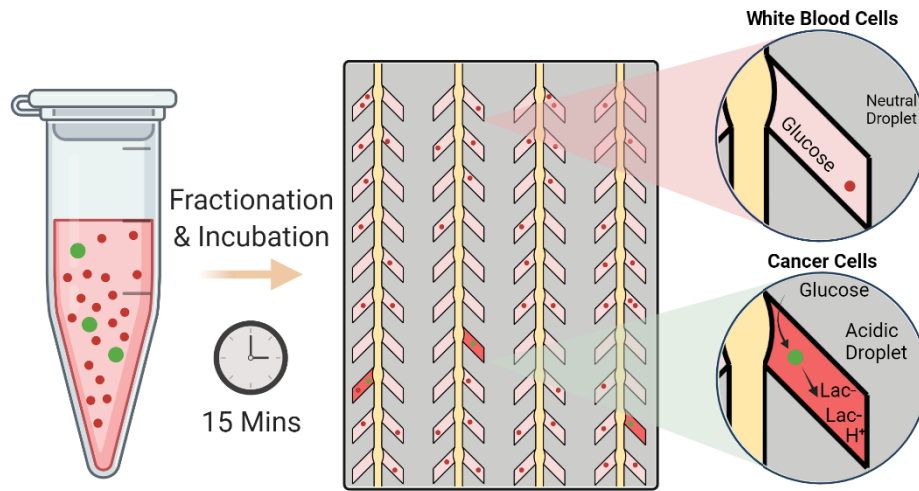
5.2.8 Oestrogen Deprivation of MCF-7 Cells

In order to achieve oestrogen deprived MCF-7 cells, a cell batch was cultured in phenol-red-free RPMI media (Gibco, Australia) supplemented with 10% dextran charcoal-stripped Foetal Bovine Serum (FBS), as described by Darbre et al. [169, 170]. For charcoal-stripping FBS to deplete hormones, we briefly incubated dextran-coated charcoal (Sigma-Aldrich, USA) at 4°C in 10mM HEPES, pH 7.4. Then, the solution was centrifuged at 500×g for 10 minutes. The supernatant was removed and replaced with the same volume of FBS. Lastly, the tube was vortexed to thoroughly mix the charcoal with serum and incubated at 4°C for 12 hours.

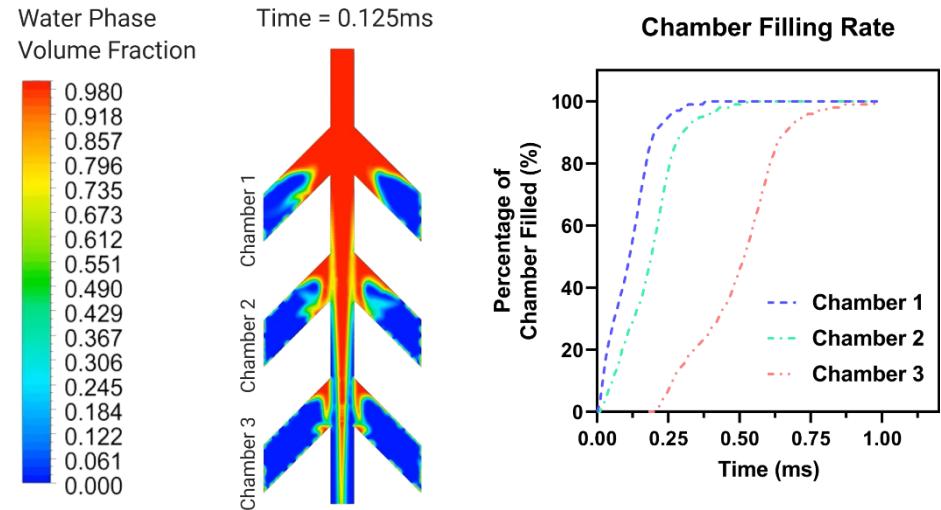
5.2.9 Preclinical Validation

The mouse experiments were performed in biological testing facility at Garvan Institute of Medical Research under the approval of the St. Vincent's Hospital Animal Ethics Committee (AEC) #19/02 (previous) and AEC #22/03 (current). Blood was collected from breast cancer mouse models at endpoint, mice bearing 67NR and 4T1.2 tumours were sacrificed 24-25 days after cell implantation and MMTV-PyMT mice were sacrificed at 100 days old, as previously described by Gallego-Ortega et al. and Valdes-Mora et al. [171, 172]. The blood was processed similar to the procedure described in the "Device Loading and Operation" section. Briefly, erythrocytes were removed via osmotic cell lysis and the sample was enriched for CTCs based on size using the spiral microfluidic device, followed by sample suspension in 5 μ L of pHrodo dye solution and was injected into the high-throughput SDM device. After 15 minutes of incubation, the entire device was imaged and analysed for metabolic activity based on the fluorescent intensity of each droplet.

A) Detection Mechanism



B) CFD Analysis



C) Image Analysis Workflow

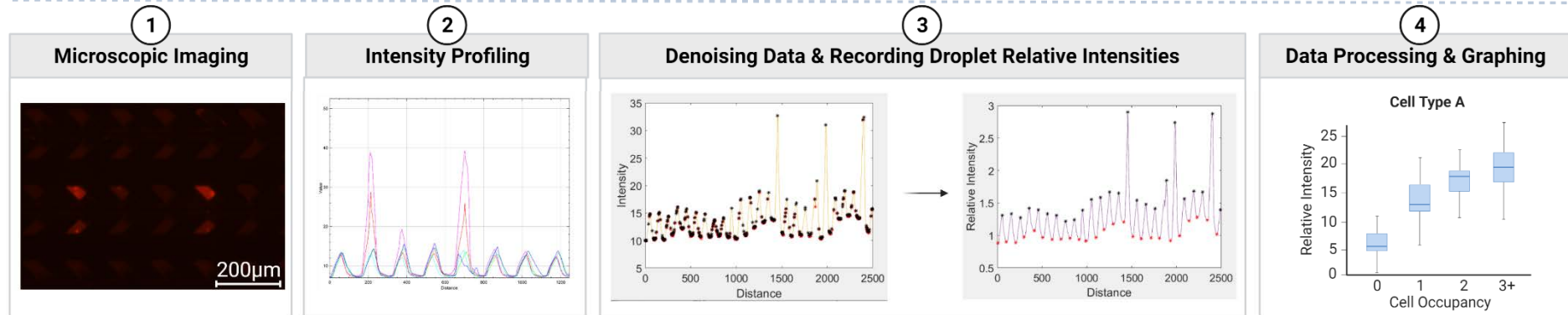


Figure 5.2 – Working principle of Static Droplet Microfluidic (SDM) device. A) Detection mechanism relies on the fractionation of liquid down to picolitres, uptake of excess uptake of glucose and secretion of lactate from cancer cells compared to white blood cells, resulting in an acidic droplet environment. B) Computational Fluid Dynamics (CFD) analysis of 3 chambers in a row, showing the chamber filling rates over time. C) Post incubation and imaging the SDM device, to determine the metabolically active cells, the intensity of each droplet was profiled using ImageJ, and subsequently the intensity profiles were denoised using MATLAB and lastly the data is processed and analysed.

5.3 Automated Droplet Intensity Analyser

5.3.1 Programming Workflow

The proposed program was developed using MATLAB (United States) and provided as supplementary to this manuscript. The working principle of the program developed in this work is illustrated in Figure 5.3. Briefly, the program starts by requiring the user to input variables including: 1) number of images to be processed, 2) value of “off threshold”, 3) “minimum droplet size” (in pixels) and 4) value of “on threshold”.

The software starts initialising by creating a two-dimensional matrix from the image and converting the intensity of each pixel to a single numerical value. In the next step, the program starts gridding matrix/image by turning the rows and columns between droplets to 0 intensity value. The gridding is done through a simple yet effective approach; the rows and columns with values of the entire row/column below the “off threshold” is equated zero. To eliminate background noises and smaller sized autofluorescence points/particles, droplets smaller than “minimum droplet size” are eliminated. In the final step, an “on threshold” is defined and each droplet containing an average intensity value above the threshold is recorded and normalised against “off droplets”.

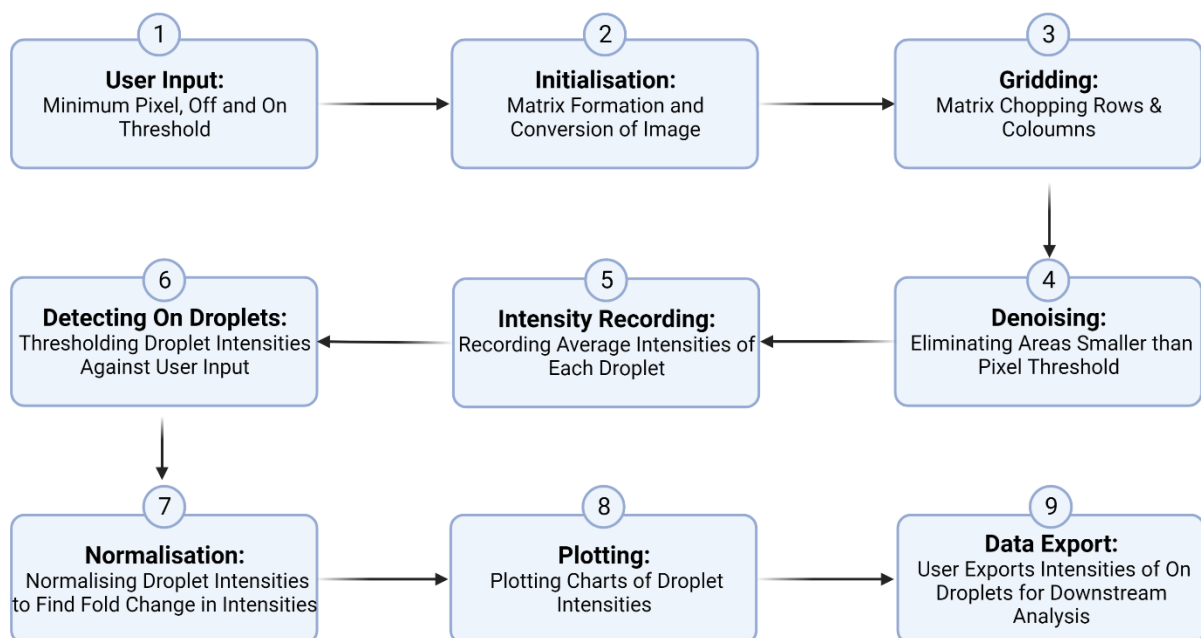


Figure 5.3 – Programming workflow for analysing droplets. The program workflow consists of 9 key steps in which the microscopic images of static droplets is analysed. The program starts with user inputting variables including minimum pixel, off threshold and on threshold. It is then followed by an

initialisation step which image is converted into a matrix containing a single intensity value for each pixel. Based on the user inputs, the software performs gridding to isolate droplets from background pixels and conducts a denoising step to remove smaller size particles. After detecting the droplets, average intensity of each droplet is recorded, normalised and plotted on a chart where the user can export the on-droplet intensity values from the software.

5.3.2 Image Analysis

For an easier illustration and a pilot study, an image with dark background (with low intensity) and grey circles of different intensities were used to mimic the microscopic image of droplets (Figure 5.2A). As discussed earlier, after inputting the required variables, the program initiates by gridding the rows (Figure 5.2B) and columns (Figure 5.2C). If there were any smaller sized noise/autofluorescence particles, they get eliminated via size thresholding. In the next step, all droplets are shown on a chart based on their absolute intensity values (Figure 5.2D). At this point, the user defines an “on-threshold” and the program eliminates the off droplets and plots two charts of the absolute (Figure 5.2E) and normalised intensities (Figure 5.2F).

Furthermore, an actual microscopic image was taken from a static droplet device used for screening metabolic activity of cancer cells [128]. As shown in Figure 5.3, the program successfully detects the diagonally/arrowed shaped droplets and plots the absolute and normalised droplet intensities. It is worth mentioning that diagonally shaped droplets would be among the most complex geometries for the program to detect due to its complex shape. Similar to Figure 5.2, each step is illustrated in Figure 5.3A-F for better showcasing the use case of the program in the real case scenario.

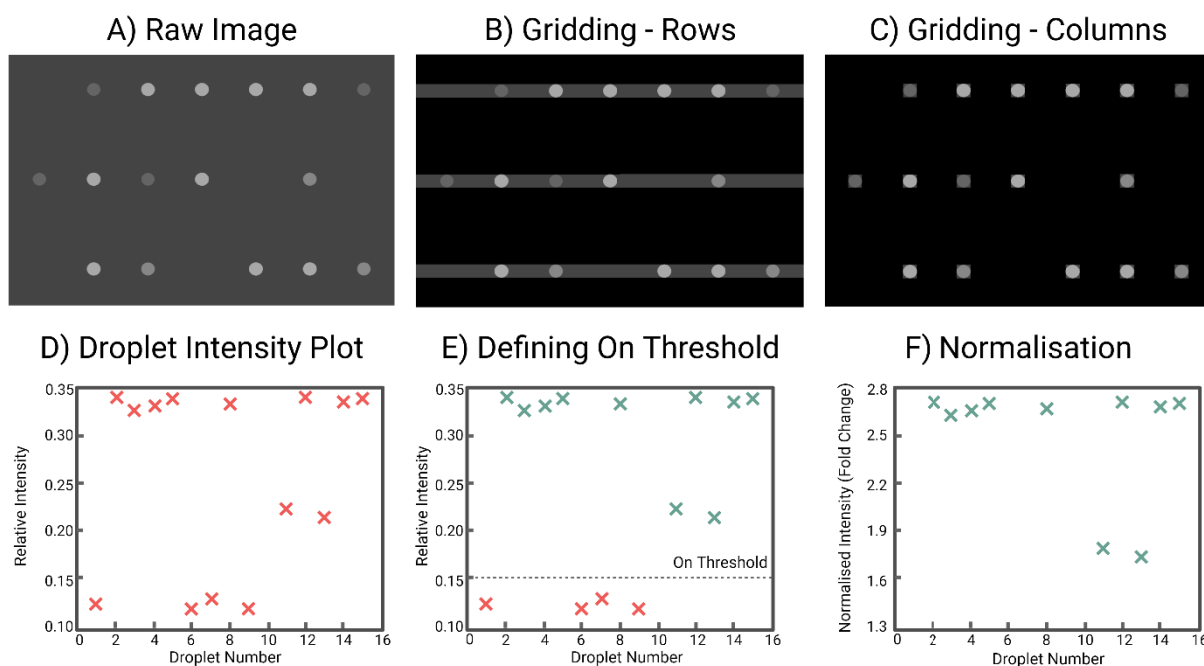


Figure 5.4 – Analysis of Sample Image. A sample image containing circles with different grayscale intensity was used to optimise the program. The figure illustrates different steps of A) importing raw image, B) gridding rows, C) gridding columns, D) plotting droplet intensities, E) defining on threshold and F) normalisation of on droplets in terms of fold change of intensities compared to the off droplets.

5.3.3 Application Use Cases

While the use case of droplet/micro-array analysis remain endless, the proposed program aims to provide a versatile and simple approach for users without major programming knowledge. The program was written using MATLAB software and can analyse multiple images simultaneously. The image analysis conducted in Figures 2 and 3 are provided as a supplementary document to this manuscript which can be used as a reference for practice.

Firstly, ensure MATLAB software is installed on your computer and simply place the program in the same folder as your image(s) to be analysed. The images are meant to be names with the following format: image### - i.e. the first image should be named image001. After opening and starting the program, the few prompt boxes will appear for user to input variable values. The first box requires user to input number of images being analysed, followed by an “off-threshold”. Setting “off threshold” would differ based on each image and might require optimisation. However, the default value of 0.12 is a reasonable start point for most images. In the next step, software requires the minimum pixel threshold to eliminate the background noise, which can be simply measured by software like paint, ImageJ and Photoshop. The

minimum pixel threshold should be chosen to be smaller than the pixel size of the droplets to ensure droplets are not eliminated – e.g., minimum pixel threshold to be half of the droplet size. After setting the initial inputs, the software shows 5 figures of each step to ensure the inputs were valid, as shown in Figure 2 and 3. First two figures are the gridding steps and third figure in the MATLAB file would be the pre-denoising. Fourth figure is the denoised image while showing the droplets. The fifth MATLAB figure is a chart containing the intensity value of each droplet which can be used as a guide for the user to enter the “on threshold”. At this stage the program has finished analysing the image and sixth MATLAB figure illustrates the “on droplets” along with seventh and eighth figure which plot the intensity charts of absolute and normalised droplet intensities. The process can be repeated and adjusted to optimise each variable and ensure the results are accurately interpreted. In the case that intensities are required, they can be accessed in MATLAB under the workspace section (often placed on the right). While all variables are accessible in the MATLAB file, the two matrices of “droplet_intensity_on” and “droplet_intensity_on_normalised” contain the values of the last two charts.

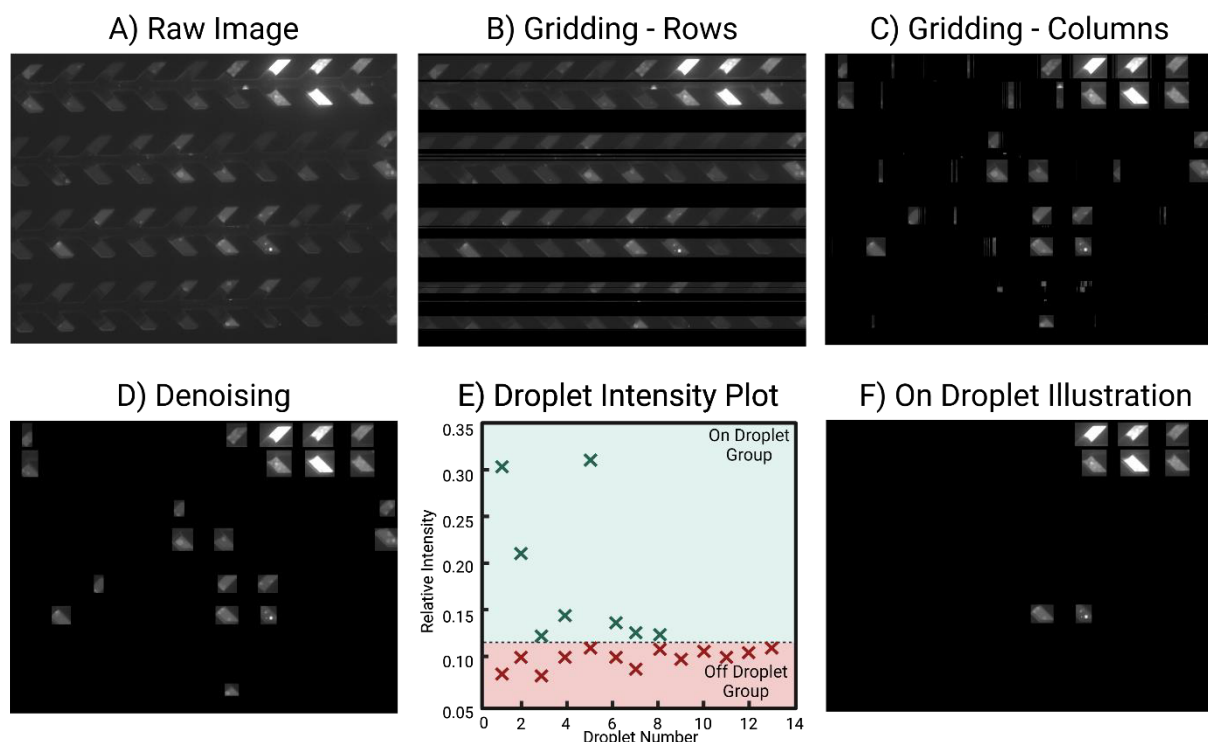


Figure 5.5 – Analysis of a Static Droplet Microfluidic Device Image. An actual microscopic image of a static droplet microfluidic device was taken after analysing cancer cell metabolic activity using pH sensitive dyes. The figure illustrates different steps of A) importing the raw image, B) gridding rows,

C) gridding columns, D) denoising and elimination of background noise, E) plotting the droplet intensities and F) illustration of the on droplets based on the threshold defined by the user.

5.4 Results and Discussion

5.4.1 Static Droplet Microfluidic: Concept Design and Development

The ability to fractionate liquid into nano-picolitre segments via dynamic droplet microfluidics has revolutionised the single-cell analysis field [84]. But technical complications, including reliance on skilled operators, specialised equipment and costly reagents, have limited the clinical applicability of this method [4]. As an alternative approach, static droplets have been developed in recent years to overcome the abovementioned limitations [143, 149, 153, 154, 173]. However, low-throughput and low-flexibility in down-sizing droplets (i.e., inability to generate sub-picolitre droplets) have remained a major barrier for these devices, only allowing them to be suitable for a limited number of applications that deals with small samples [4]. In contrast to the conventional static droplet devices and to overcome both the throughput and volume limitations, we investigated potential approaches for liquid entrapment without relying on fabricating an air vent inside each chamber. Initially, an in-depth Computational Fluid Dynamics (CFD) simulation was conducted to explore the potential of filling the side chambers by providing a negative pressure inside the device prior to filling (Figure 5.2B). Building on this understanding, several designs were fabricated and experimentally validated using pre-vacuumed PDMS devices. Both numerical and experimental simulations showed the devices are filled within a second, which facilitates rapid sample injection and fraction inside the chip. Among all, arrow-shaped static droplets were found to have the best filling while allowing a maximum number of droplets in a given area. As a result, in this work we developed SDM devices with different droplet volumes ranging from 5nL to 125pL to thoroughly investigate the potential of entrapping single cancer cells and consequently measuring their metabolic activity.

5.4.2 Device and Workflow Optimisation

In order to understand and characterise the SDM device, we studied and optimised different volumes of droplets, time of incubation and cell trapping characterisation based on the metabolic screening of the DU-145 cancer cell line using the pHrodo dye (a pH sensitive fluorescent dye). Throughout all the characterisation steps, the recorded fluorescent intensities were normalised against the base fluorescent intensity of PDMS boundaries as the

reference in each image. This allows a clear distinction between the PDMS boundaries, “off” droplets (droplets with no metabolically active cell) and “on” droplets (droplets with metabolically active cells). Also, this normalisation of recorded fluorescent intensities enabled a direct comparison of results across different cell types and occupancies by eliminating chip-to-chip and batch-to-batch variations (Figure 5.2C).

Volume Characterisation. Initially, we investigated the effect of droplet volume on the acidification rate of the droplets and consequently the fluorescent intensity emitted by the pHrodo dye. The concept relies on entrapping an individual cell inside a tiny droplet, where the excessive lactate production of the cancer cell results in acidification of the droplet that can be detected and quantified via pHrodo dye. Hence, the volume of each droplet plays a key role on the threshold of detection. To discover the optimum volume of liquid, as shown in Figure 5.3A, we tested 5nL, 1.25nL, 750pL and 125pL SDM devices. For the 5nL device, the mean fluorescent intensity of empty and single occupancy droplets was 1.497 ± 0.5860 and 1.686 ± 0.5598 , respectively. Similarly, the mean fluorescent intensity of the empty and single occupancy droplets in the 1.25nL device was 1.447 ± 0.2919 and 1.622 ± 0.4284 , respectively. Additionally, the mean fluorescent intensity of empty and single occupancy droplets in the 0.75nL device was 1.532 ± 0.2184 and 2.329 ± 0.2389 , respectively. Lastly, the 0.125nL device indicated a mean fluorescent intensity of 1.458 ± 0.211 for the empty droplets and 2.828 ± 0.7714 for the droplets with single cell occupancy.

The results obtained from 5nL and 1.25nL devices indicated no clear distinction among empty and single occupancy droplets which is clearly observed in the box and whisker charts shown in Figure 5.3A. In contrast to the larger devices, sub-picolitre devices indicated a clear difference between the fluorescent intensity of empty and single cell occupancy droplets. The results matched with the hypothesis that smaller droplet volumes result in a lower limit-of-detection due to faster acidification rate and higher effective concentration of the pHrodo dye. Therefore, the 125pL device was chosen as the optimum droplet volume throughout this manuscript.

Time Characterisation. The incubation time of cells plays a key role in defining the threshold of detection. In order to understand the effect of time, we injected and incubated DU-145 cells at 37°C over 15-, 30-, 45- and 60-minute periods inside the 0.125pL device, and the

results of the mean fluorescent intensity of the single cell occupancy droplets were 2.239 ± 0.2791 , 3.469 ± 1.558 , 4.749 ± 1.673 and 5.644 ± 0.3293 , respectively.

As expected, with a longer incubation time, a greater difference between the empty and single-cell occupancy droplets was observed. Based on the results shown in Figure 5.3B, along with experimental observations, 15-minute incubation of the droplets is sufficient to effectively detect droplets containing cancer cells, and 30-minute incubation is most ideal for applications that involve quantification and/or comparison of metabolic activity of cells. Shorter incubation than 15 minutes often leads to a high signal-to-noise ratio and complicates the detection process. On the other hand, longer incubation than 30 minutes results in over-saturation of the signals which does not allow for an appropriate quantification of the results.

Cell Trapping Efficiency. Lastly, the cell trapping efficiency was optimised to achieve the maximum single-cell trapping rate. The lower cell concentration at injection resulted in a higher single-cell isolation rate and consequently a higher number of empty droplets. For this work, 5 concentrations of 2,000, 4000, 6000, 8000 and 10,000 cells per μL of liquid was tested, achieving a single-cell isolation rate of $86.8\% \pm 7.86\%$, $75.4\% \pm 7.71\%$, $64.8\% \pm 4.26\%$, $47\% \pm 8.49\%$ and $45.6\% \pm 7.42\%$, respectively. The single-cell isolation rates were calculated based on the number of cells encapsulated individually over the total number of injected cells. The cell occupancy of droplets follows a Poisson distribution, thus lower cell concentration leads to the highest single-cell isolation rate [5]. Our results indicate the highest single-cell isolation rate at the concentration of 2000 cells per μL .

5.4.3 Classification of Cancer Cell Metabolic Activity at Single-Cell Resolution

After understanding and characterising the SDM device and experimental parameters, we analysed and compared the metabolism of 3 different human cancer cell lines, including the prostate cancer cell line, DU-145, and breast cancer cell lines, MCF-7 and MDA-MB-231. Then the values were compared with healthy human white blood cells. The mean fluorescent intensity of empty, singlet, doublet and triplet+ occupancy of DU-145 cells were recorded as 1.463 ± 0.2168 , 2.493 ± 0.7957 , 3.301 ± 0.4206 and 5.739 ± 1.377 , respectively. Similarly, for the MCF-7 cells, a mean fluorescent intensity of 1.312 ± 0.1392 , 1.843 ± 0.2437 , 2.274 ± 0.3831 , 2.726 ± 0.557 were obtained for the empty, singlet, doublet and triplet+ cell occupancy droplets, respectively. Furthermore, MDA-MB-231 cells expressed a mean fluorescent intensity of 1.224 ± 0.1218 , 1.822 ± 0.3225 , 2.345 ± 0.3643 and 3.077 ± 0.8225 for

the empty, singlet, doublet and triplet+ cell occupancy droplets, respectively. Lastly, in order to compare the cancer cell line metabolic activity, white blood cells of healthy donors were encapsulated in the droplets. The results indicated no major differences across the metabolic activity of droplets containing one or more white blood cells, compared to empty droplets.

The metabolomic screening of different cancer cell types in comparison with white blood cells indicated a clear correlation between cell occupancy and fluorescent intensity of the droplets (Figure 5.3C). While the normalised fluorescent intensity of the empty droplets across all experiments remained within a similar range of 1.224 to 1.447, the fluorescent intensity of droplets containing cancer cells was above a minimum mean value of 1.843. Within each cancer cell type, the higher cell occupancy corresponded with a higher fluorescent intensity of the droplets which further validates our hypothesis of the excessive glucose uptake and lactate production of cancer cells that results in acidification of their droplet environment. Interestingly, owing to the benefits of miniaturisation down to picolitres, the proposed SDM device is capable of precisely distinguishing between the metabolic activity of different cancer cell types. Based on the results shown in Figure 5.3C, DU-145 had the highest lactate secretion rate followed by MDA-MB-231 and MCF-7. Interestingly, these results is consistent with the lactate production measured by Lee et al., who also emphasised the importance of understanding the metabolic switch from aerobic mitochondrial oxidative phosphorylation to glycolysis of cancer cells which not only facilitates their survival and growth but also acquired invasiveness and resistance to chemotherapy induced apoptosis [174]. Additionally, the DU-145 cells showed the greatest level of heterogeneity in terms of lactate production. In contrast to the cancer cells, white blood cells did not indicate any signs of droplet acidification within the experimental timeframe, regardless of the droplet cell occupancy. The ability to distinguish between droplets containing cancer cells versus white blood cells provides a unique opportunity to detect and characterise the metabolic activity of circulating tumour cells in peripheral blood, as one of the key applications of our device.

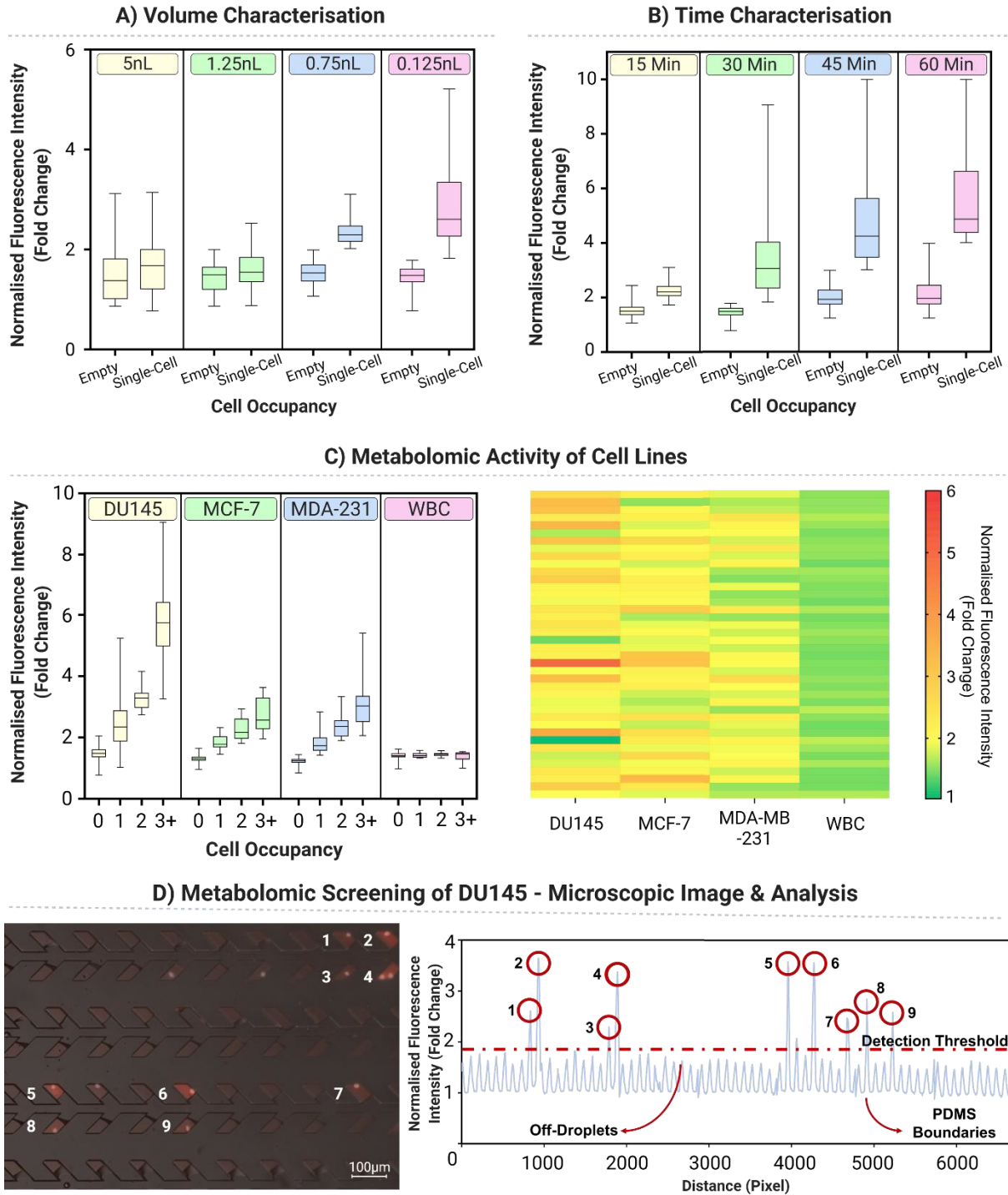


Figure 5.6 – Static Droplet Microfluidics (SDM) device characterisation for trapping and monitoring metabolic activity of cells. A) Characterisation of metabolic activity using SDM device and pH sensitive dye based on different droplet volumes (ranging from 5nL to 125pL) and occupancy. B) Characterisation of metabolic activity using SDM device and pH sensitive dye based on different incubation periods (ranging from 15 to 60 minutes) and occupancy. C) Characterisation of metabolic activity using SDM device and pH sensitive dye based on different cell types and occupancy. D) An actual microscopic image (mCherry and bright field channels overlaid) of DU145 cell line inside the

SDM device and corresponding denoised & normalised intensity profile, indicating droplets with metabolically active cells.

5.4.4 Metabolic Classification of ER+ Breast Cancer Cells

Oestrogens and oestrogen receptor alpha (ER α) play a key role in development and progression of more than three-quarters of breast cancers [175]. Anti-oestrogen therapy is the mainstream treatment for ER+ breast cancer, however, a large proportion of patients eventually develop resistance to this treatment [176]. Thus, the ability to precisely monitor metabolic activity of breast cancer cells might have clinical implications such as monitoring patient's treatment efficacy. To explore the potential application of the SDM device for metabolomic screening of breast cancer cells, we investigated the effect of oestrogen deprivation of MCF-7 cell line on the secretion rate of lactate at single-cell resolution. MCF-7 cells were oestrogen deprived for a week in phenol-red free medium with charcoal-stripped foetal bovine serum. The metabolic activity of the oestrogen deprived cells were screened at single-cell resolution and compared it to a control group of MCF-7 cultured simultaneously in complete medium. As shown in Figure 5.4A and 5.4B, oestrogen deprived MCF-7 group had a minor metabolic activity with a mean fluorescent intensity of 1.823 ± 0.2973 and 2.136 ± 0.3175 for the empty and single-cell occupancy droplets. It is noteworthy that a mean cell viability of $78\% \pm 2.97\%$ was observed among the oestrogen deprived MCF-7 groups. Besides, the metabolomic activity of the normal MCF-7 group was recorded as 1.407 ± 0.2066 and 2.983 ± 1.406 for the empty and single-cell occupancy droplets.

Using our SDM device we were able to classify the metabolic activity of the ER+ MCF7 cell line in response to oestrogen. Based on the obtained results, the ability to precisely monitor and measure the metabolic activity of cancer cells, would potentially allow for clinical utilisation of the proposed SDM device as a scalable technique to assess the effect of anticancer therapies that result in differential metabolic activity across different cancer types.

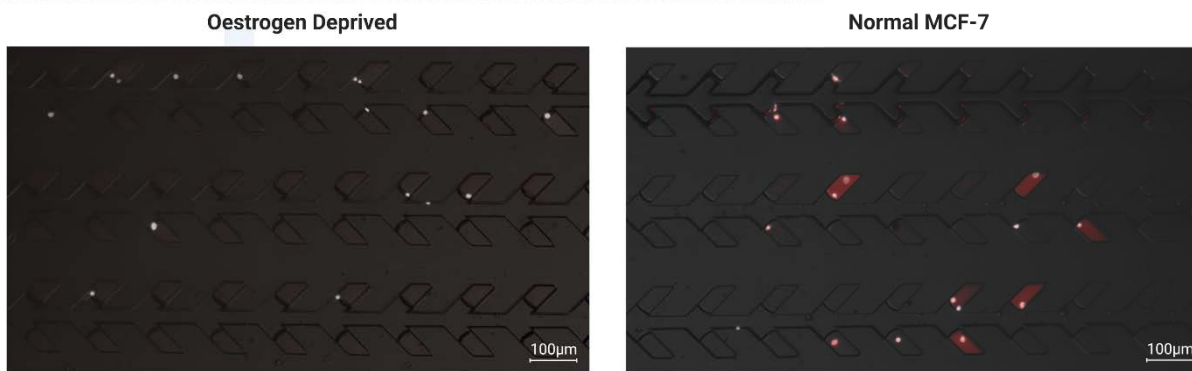
5.4.5 Metabolic Classification of CTCs in Blood Samples

In order to assess the applicability of our SDM device for the detection of CTCs from peripheral blood, we developed a high-throughput SDM device containing 38,400 droplets with 125pL volume each. Based on our previous studies on CTC enrichment using inertial microfluidics, typically a range of 1-10 CTCs are found among 1,000-2,000 leukocytes in 1mL of a cancer patient's blood [146]. To mimic this scenario, we spiked a different number of Hoechst-

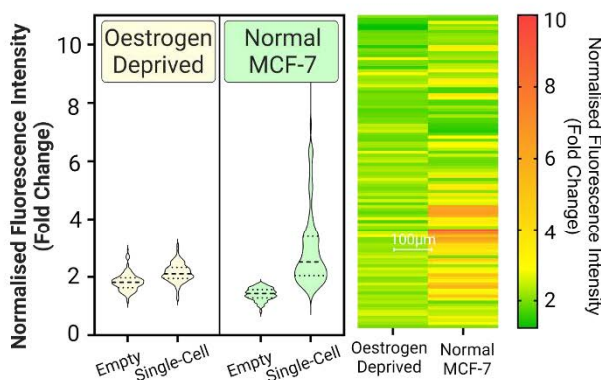
stained DU-145 cancer cells in 5mL of healthy human blood. Blood erythrocytes were removed via osmotic cell lysis and the sample was enriched based on size for CTCs using a spiral microfluidic device [146]. The CTC-enriched fraction was then centrifuged, resuspended in 5 μ L of pHrodo dye solution and subsequently injected into our pre-vacuumed high-throughput SDM device and incubated for 15 minutes. Finally, fluorescent imaging of the chip and image analysis was used to detect and classify the number of metabolically active cells. We spiked 50, 100, 500 and 1000 cancer cells in 5mL of healthy blood and detected a mean value of 25.20 ± 27.33 , 73.40 ± 25.98 , 375 ± 195.8 and 821 ± 429.1 metabolically active cells respectively. Each group was repeated 5 times to reduce the human error involved in the process.

As shown in Figure 5.4C, there is a linear correlation between the number of spiked cells versus the number of detected cells. It is noteworthy that the number of spiked cells was estimated by manually counting the cell concentration of a harvested DU-145 cell batch serially diluted. Thus, a level of uncertainty in the number of spiked cells exists which might have potentially contributed to a lower number of detected cancer cells versus the spiked in values. Interestingly, we observed that co-trapping leukocytes with cancer cells do not affect the detection process, as far as the droplets are not over-concentrated with cells (i.e., more than 15 cells per droplet). Hence, given the rarity of cancer cells, our 38,400 pocket SDM device is capable of processing up to 192,000 cells in 5 μ L of liquid per device (Figure 5.4D). Given the small footprint and large capacity of our high-throughput SDM device, less efficient CTC enrichment approaches (e.g., leukocyte depletion-based techniques) can also be used. Our SDM device not only overcomes the limitations associated with CTC isolation using current commercial single-cell analysis platforms (ref, such as?) but also provides an alternative approach for the detection of metabolically active cancer cells in peripheral blood. Additionally, the proposed SDM device eliminates the need for skilled operators, specialised laboratories and expensive reagents/equipment to fractionate liquid and monitor the metabolic activity of individual cells. Instead, the entire operation can be conducted by general laboratory equipment and non-experienced technicians. Thus, we believe this is a crucial step towards clinical utility of static droplet microfluidic devices for monitoring metabolomic activity of single cells.

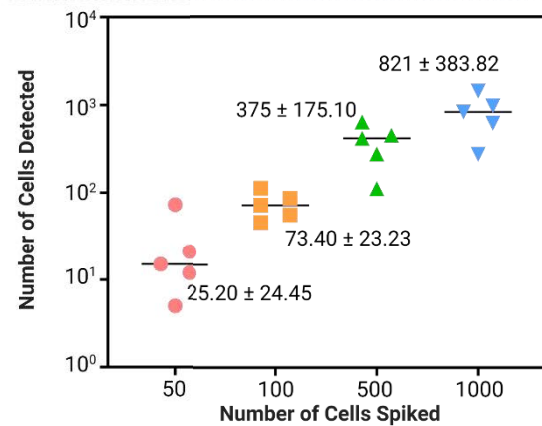
A) Oestrogen Deprivation of MCF-7 Cells



B) Oestrogen Deprivation Quantitative Analysis



C) Cancer Cell Spiking in Human Blood



D) Metabolomic Screening of DU145 Spiked in Human Blood

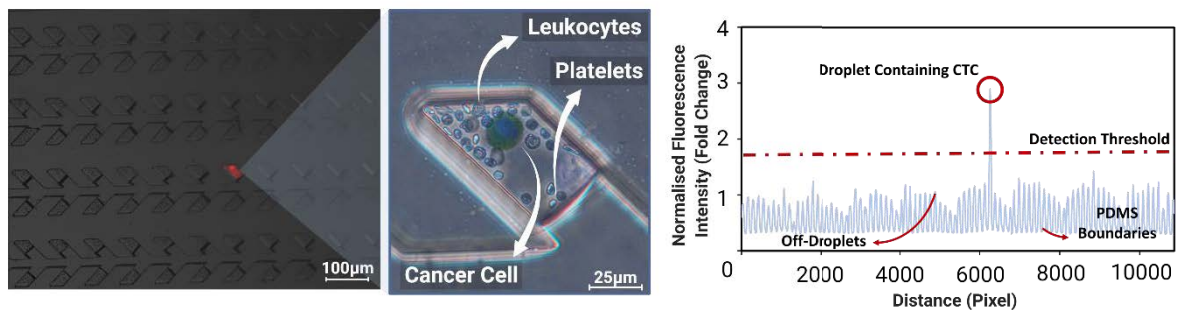


Figure 5.7 – Static Droplet Microfluidics (SDM) device applications for screening cancer cells. A) Microscopic images of SDM device used to track metabolic activity of MCF-7 cancer cells under oestrogen deprivation and untreated conditions, B) Quantitative analysis of metabolic activity of oestrogen deprived and normal MCF-7 cells using the SDM device. C) Comparing number of cells spiked in healthy human blood versus numbers of active cells found using the SDM device. D) Microscopic images showing a real case scenario, where one metabolically active DU-145 cancer cell is co-trapped with peripheral blood cells. The close-up picture shows DAPI and brightfield channels overlaid of the active droplet that contains a single cancer cell stained with DAPI antibodies. The corresponding intensity graph indicating only one active droplet.

5.4.6 Pre-clinical Verification of the SDM Device utility for CTC Detection Based on Metabolic Activity

Lastly, to further validate the potential of using the proposed SDM device for identifying highly metabolically active cancer cells in peripheral blood, the workflow was tested on several mammary mouse models (Figure 5.5A). Firstly, experiments were conducted on syngeneic 67NR and 4T1.2 models with Triple-Negative Breast Cancer (TNBC) cell lines orthotopically injected in Balb/c hosts. The 67NR is a non-metastatic TNBC model and thus was used as a negative control as no circulating cancer cells were expected to be found. Terminal bleeding from two 67NR tumour bearing female mice 4 weeks post-implantation was collected and processed as described in the materials and methods section. The image analysis of both samples indicated no metabolic active cells with a maximum normalised intensity of 2.1683, consistent with the results discussed in earlier sections. This value was used as the baseline and cut-off point for indicating active cancer cells. Similarly, entire blood from four 4T1.2 tumour bearing female mice was collected and analysed using a similar workflow. Interestingly, as show in Figure 5.5B, the number of metabolically active cancer cells found in each mouse was 1,584; 2,640; 8,448 and 6,400. Numbers were consistent with the high metastatic burden of the 4T1.2 model.

To further validate the potential of detecting circulating cancer cells in cancer patients, terminal bleeding samples from two 12-week-old MMTV-PyMT mouse mammary tumour models was collected and analysed. The MMTV-PyMT mouse model spontaneously develops mammary tumours closely resembling the human disease [177-180]. During the analysis, 677 and 592 metabolically active cells were found in the samples. Interestingly, the number of metabolically active CTCs identified with the SDM device correlated with the metastatic burden of each mouse model, as confirmed by the histological analysis of cross-sections of the lungs, underscoring the prognostic utility of this technique.

All together, these results confirmed the potential of using our workflow for detecting metabolically active circulating cancer cells in blood. In future, beside the quantification of metabolically active cells, correlating the level of metabolomic activity with the stage and type of cancer can provide an opportunity for clinical integration of the proposed workflow for non-invasive, rapid and low-cost diagnosis and prognosis of cancer patients.

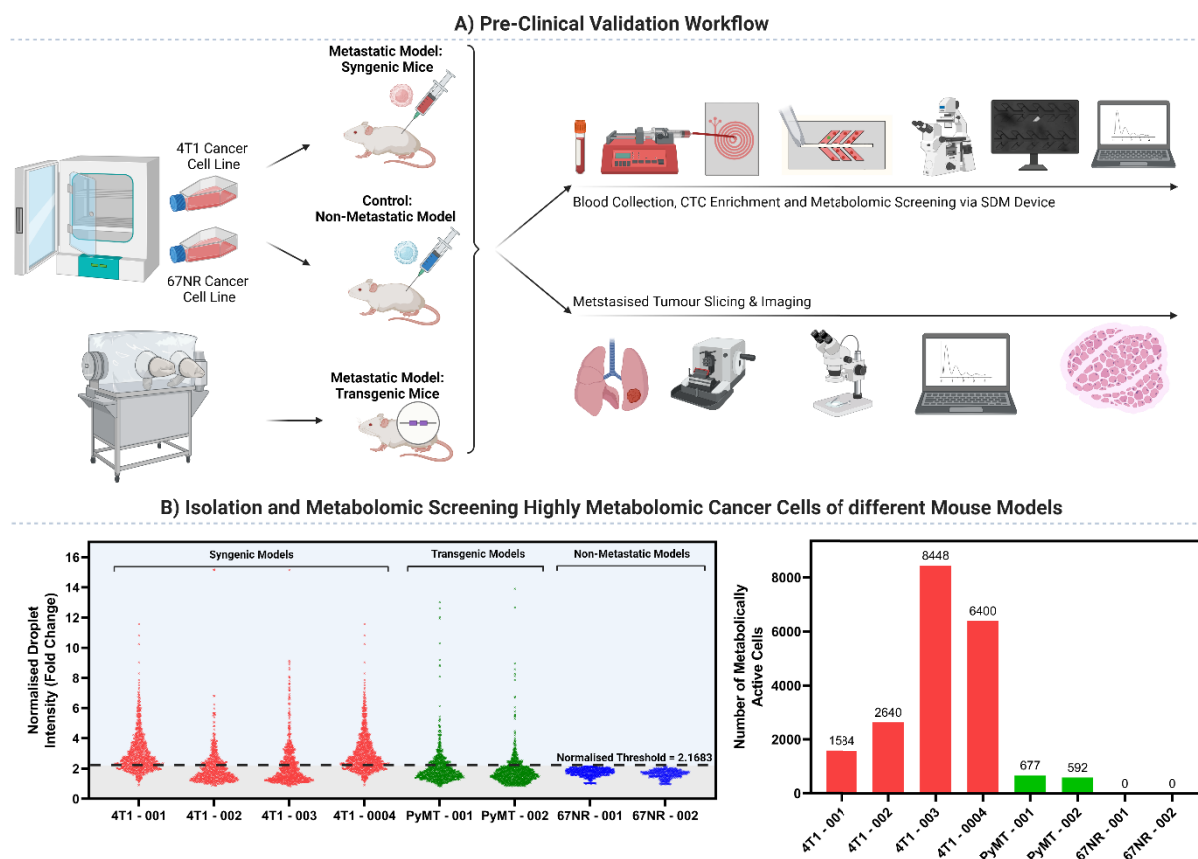


Figure 5.8 – Pre-clinical validation via detection of circulating cancer cells in the blood of mouse models. A) The workflow used for handling and processing mouse models of 67NR (non-metastatic syngeneic model), 4T1.2 (metastatic syngeneic model) and MMTV-PyMT (transgenic model). B) Metabolomic screening of CTC-enriched samples from 8 different mice.

5.5 Conclusion

In conclusion, we developed a simple, versatile and precise Static Droplet Microfluidic (SDM) platform for metabolomic studies. Our SDM device is useful to monitor the metabolic activity and classify cancer cells at single-cell resolution, in a high-throughput manner and without the need of expensive equipment. We demonstrated the ability to accurately distinguish between cancer and peripheral blood cells via monitoring their lactate production, allowing this tool to be an ideal candidate for detection and monitoring of Circulating Tumour Cells (CTCs) in the blood of cancer patients. Furthermore, we also evaluated the potential of using this technique for in-vitro assessment and tracking of cellular activities under different conditions – relevant for breast cancer therapy. Overall, we envision that our proposed SDM device will be valuable for diagnosis and prognosis of cancer patients and enable clinics to

undertake in-depth single cell metabolomic analysis. It is noteworthy that the integration of machine learning or automated image analysis tools can automate the screening process and reduce potential human errors. Additionally, the entire workflow could be enhanced by integrating an all-in-one device, where CTC enrichment, trapping and metabolomic screening take place inside a single system which can significantly reduce labour intensiveness and operator errors. While the proposed device is simple-to-operate and allows for high-throughput screening of metabolically active cells with great clinical potential, further studies on a large cohort of patients with different cancer types is required to completely understand the relationship between the number of metabolically active cells and overall survival of patients, treatment outcomes and disease progression. Additionally, further integration of other biological assays can improve the clinical significance of this method. For example, the incorporation of an on-chip single-cell proteomic study to analyse secretion products and/or on-chip detection of mutations (on-chip PCR) would allow multi-dimensional assessment of sample and provide a better understanding of patient's disease conditions.

Chapter 6 – The Correlation of Epithelial-Mesenchymal Transition and Lactate Metabolism in Human Breast Cancer

Summary

This chapter explores the relationship between lactate secretion and epithelial-mesenchymal transition (EMT) state of cancer cells. While EMT state of cancer cells is one of the major steps in the metastasis of cancer, often cannot be used as a diagnostic approach due to its complexity for measurement. Herein, the potential of correlating lactate production of cancer cells in breast cancer patients with their EMT state was explored as a potential biomarker for clinical integration of this technique. This chapter was greatly impacted by COVID-19 restrictions and thus we were not able to complete all the experiments and there will ongoing work to finalise and publish this chapter. This chapter is aimed for submission to the journal of PNAS as a communication journal*.

*Radfar P, Ding L, Aboulkheyr H, Warkiani ME. Rapid Fabrication of Static Droplet Microfluidic Devices.

6.1 Introduction

Breast cancer is the most prevalent diagnosed cancer types in women globally with over 2.3 million new cases and 685,000 deaths [181]. Breast cancer has replaced lung cancer as the most commonly diagnosed cancer type globally and its burden has been increasing in the past years [21]. Breast cancers are categorised into major subtypes based on their immunohistochemistry expression of classic hormones and growth factors such as oestrogen receptor (ER), progesterone receptor (PR) and human epidermal growth factor receptor 2 (HER2). Among the subtypes, Triple-negative breast cancer (TNBC) lacks expression of the ER, PR and HER2, while being significantly associated with high metastatic potential and poor diagnosis/prognosis [182]. TNBC is accountable for the most breast cancer-related deaths and given the difficulty in diagnosis and treatment of them, further research is critical to reduce the burden of this disease [183]. Among the hallmarks of cancer, metastasis is known to be the responsible for most cancer-related deaths [184]. Metastasis is the mechanism in which cancer spread to a part of body that is different to the primary tumour. During metastasis, cancer cells disseminate from the original tumour and enter the vascular system [123]. The cancer cells in the circulations are often known as circulating tumour cells (CTCs) which travel to a distant site and colonise a secondary organ and form a tumour. CTCs can travel in singular or cluster format and the number of CTCs in the blood of patients is known to be directly correlated with the stage of the cancer [185].

An important aspect of cancer metastasis is the Epithelial-Mesenchymal Transition (EMT) of cancer cells which is defined as the process of dedifferentiation of epithelial cells to mesenchymal cells [186]. Epithelial cells have strong cell-cell and cell-basal adherence, and basement membrane separates the epithelial lining from the stroma and connective tissues. On the other hand, mesenchymal cells lack cell-cell adhesion and have a fibroblast-like morphology [187]. For cancer cells to spread, the EMT can be activated in the epithelial cancer cells and cause them to downregulate adhesion junctions, acquire invasive properties and develop metastatic growth characteristics [188].

Furthermore, cancer cells are known to be metabolically more active than normal human cells. In 1920s, Otto Warburg was first to discover the increased lactate production of cancer cells as a result of increased glycolysis which results in the acidification of the tumour microenvironment [189]. However, lactate is not only a waste product of glycolysis and

recently studies have found that lactate can be a major energy fuel for oxidative tumour cells and act as nutrient source [190]. Additionally, lactate molecules play a crucial role as a signalling agent in cancer progression and metastasis by promoting migration, immune escape and angiogenesis [191-193].

Although there is a growing interest in studying lactate metabolism of cancer cells, the concept of lactate metabolism in metastatic transformation and particularly EMT remains unexplored [188]. In this work, we performed an In Silico study on breast cancer cell lines and patient genomic data to understand the correlation between lactate metabolism and epithelial/mesenchymal state of the cells. Furthermore, an in-depth single cell metabolic study was performed on EMT induced MCF-7 cells and showed a correlation between EMT and lactate production. Lastly, we elaborated on the potential to use lactate as a biomarker for assessing cells to indicate their metastatic potential, EMT status and invasion ability.

6.2 Results and Discussion

6.2.1 In Silico Studies

In order to perform a preliminary study and understand the relationship between breast cancer cell line, an In Silico study was conducted on 7 lactate related gene of SLC16A2, SLC16A3, SLC16A4, SLC16A7, SLC16A1, LDHB and LDHA across over 40 breast cancer cell lines (Figure 7.1A). Furthermore, the EMT score of each breast cancer cell line is compared to understand the epithelial or mesenchymal status of the cells. As illustrated in the chart, cell lines with high mesenchymal score also highly express lactate production related genes. In the next step, the 7 lactate related genes were analysed and given a Gene Set Enrichment Score (GSVA) across four subtypes of breast cancer. As shown in Figure 6.1B, the expression of the 7 related gene is directly related to the aggressiveness of the cancer – e.g., Basal type of cancer has the highest GSVA score. Furthermore, in Figure 6.1C, the hallmark of oestrogen response across early and late stages of the breast cancer compared with the hallmark of the EMT. Based on the analysed results and the enrichment scores, cells that have an oestrogen early and late response pathway also express a high level of lactate production related genes. In other words, from Figure 7.1A, B and C, are illustrating the lactate association with EMT, distribution across cancer cell types and lactate pathways are enriched with aggressive cancer types. Moreover, Figure 7.1D illustrates the GSVA score of the lactate associated genes is directly correlated with EMT pathway.

To further explore the correlations of lactate production related genes with breast cancer type, single cell genomic data were analysed in Figure 7.1E. The single cell analysis genomic data were evaluated against PAM50 genes, breast cancer subtypes, expression of LDHA and LDHB (leading lactate production related genes). The result indicates the subpopulation cells that are Basal (more aggressive based on Figure 6.1B), are also from a triple negative breast cancer nature with higher expression of LDHA and LDHB. Lastly, the correlation of mesenchymal state of breast cancer cells with expression of LDHA and LDHB was analysed and a positive correlation is shown in the Figure 6.2A and B.

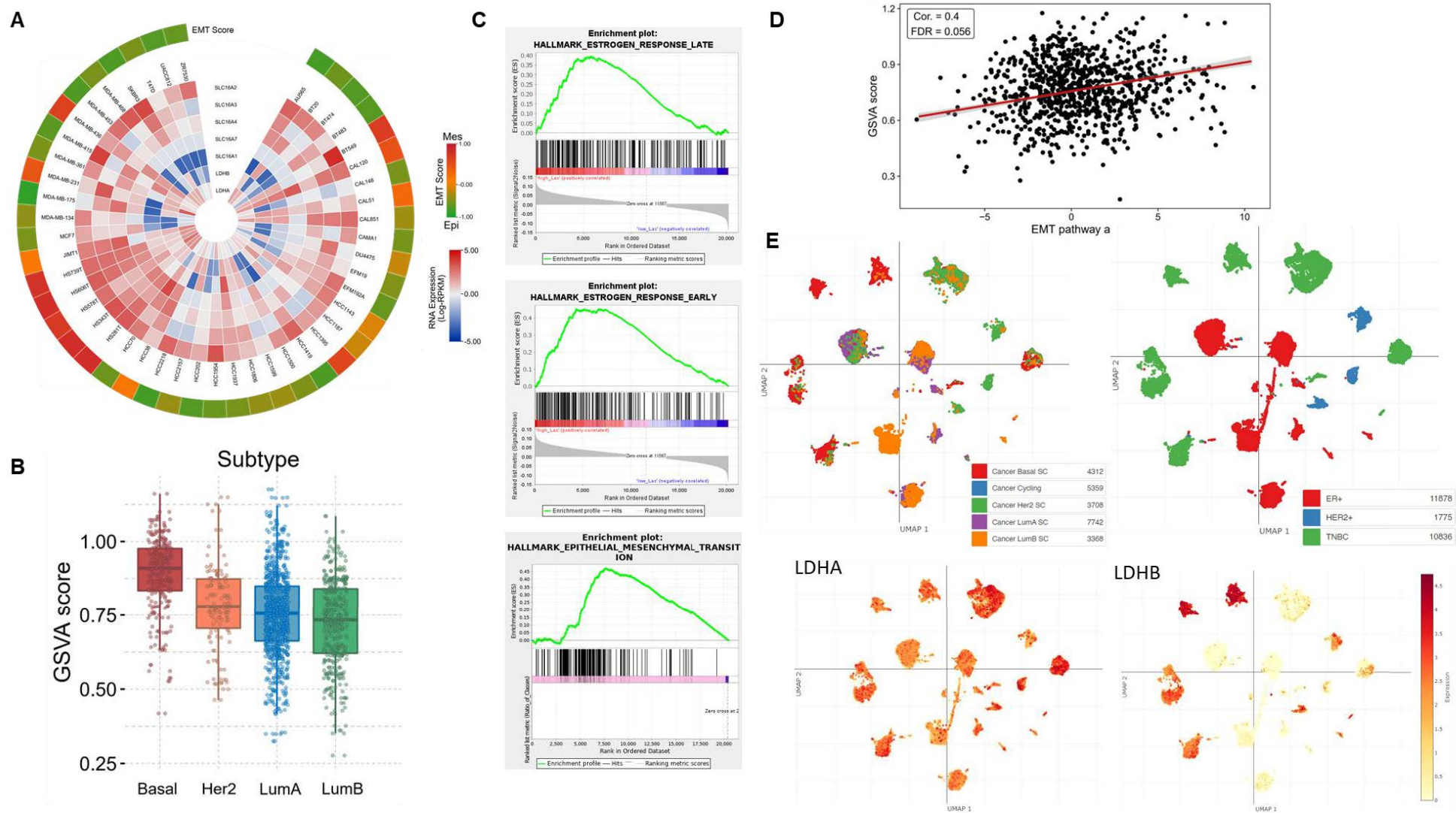


Figure 6.1 – In Silico Study of Breast Cancer Cell Lines and Patients. A) Comparison of 7 lactate related genes of SLC16A2, SLC16A3, SLC16A4, SLC16A7, SLC16A1, LDHB and LDHA across over 40 breast cancer cell lines along with their epithelial mesenchymal transition (EMT) score. B) Statistical analysis of the

7 lactate related genes and perform a Gene Set Enrichment Score (GSVA Score) across four subtypes of breast cancers. C) Hallmark of oestrogen response across early and late stages of breast cancer compared with the hallmark of epithelial-mesenchymal transition. D) GSVA score of the lactate associated genes with EMT pathway. E) Single cell genomic data analysed based on different classification of PAM50, cancer type, expression of LDHA and LDHB.

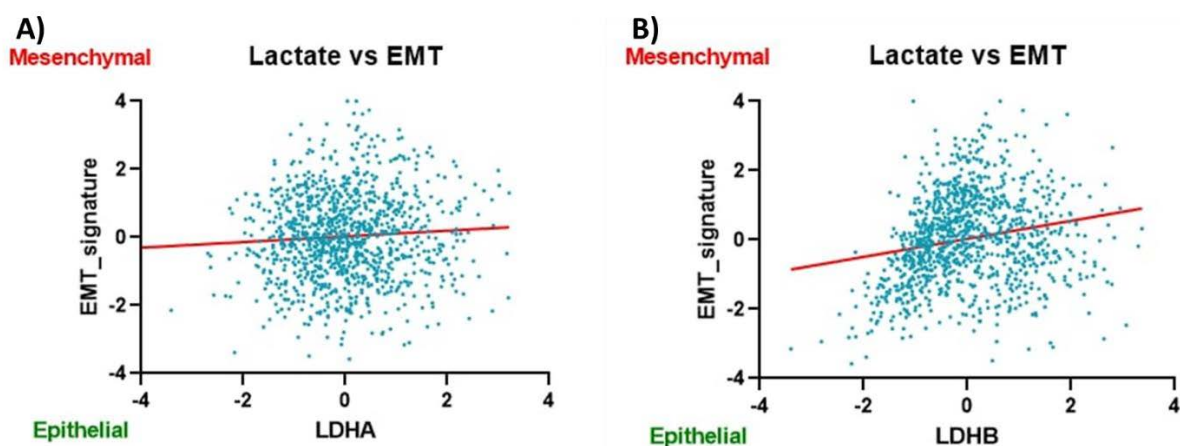


Figure 6.2 – Comparison of mesenchymal/epithelial state of cancer cells in respect to expression of A) LDHA and B) LDHB.

6.2.2 Lactate Metabolic Screening

To further explore and unravel the relation between lactate production and EMT state of the cells, an *in vitro* study was designed and conducted on MCF-7 cells. Based on the *in silico* studies (Figure 6.1A), MCF-7 cells express relatively low level of lactate related genes (particularly LDHA and LDHB) while having an epithelial state. Thus, the *in vitro* study aimed to induce the EMT on the MCF-7 cells to transition them into a mesenchymal state and compare their lactate production level. However, one major challenge in study of cell populations at bulk is the heterogeneity of cells and the inability to distinguish between subpopulation of cells, specially in terms of metabolism and cell activities [194]. To address this challenge and distinguish the highly metabolic active cancer cells at different EMT state, we used a static droplet microfluidic (SDM) device to monitor lactate production and acidification of 125pL droplets at single-cell resolution [185].

The concept relies on fractionating a cell sample into 125pL where the tiny lactate production of cells in the miniaturised droplets result in rapid acidification. Thus, by leveraging the rapid acidification of the droplets, a pH sensitive fluorescent dye enables an accurate analysis and quantification of lactate production of each cell. Figure 6.3A shows the working principle of the SDM device through 3 steps of injection, droplet formation and metabolomic screening. Figure 7.3B illustrates the microscopic image of the control and EMT induced MCF-7 groups and their lactate production under the microscope. There is a clear distinction in the droplet intensities of the epithelial and mesenchymal group. Furthermore, the EMT induction was

monitored over three days and compared with the control group. Interestingly, there is a clear correlation between the time of EMT induction versus their lactate production suggesting potential of using lactate production as a biomarker for understanding the state of a disease.

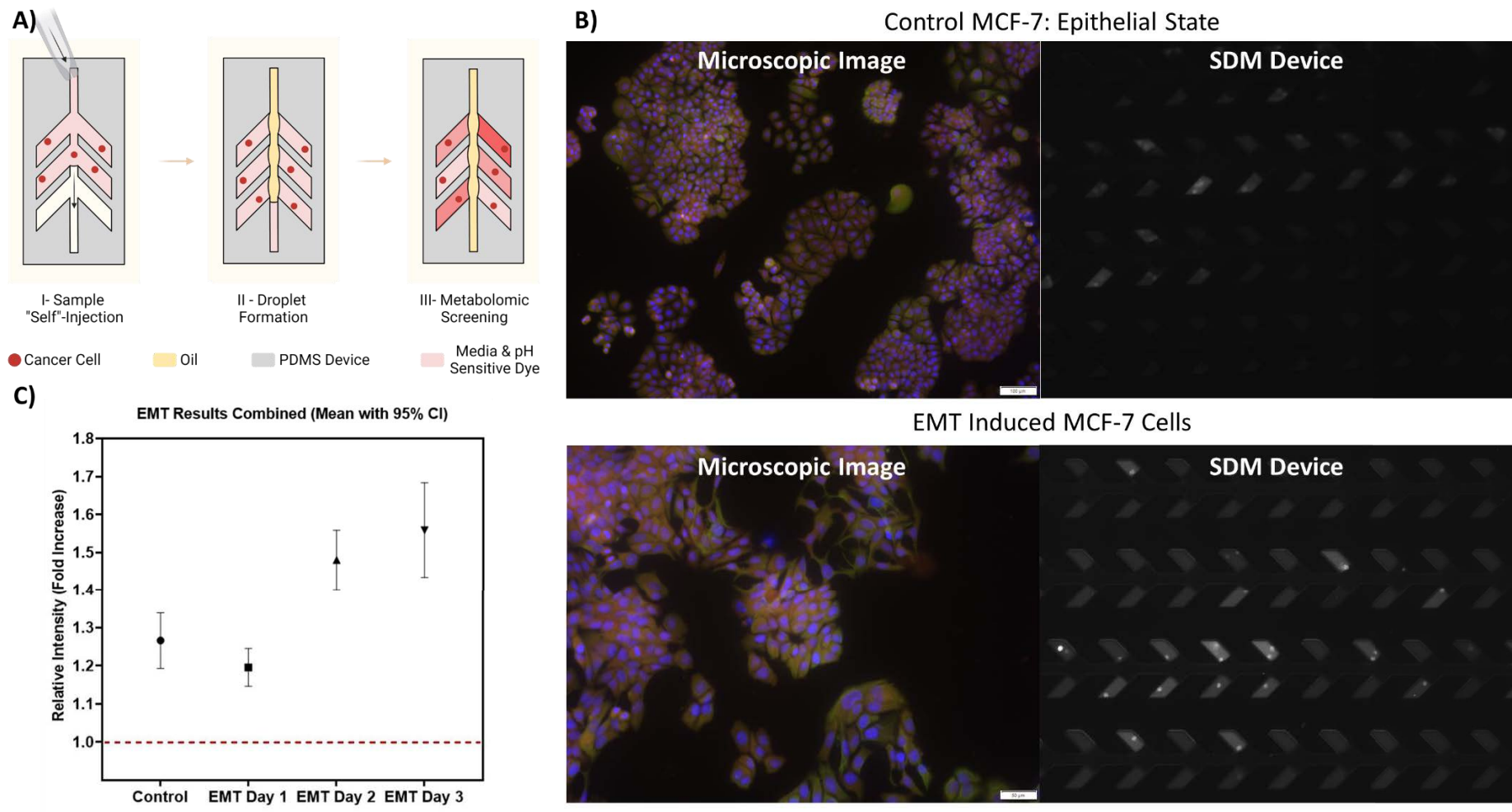


Figure 6.3 – Static Droplet Microfluidic Device for Analysis of EMT Induced MCF-7 Cells. A) Static Droplet Microfluidic (SDM) device working principle. B) Comparison of EMT induced MCF-7 and tracking their metabolic activity through the SDM device. C) Analysis of the effect of EMT induction kit over 3 days on lactate production and relative intensity of the droplets.

6.3 Conclusion and Future Works

In this paper, the correlation between EMT state of breast cancer cells and their lactate production were studied. Firstly, through an in-silico study, we analysed over 7 lactate related gene expressions across cell lines and breast cancer types and compared it with their EMT state. Furthermore, a static droplet microfluidic device was deployed to metabolically study MCF-7 cells at single-cell resolution as a non-metastatic and epithelial breast cancer cell line. The studies confirmed the correlation between EMT state and the level of lactate production.

Despite the interesting preliminary results obtained in this project, there is a need for considerable amount of experiment prior to drawing any conclusions. The future works include further in-depth study of different breast cancer types, different EMT inducing and inhibiting approaches, molecular and metabolic study of cells undergoing EMT. Furthermore, a study on large cohort of patients with different subtype of breast cancer, metastatic and non-metastatic profiles. By conducting the abovementioned studies, the lactate production could potentially be considered as a key biomarker for understanding the patient's disease state and even treatment outcomes.

Chapter 7 - Conclusion and Future Work

In this thesis, microfluidic tools were developed to characterise and analyse circulating tumour cells (CTCs) at single cell resolution with a focus for clinical implementation of them via reducing the need for specialised equipment or skilled operators. Firstly, methods for rapid prototyping and microfabrication of static droplet microfluidic devices were developed which was used to fabricate a device for single-cell molecular studies of CTCs using common laboratory equipment. Static droplet microfluidic device was to fractionate the blood sample post enrichment and isolate single cells inside 20nL droplets. By leveraging the temporary bonding of the device, rapid freezing of the sample and peeling off the device, the tiny droplets containing single cancer cells were recovered and transferred to for molecular studies using a handheld pipette. Furthermore, a detailed study on cancer cell metabolism was conducted to understand the potential of utilising lactate production level as a biomarker to distinguish cancer cells from the peripheral blood cells. Although measuring lactate of single CTCs at bulk is not possible, the miniaturisation effect of droplet microfluidics was utilised to precisely measure the lactate production of each cell using a pH sensitive fluorescent dye. It was successfully shown that CTCs produce significantly higher level of lactate resulting in rapid acidification of the 125pL droplet environment. The cancer cell activity was clearly shown to be distinguishable from peripheral blood cells and the workflow was further validated using spiked cells in healthy human blood as well as preclinical mammary mouse models. Moreover, further abilities to study oestrogen deprivation of MCF-7 cells were explored and shown the capability of the device on different use cases for diagnosis and prognosis of cancer patients. In line with the static droplet microfluidic device for analysis of thousands of droplets simultaneously, a MATLAB based program was developed to automate the droplet analysis process and more importantly eliminate room for human errors. Additionally, given the ability to precisely characterise the lactate production of cancer cells, an in-depth study was conducted to understand the correlation of lactate production and epithelial mesenchymal transition (EMT) state of cells. An In Silico study was conducted and shown the correlation of expression of 7 lactate production related genes with EMT score of various breast cancer cell lines and cancer subtypes. Lastly, a preliminary in vivo study was conducted on EMT induced MCF-7 cells and the lactate production was measured at single cell resolution using a high throughput static droplet

microfluidic device. The results are indicating a direct correlation between mesenchymal state of the cells with higher lactate production. This potentially could be further studied for implementation as a biomarker for understanding patient disease state.

In overall, multiple microfluidic devices/tools were developed to study single CTCs based on their phenotype, molecular and metabolic profile. While each device provides a range of benefits for potential clinical utilisation, further research must be carried out to validate and ensure the broad applications of the potential devices. First and foremost, samples from large cohort of patients across different cancer type must be tested with a clear overall aim/goal on targeting specific genes, studying metabolic activity of different cancer cell types and correlating those with cancer patients and their treatment outcomes. Furthermore, linking the patient disease state with number of CTCs, CTC EMT score, lactate production level and expression of specific genes based on the cancer type can provide crucial knowledge on potential clinical integration of the device. Moreover, the proposed devices offer a simple workflow in terms of operations. However, analysis of the droplets including the image taking process requires improvement prior to clinical utility of the devices. Thus, automation of the process such as integration of the image analysis program with the microscopes software to automatically image the chip and analyse the results in one step, would be critical for clinical integration of these devices. Lastly, most of the concept proposed in this thesis were introduced for the first time and further engineering optimisation would also be beneficial for improvement of the sample handling and minimise the sample loss. To provide a summary, Figure 7.1 provides an overview of potential future works that could be conducted as the next step for clinical integration of single-cell devices for assessing circulating tumour cells (CTCs) of cancer patients. Briefly, improvement of CTC isolation devices to isolate and characterise CTC cluster would be a vital step forward. Additionally, clinical integration of single-cell imaging and analysis techniques to accommodate for CTC cluster is one of the key steps to further expand the potential of assessing patient's disease state. These techniques can be combined with biological tools such as droplet digital PCR, single-cell RNA sequencing, digital spatial profiling (for CTC clusters) and in-depth bioinformatic analysis with potentials for leveraging artificial intelligence.

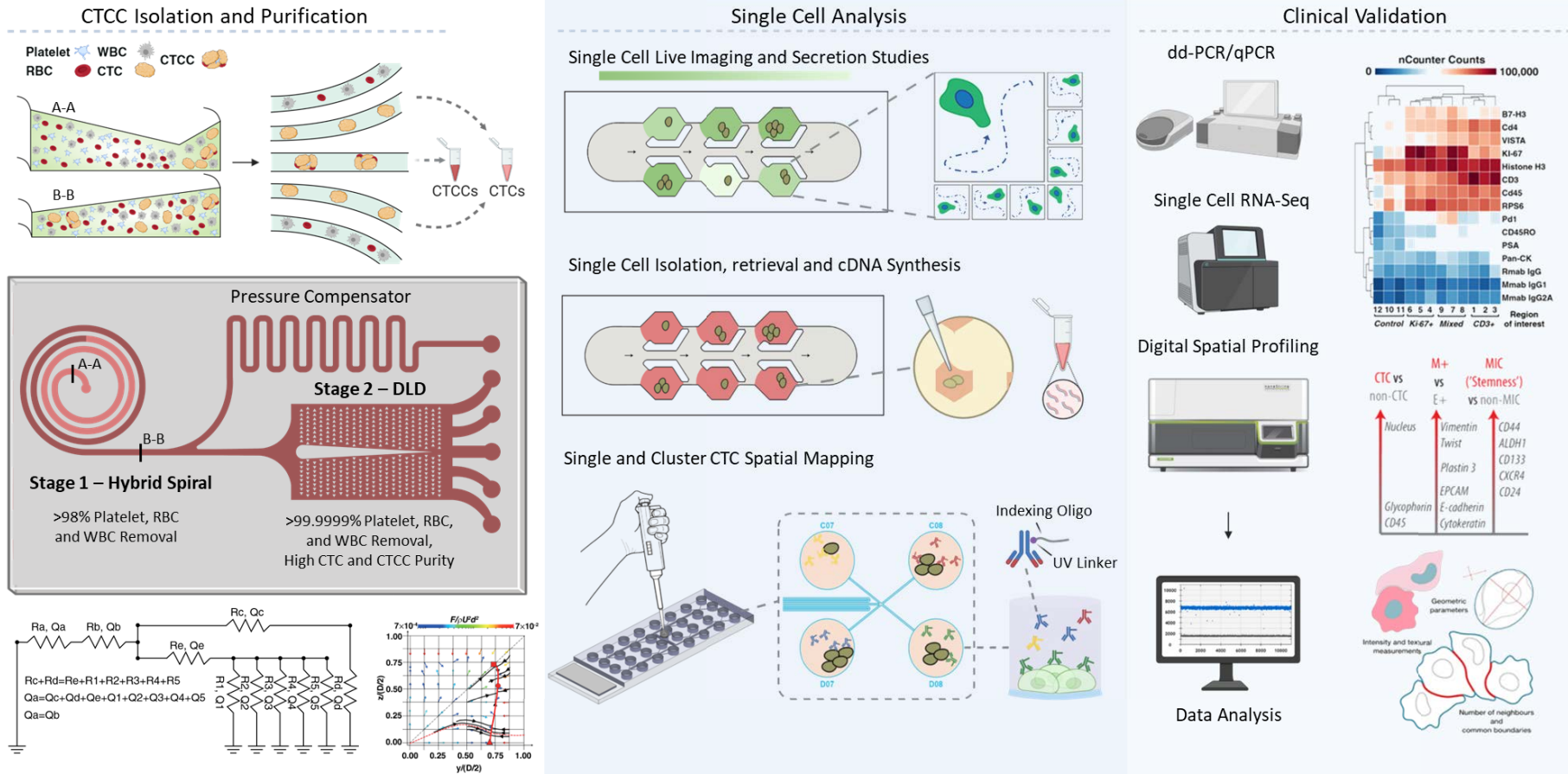


Figure 7.1 – Future pathway for analysis of circulating tumour clusters. There is a vital need for development of a novel label-free device for enrichment of CTC clusters, followed by single-cell analysis tools capable of imaging and characterising them. Additionally, the current biological analysing techniques such as droplet digital PCR, single cell RNA-sequencing and digital spatial profiling can be used to assess these CTC clusters to provide additional insight on patients’ state.

References

1. Toriello, N.M., et al., *Integrated microfluidic bioprocessor for single-cell gene expression analysis*. Proceedings of the National Academy of Sciences, 2008. **105**(51): p. 20173-20178.
2. Smietanka, U., et al., *Clusters, Assemblies and Aggregates of Tumor Cells in the Blood of Breast Cancer Patients; Composition, Mode of Action, Detection and Impact on Metastasis and Survival*. International Journal of Translational Medicine, 2021. **1**(1): p. 55-68.
3. Costa, C., et al., *Analysis of a Real-World Cohort of Metastatic Breast Cancer Patients Shows Circulating Tumor Cell Clusters (CTC-clusters) as Predictors of Patient Outcomes*. Cancers, 2020. **12**(5): p. 1111.
4. Rezaei, M., et al., *Simple-to-Operate Approach for Single Cell Analysis Using a Hydrophobic Surface and Nanosized Droplets*. Analytical Chemistry, 2021. **93**(10): p. 4584-4592.
5. Ding, L., et al., *An easy-to-operate method for single-cell isolation and retrieval using a microfluidic static droplet array*. Microchimica Acta, 2021. **188**(8): p. 242.
6. Gierahn, T.M., et al., *Seq-Well: portable, low-cost RNA sequencing of single cells at high throughput*. Nature Methods, 2017. **14**(4): p. 395-398.
7. Tang, X., et al., *The single-cell sequencing: new developments and medical applications*. Cell & Bioscience, 2019. **9**(1): p. 53.
8. Wiedmeier, J.E., et al., *Single-Cell Sequencing in Precision Medicine*. Cancer Treat Res, 2019. **178**: p. 237-252.
9. Wu, X., et al., *Research Techniques Made Simple: Single-Cell RNA Sequencing and its Applications in Dermatology*. The Journal of investigative dermatology, 2018. **138**(5): p. 1004-1009.
10. Au - Peterson, S.M. and J.L. Au - Freeman, *RNA Isolation from Embryonic Zebrafish and cDNA Synthesis for Gene Expression Analysis*. JoVE, 2009(30): p. e1470.
11. Tomlinson, M.J., et al., *Cell separation: Terminology and practical considerations*. Journal of Tissue Engineering, 2013. **4**: p. 2041731412472690.
12. Takaishi, S., et al., *Identification of Gastric Cancer Stem Cells Using the Cell Surface Marker CD44*. Stem Cells, 2009. **27**(5): p. 1006-1020.
13. Hu, P., et al., *Single Cell Isolation and Analysis*. Frontiers in Cell and Developmental Biology, 2016. **4**.
14. Terry, V.H., I.C.D. Johnston, and C.A. Spina, *CD44 MicroBeads accelerate HIV-1 infection in T cells*. Virology, 2009. **388**(2): p. 294-304.
15. Sabnis, A.J. and T.G. Bivona, *Principles of Resistance to Targeted Cancer Therapy: Lessons from Basic and Translational Cancer Biology*. Trends Mol Med, 2019. **25**(3): p. 185-197.
16. Schreier, S. and W. Triampo, *The Blood Circulating Rare Cell Population. What Is It and What Is It Good for?* Cells, 2020. **9**(4): p. 790.
17. Mishima, Y., et al., *The Mutational Landscape of Circulating Tumor Cells in Multiple Myeloma*. Cell Rep, 2017. **19**(1): p. 218-224.
18. Rezaei, M., et al., *A Reappraisal of Circulating Fetal Cell Noninvasive Prenatal Testing*. Trends in Biotechnology, 2019. **37**(6): p. 632-644.

19. Winter, M., et al., *Isolation of Circulating Fetal Trophoblasts Using Inertial Microfluidics for Noninvasive Prenatal Testing*. Advanced Materials Technologies, 2018. **3**(7): p. 1800066.
20. He, X., et al., *A meta-analysis of the prognostic value of circulating tumor cells in ovarian cancer*. American Journal of Translational Research, 2022. **14**(6): p. 3574.
21. Sung, H., et al., *Global Cancer Statistics 2020: GLOBOCAN Estimates of Incidence and Mortality Worldwide for 36 Cancers in 185 Countries*. CA: A Cancer Journal for Clinicians, 2021. **71**(3): p. 209-249.
22. Zugazagoitia, J., et al., *Current Challenges in Cancer Treatment*. Clinical Therapeutics, 2016. **38**(7): p. 1551-1566.
23. Ferlay, J., et al., *Cancer statistics for the year 2020: An overview*. International Journal of Cancer, 2021. **149**(4): p. 778-789.
24. Ngwa, W., et al., *Potential for information and communication technologies to catalyze global collaborations in radiation oncology*. International journal of radiation oncology, biology, physics, 2015. **91**(2): p. 444-447.
25. Ganesh, K. and J. Massagué, *Targeting metastatic cancer*. Nat Med, 2021. **27**(1): p. 34-44.
26. Gkoutela, S., et al., *Circulating Tumor Cell Clustering Shapes DNA Methylation to Enable Metastasis Seeding*. Cell, 2019. **176**(1): p. 98-112.e14.
27. Wang, W.-C., et al., *Survival Mechanisms and Influence Factors of Circulating Tumor Cells*. BioMed Research International, 2018. **2018**: p. 6304701.
28. Chambers, A.F., A.C. Groom, and I.C. MacDonald, *Dissemination and growth of cancer cells in metastatic sites*. Nat Rev Cancer, 2002. **2**(8): p. 563-72.
29. Maheswaran, S., et al., *Detection of mutations in EGFR in circulating lung-cancer cells*. N Engl J Med, 2008. **359**(4): p. 366-77.
30. Olmos, D., et al., *Circulating tumour cell (CTC) counts as intermediate end points in castration-resistant prostate cancer (CRPC): a single-centre experience*. Annals of Oncology, 2009. **20**(1): p. 27-33.
31. Radfar, P., et al., *Single-cell analysis of circulating tumour cells: enabling technologies and clinical applications*. Trends in Biotechnology, 2022.
32. Bathth, I.S., et al., *CTC analysis: an update on technological progress*. Translational Research, 2019. **212**: p. 14-25.
33. Allard, W.J., et al., *Tumor cells circulate in the peripheral blood of all major carcinomas but not in healthy subjects or patients with nonmalignant diseases*. Clin Cancer Res, 2004. **10**(20): p. 6897-904.
34. Del Ben, F., et al., *A Method for Detecting Circulating Tumor Cells Based on the Measurement of Single-Cell Metabolism in Droplet-Based Microfluidics*. Angew Chem Int Ed Engl, 2016. **55**(30): p. 8581-4.
35. Hou, H.W., et al., *Isolation and retrieval of circulating tumor cells using centrifugal forces*. Scientific Reports, 2013. **3**(1): p. 1259.
36. Hamza, B., et al., *Optofluidic real-time cell sorter for longitudinal CTC studies in mouse models of cancer*. Proceedings of the National Academy of Sciences, 2019. **116**(6): p. 2232-2236.
37. Lohr, J.G., et al., *Whole-exome sequencing of circulating tumor cells provides a window into metastatic prostate cancer*. Nature biotechnology, 2014. **32**(5): p. 479-484.
38. Fachin, F., et al., *Monolithic Chip for High-throughput Blood Cell Depletion to Sort Rare Circulating Tumor Cells*. Scientific Reports, 2017. **7**(1): p. 10936.

39. Ozkumur, E., et al., *Inertial Focusing for Tumor Antigen-Dependent and -Independent Sorting of Rare Circulating Tumor Cells*. *Science Translational Medicine*, 2013. **5**(179): p. 179ra47-179ra47.
40. Hanahan, D. and R.A. Weinberg, *Hallmarks of cancer: the next generation*. *Cell*, 2011. **144**(5): p. 646-74.
41. Meng, S., et al., *Circulating Tumor Cells in Patients with Breast Cancer Dormancy*. *Clinical Cancer Research*, 2004. **10**(24): p. 8152-8162.
42. Lim, S.B., C.T. Lim, and W.-T. Lim, *Single-Cell Analysis of Circulating Tumor Cells: Why Heterogeneity Matters*. *Cancers*, 2019. **11**(10): p. 1595.
43. Kallergi, G., et al., *Apoptotic circulating tumor cells in early and metastatic breast cancer patients*. *Mol Cancer Ther*, 2013. **12**(9): p. 1886-95.
44. Khoo, B.L., et al., *Single-cell profiling approaches to probing tumor heterogeneity*. *International Journal of Cancer*, 2016. **139**(2): p. 243-255.
45. Cortes-Hernandez, L.E., et al., *Molecular and Functional Characterization of Circulating Tumor Cells: From Discovery to Clinical Application*. *Clin Chem*, 2019.
46. Sun, G., et al., *Single-cell RNA sequencing in cancer: Applications, advances, and emerging challenges*. *Molecular Therapy - Oncolytics*, 2021. **21**: p. 183-206.
47. Keller, L. and K. Pantel, *Unravelling tumour heterogeneity by single-cell profiling of circulating tumour cells*. *Nature Reviews Cancer*, 2019. **19**(10): p. 553-567.
48. Yang, Y.-P., T.M. Giret, and R.J. Cote, *Circulating Tumor Cells from Enumeration to Analysis: Current Challenges and Future Opportunities*. *Cancers*, 2021. **13**(11): p. 2723.
49. Aktas, B., et al., *Stem cell and epithelial-mesenchymal transition markers are frequently overexpressed in circulating tumor cells of metastatic breast cancer patients*. *Breast Cancer Res*, 2009. **11**(4): p. R46.
50. Tan, T.Z., et al., *Epithelial-mesenchymal transition spectrum quantification and its efficacy in deciphering survival and drug responses of cancer patients*. *EMBO Molecular Medicine*, 2014. **6**(10): p. 1279-1293.
51. Gooding, A.J. and W.P. Schiemann, *Epithelial–Mesenchymal Transition Programs and Cancer Stem Cell Phenotypes: Mediators of Breast Cancer Therapy Resistance*. *Molecular Cancer Research*, 2020. **18**(9): p. 1257-1270.
52. Markiewicz, A., et al., *Spectrum of Epithelial-Mesenchymal Transition Phenotypes in Circulating Tumour Cells from Early Breast Cancer Patients*. *Cancers (Basel)*, 2019. **11**(1).
53. Aya-Bonilla, C.A., et al., *Isolation and detection of circulating tumour cells from metastatic melanoma patients using a slanted spiral microfluidic device*. *Oncotarget*, 2017. **8**(40).
54. Lohr, J.G., et al., *Whole-exome sequencing of circulating tumor cells provides a window into metastatic prostate cancer*. *Nat Biotechnol*, 2014. **32**(5): p. 479-84.
55. Hou, H.W., et al., *Isolation and retrieval of circulating tumor cells using centrifugal forces*. *Sci Rep*, 2013. **3**: p. 1259.
56. Warkiani, M.E., et al., *Slanted spiral microfluidics for the ultra-fast, label-free isolation of circulating tumor cells*. *Lab Chip*, 2014. **14**(1): p. 128-37.
57. Kulasinghe, A., et al., *Short term ex-vivo expansion of circulating head and neck tumour cells*. *Oncotarget*, 2016. **7**(37): p. 60101-60109.
58. Kulasinghe, A., L. Kenny, and C. Punyadeera, *Circulating tumour cell PD-L1 test for head and neck cancers*. *Oral Oncol*, 2017. **75**: p. 6-7.

59. Kulasinghe, A., M.E. Warkiani, and C. Punyadeera, *The Isolation and Characterization of Circulating Tumor Cells from Head and Neck Cancer Patient Blood Samples Using Spiral Microfluidic Technology*. *Methods Mol Biol*, 2019. **2054**: p. 129-136.
60. Alix-Panabières, C. and K. Pantel, *Challenges in circulating tumour cell research*. *Nature Reviews Cancer*, 2014. **14**(9): p. 623-631.
61. Diamantopoulou, Z., F. Castro-Giner, and N. Aceto, *Circulating tumor cells: Ready for translation?* *Journal of Experimental Medicine*, 2020. **217**(8).
62. Cappelletti, V., et al., *Analysis of Single Circulating Tumor Cells in Renal Cell Carcinoma Reveals Phenotypic Heterogeneity and Genomic Alterations Related to Progression*. *International Journal of Molecular Sciences*, 2020. **21**(4): p. 1475.
63. Rita, Z. and E. Rossi, *Single-cell analysis of Circulating Tumor Cells: How far we come with omics-era?* *Frontiers in genetics*, 2019. **10**: p. 958.
64. Lambros, M.B., et al., *Single-Cell Analyses of Prostate Cancer Liquid Biopsies Acquired by Apheresis*. *Clin Cancer Res*, 2018. **24**(22): p. 5635-5644.
65. Paoletti, C., et al., *Comprehensive Mutation and Copy Number Profiling in Archived Circulating Breast Cancer Tumor Cells Documents Heterogeneous Resistance Mechanisms*. *Cancer Res*, 2018. **78**(4): p. 1110-1122.
66. Werner, S., et al., *Suppression of early hematogenous dissemination of human breast cancer cells to bone marrow by retinoic Acid-induced 2*. *Cancer Discov*, 2015. **5**(5): p. 506-19.
67. Nong, J., et al., *Circulating tumor DNA analysis depicts subclonal architecture and genomic evolution of small cell lung cancer*. *Nat Commun*, 2018. **9**(1): p. 3114.
68. Powell, A.A., et al., *Single cell profiling of circulating tumor cells: transcriptional heterogeneity and diversity from breast cancer cell lines*. *PLoS One*, 2012. **7**(5): p. e33788.
69. Sun, Y.-F., et al., *Dissecting spatial heterogeneity and the immune-evasion mechanism of CTCs by single-cell RNA-seq in hepatocellular carcinoma*. *Nature Communications*, 2021. **12**(1): p. 4091.
70. Gross, A., et al., *Technologies for Single-Cell Isolation*. *International Journal of Molecular Sciences*, 2015. **16**(8): p. 16897-16919.
71. Gierahn, T.M., et al., *Seq-Well: portable, low-cost RNA sequencing of single cells at high throughput*. *Nat Methods*, 2017. **14**(4): p. 395-398.
72. Antonarakis, E.S., et al., *Clinical Significance of Androgen Receptor Splice Variant-7 mRNA Detection in Circulating Tumor Cells of Men With Metastatic Castration-Resistant Prostate Cancer Treated With First- and Second-Line Abiraterone and Enzalutamide*. *J Clin Oncol*, 2017. **35**(19): p. 2149-2156.
73. Xu, M., et al., *An Integrated Microfluidic Chip and Its Clinical Application for Circulating Tumor Cell Isolation and Single-Cell Analysis*. *Cytometry Part A*, 2020. **97**(1): p. 46-53.
74. Nelep, C. and J. Eberhardt, *Automated rare single cell picking with the ALS cellselector™*. *Cytometry. Part A : the journal of the International Society for Analytical Cytology*, 2018. **93**(12): p. 1267-1270.
75. Reinhardt, F., et al., *Diagnostic Leukapheresis Enables Reliable Transcriptomic Profiling of Single Circulating Tumor Cells to Characterize Inter-Cellular Heterogeneity in Terms of Endocrine Resistance*. *Cancers (Basel)*, 2019. **11**(7).
76. Espina, V., et al., *Laser capture microdissection technology*. *Expert Rev Mol Diagn*, 2007. **7**(5): p. 647-57.

77. Zhang, K., et al., *Hand-Held and Integrated Single-Cell Pipettes*. Journal of the American Chemical Society, 2014. **136**(31): p. 10858-10861.
78. Park, E.S., et al., *Isolation and genome sequencing of individual circulating tumor cells using hydrogel encapsulation and laser capture microdissection*. Lab on a Chip, 2018. **18**(12): p. 1736-1749.
79. Zhu, Y., et al., *Proteome Profiling of 1 to 5 Spiked Circulating Tumor Cells Isolated from Whole Blood Using Immunodensity Enrichment, Laser Capture Microdissection, Nanodroplet Sample Processing, and Ultrasensitive nanoLC–MS*. Analytical Chemistry, 2018. **90**(20): p. 11756-11759.
80. Valihrach, L., P. Androvic, and M. Kubista, *Platforms for single-cell collection and analysis*. International journal of molecular sciences, 2018. **19**(3): p. 807.
81. Au - Basu, S., et al., *Purification of Specific Cell Population by Fluorescence Activated Cell Sorting (FACS)*. JoVE, 2010(41): p. e1546.
82. Wang, Y., et al., *Single nucleotide variant profiles of viable single circulating tumour cells reveal CTC behaviours in breast cancer*. Oncol Rep, 2018. **39**(5): p. 2147-2159.
83. Nguyen, A., et al., *Single Cell RNA Sequencing of Rare Immune Cell Populations*. Frontiers in Immunology, 2018. **9**(1553).
84. Matuła, K., F. Rivello, and W.T.S. Huck, *Single-Cell Analysis Using Droplet Microfluidics*. Advanced Biosystems, 2020. **4**(1): p. 1900188.
85. Rakszewska, A., et al., *One drop at a time: toward droplet microfluidics as a versatile tool for single-cell analysis*. NPG Asia Materials, 2014. **6**(10): p. e133-e133.
86. Brechbuhl, H.M., et al., *Analysis of circulating breast cancer cell heterogeneity and interactions with peripheral blood mononuclear cells*. Molecular Carcinogenesis, 2020. **59**(10): p. 1129-1139.
87. D'Avola, D., et al., *High-density single cell mRNA sequencing to characterize circulating tumor cells in hepatocellular carcinoma*. Scientific Reports, 2018. **8**(1): p. 11570.
88. Teh, S.Y., et al., *Droplet microfluidics*. Lab Chip, 2008. **8**(2): p. 198-220.
89. Seemann, R., et al., *Droplet based microfluidics*. Rep Prog Phys, 2012. **75**(1): p. 016601.
90. Del Ben, F., et al., *A Method for Detecting Circulating Tumor Cells Based on the Measurement of Single-Cell Metabolism in Droplet-Based Microfluidics*. Angewandte Chemie International Edition, 2016. **55**(30): p. 8581-8584.
91. Zhou, Y., et al., *Evaluation of Single-Cell Cytokine Secretion and Cell-Cell Interactions with a Hierarchical Loading Microwell Chip*. Cell Reports, 2020. **31**(4): p. 107574.
92. Park, S.-m., et al., *Molecular profiling of single circulating tumor cells from lung cancer patients*. Proceedings of the National Academy of Sciences, 2016. **113**(52): p. E8379-E8386.
93. Tamminga, M., et al., *Analysis of Released Circulating Tumor Cells During Surgery for Non-Small Cell Lung Cancer*. Clinical Cancer Research, 2020. **26**(7): p. 1656-1666.
94. Iyer, A., et al., *Integrative Analysis and Machine Learning Based Characterization of Single Circulating Tumor Cells*. Journal of Clinical Medicine, 2020. **9**(4): p. 1206.
95. Di Trapani, M., N. Manaresi, and G. Medoro, *DEPArray™ system: An automatic image-based sorter for isolation of pure circulating tumor cells*. Cytometry Part A, 2018. **93**(12): p. 1260-1266.
96. Schochter, F., et al., *53BP1 Accumulation in Circulating Tumor Cells Identifies Chemotherapy-Responsive Metastatic Breast Cancer Patients*. Cancers, 2020. **12**(4): p. 930.

97. Boyer, M., et al., *Circulating Tumor Cell Detection and Polyomavirus Status in Merkel Cell Carcinoma*. Scientific Reports, 2020. **10**(1): p. 1612.
98. Tucci, M., et al., *Dual-procedural separation of CTCs in cutaneous melanoma provides useful information for both molecular diagnosis and prognosis*. Therapeutic Advances in Medical Oncology, 2020. **12**: p. 1758835920905415.
99. Aboulkheyr Es, H., et al., *Personalized Cancer Medicine: An Organoid Approach*. Trends Biotechnol, 2018. **36**(4): p. 358-371.
100. Paolillo, C., et al., *Detection of Activating Estrogen Receptor Gene (ESR1) Mutations in Single Circulating Tumor Cells*. Clin Cancer Res, 2017. **23**(20): p. 6086-6093.
101. Jordan, N.V., et al., *HER2 expression identifies dynamic functional states within circulating breast cancer cells*. Nature, 2016. **537**(7618): p. 102-106.
102. Dagogo-Jack, I. and A.T. Shaw, *Tumour heterogeneity and resistance to cancer therapies*. Nat Rev Clin Oncol, 2018. **15**(2): p. 81-94.
103. Marchetti, A., et al., *Assessment of EGFR mutations in circulating tumor cell preparations from NSCLC patients by next generation sequencing: toward a real-time liquid biopsy for treatment*. PLoS One, 2014. **9**(8): p. e103883.
104. Maheswaran, S., et al., *Detection of Mutations in EGFR in Circulating Lung-Cancer Cells*. New England Journal of Medicine, 2008. **359**(4): p. 366-377.
105. Pailler, E., et al., *High level of chromosomal instability in circulating tumor cells of ROS1-rearranged non-small-cell lung cancer*. Ann Oncol, 2015. **26**(7): p. 1408-15.
106. Pailler, E., et al., *Method for semi-automated microscopy of filtration-enriched circulating tumor cells*. BMC Cancer, 2016. **16**: p. 477.
107. Pailler, E., et al., *Circulating Tumor Cells with Aberrant ALK Copy Number Predict Progression-Free Survival during Crizotinib Treatment in ALK-Rearranged Non-Small Cell Lung Cancer Patients*. Cancer Res, 2017. **77**(9): p. 2222-2230.
108. Liu, Y., et al., *Meta-analysis of the mutational status of circulation tumor cells and paired primary tumor tissues from colorectal cancer patients*. Oncotarget, 2017. **8**(44): p. 77928-77941.
109. Schneck, H., et al., *Analysing the mutational status of PIK3CA in circulating tumor cells from metastatic breast cancer patients*. Mol Oncol, 2013. **7**(5): p. 976-86.
110. Gasch, C., et al., *Frequent detection of PIK3CA mutations in single circulating tumor cells of patients suffering from HER2-negative metastatic breast cancer*. Mol Oncol, 2016. **10**(8): p. 1330-43.
111. Pestrin, M., et al., *Heterogeneity of PIK3CA mutational status at the single cell level in circulating tumor cells from metastatic breast cancer patients*. Mol Oncol, 2015. **9**(4): p. 749-57.
112. Markou, A., et al., *Multiplex Gene Expression Profiling of In Vivo Isolated Circulating Tumor Cells in High-Risk Prostate Cancer Patients*. Clin Chem, 2018. **64**(2): p. 297-306.
113. Yu, M., et al., *Circulating breast tumor cells exhibit dynamic changes in epithelial and mesenchymal composition*. Science, 2013. **339**(6119): p. 580-4.
114. Carter, L., et al., *Molecular analysis of circulating tumor cells identifies distinct copy-number profiles in patients with chemosensitive and chemorefractory small-cell lung cancer*. Nat Med, 2017. **23**(1): p. 114-119.
115. Jolly, M.K., et al., *Phenotypic Plasticity, Bet-Hedging, and Androgen Independence in Prostate Cancer: Role of Non-Genetic Heterogeneity*. Front Oncol, 2018. **8**: p. 50.
116. Miyamoto, D.T., et al., *RNA-Seq of single prostate CTCs implicates noncanonical Wnt signaling in antiandrogen resistance*. Science, 2015. **349**(6254): p. 1351-6.

117. Tsao, S.C., et al., *Characterising the phenotypic evolution of circulating tumour cells during treatment*. Nat Commun, 2018. **9**(1): p. 1482.
118. Chen, P.Y., et al., *Adaptive and Reversible Resistance to Kras Inhibition in Pancreatic Cancer Cells*. Cancer Res, 2018. **78**(4): p. 985-1002.
119. Oser, M.G., et al., *Transformation from non-small-cell lung cancer to small-cell lung cancer: molecular drivers and cells of origin*. Lancet Oncol, 2015. **16**(4): p. e165-72.
120. Beltran, H., et al., *The Initial Detection and Partial Characterization of Circulating Tumor Cells in Neuroendocrine Prostate Cancer*. Clin Cancer Res, 2016. **22**(6): p. 1510-9.
121. Magbanua, M.J.M., et al., *Expanded Genomic Profiling of Circulating Tumor Cells in Metastatic Breast Cancer Patients to Assess Biomarker Status and Biology Over Time (CALGB 40502 and CALGB 40503, Alliance)*. Clin Cancer Res, 2018. **24**(6): p. 1486-1499.
122. Diamantopoulou, Z., F. Castro-Giner, and N. Aceto, *Circulating tumor cells: Ready for translation?* J Exp Med, 2020. **217**(8).
123. Radfar, P., et al., *Single-cell analysis of circulating tumour cells: enabling technologies and clinical applications*. Trends in Biotechnology, 2022. **40**(9): p. 1041-1060.
124. Kapeleris, J., et al., *The Prognostic Role of Circulating Tumor Cells (CTCs) in Lung Cancer*. Frontiers in Oncology, 2018. **8**.
125. Kulasinghe, A., et al., *Enrichment of circulating head and neck tumour cells using spiral microfluidic technology*. Scientific Reports, 2017. **7**(1): p. 42517.
126. Herath, S., et al., *Circulating tumor cell clusters: Insights into tumour dissemination and metastasis*. Expert Review of Molecular Diagnostics, 2020. **20**(11): p. 1139-1147.
127. Zhang, J., et al., *Fundamentals and applications of inertial microfluidics: a review*. Lab on a Chip, 2016. **16**(1): p. 10-34.
128. Radfar, P., et al., *Rapid metabolomic screening of cancer cells via high-throughput static droplet microfluidics*. Biosensors and Bioelectronics, 2022: p. 114966.
129. Radfar, P., et al., *The role of 3D printing in the fight against COVID-19 outbreak*. Journal of 3D Printing in Medicine, 2021. **5**(1): p. 51-60.
130. Hwang, B., J.H. Lee, and D. Bang, *Single-cell RNA sequencing technologies and bioinformatics pipelines*. Experimental & Molecular Medicine, 2018. **50**(8): p. 96.
131. Hu, P., et al., *Single Cell Isolation and Analysis*. Frontiers in Cell and Developmental Biology, 2016. **4**(116).
132. Nguyen, A., et al., *Single cell RNA sequencing of rare immune cell populations*. Frontiers in immunology, 2018. **9**: p. 1553.
133. Kim, H.S., T.P. Devarenne, and A. Han, *A high-throughput microfluidic single-cell screening platform capable of selective cell extraction*. Lab on a Chip, 2015. **15**(11): p. 2467-2475.
134. Li, Y., et al., *Injection Molded Microfluidics for Establishing High-Density Single Cell Arrays in an Open Hydrogel Format*. Analytical Chemistry, 2020. **92**(3): p. 2794-2801.
135. Zhang, P., et al., *Microfluidics-Based Single-Cell Protrusion Analysis for Screening Drugs Targeting Subcellular Mitochondrial Trafficking in Cancer Progression*. Analytical Chemistry, 2020. **92**(4): p. 3095-3102.
136. Stott, S.L., et al., *Isolation of circulating tumor cells using a microvortex-generating herringbone-chip*. Proceedings of the National Academy of Sciences, 2010. **107**(43): p. 18392-18397.
137. Lu, X., et al., *Parallel Label-Free Isolation of Cancer Cells Using Arrays of Acoustic Microstreaming Traps*. Advanced Materials Technologies, 2019. **4**(2): p. 1800374.

138. Shrestha, J., et al., *A rapidly prototyped lung-on-a-chip model using 3D-printed molds*. *Organs-on-a-Chip*, 2019. **1**: p. 100001.
139. Mohammadpour, J. and A. Lee, *Investigation of nanoparticle effects on jet impingement heat transfer: A review*. *Journal of Molecular Liquids*, 2020. **316**: p. 113819.
140. Mohammadpour, J., et al., *Effect of intermittent and sinusoidal pulsed flows on impingement heat transfer from a concave surface*. *International Journal of Thermal Sciences*, 2014. **76**: p. 118-127.
141. Akiyama, Y., et al., *Cryoprotectant-free cryopreservation of mammalian cells by superflash freezing*. *Proceedings of the National Academy of Sciences*, 2019. **116**(16): p. 7738-7743.
142. White, F.M., *Fluid Mechanics*. 2011: McGraw Hill.
143. Hassanzadeh-Barforoushi, A., et al., *Static droplet array for culturing single live adherent cells in an isolated chemical microenvironment*. *Lab on a Chip*, 2018. **18**(15): p. 2156-2166.
144. Karimi, A., S. Yazdi, and A.M. Ardekani, *Hydrodynamic mechanisms of cell and particle trapping in microfluidics*. *Biomicrofluidics*, 2013. **7**(2): p. 21501.
145. Warkiani, M.E., et al., *Ultra-fast, label-free isolation of circulating tumor cells from blood using spiral microfluidics*. *Nat Protoc*, 2016. **11**(1): p. 134-48.
146. Warkiani, M.E., et al., *Slanted spiral microfluidics for the ultra-fast, label-free isolation of circulating tumor cells*. *Lab on a Chip*, 2014. **14**(1): p. 128-137.
147. Winter, M., et al., *Circulating tumour cell RNA characterisation from colorectal cancer patient blood after inertial microfluidic enrichment*. *MethodsX*, 2019. **6**: p. 1512-1520.
148. Jang, T.H., et al., *Cryopreservation and its clinical applications*. *Integrative Medicine Research*, 2017. **6**(1): p. 12-18.
149. Hassanzadeh-Barforoushi, A., et al., *Capillary-assisted microfluidic biosensing platform captures single cell secretion dynamics in nanoliter compartments*. *Biosensors and Bioelectronics*, 2020. **155**: p. 112113.
150. Hassanzadeh-Barforoushi, A., et al., *Static droplet array for culturing single live adherent cells in an isolated chemical microenvironment*. *Lab on a Chip*, 2018. **18**(15): p. 2156-2166.
151. Warkiani, M.E., et al., *Slanted spiral microfluidics for the ultra-fast, label-free isolation of circulating tumor cells*. *Lab on a Chip*, 2014. **14**(1): p. 128-137.
152. Winter, M., et al., *Isolation of Circulating Fetal Trophoblasts Using Inertial Microfluidics for Noninvasive Prenatal Testing*. *Advanced Materials Technologies*, 2018: p. 1800066.
153. Shemesh, J., et al., *Stationary nanoliter droplet array with a substrate of choice for single adherent/nonadherent cell incubation and analysis*. *Proceedings of the National Academy of Sciences*, 2014. **111**(31): p. 11293-11298.
154. Boukellal, H., et al., *Simple, robust storage of drops and fluids in a microfluidic device*. *Lab on a Chip*, 2009. **9**(2): p. 331-338.
155. Vogelstein, B. and K.W. Kinzler, *The multistep nature of cancer*. *Trends in Genetics*, 1993. **9**(4): p. 138-141.
156. Rad, H.S., et al., *Understanding the tumor microenvironment in head and neck squamous cell carcinoma*. *Clinical & Translational Immunology*, 2022. **11**(6): p. e1397.
157. Chaffer, C.L. and R.A. Weinberg, *A Perspective on Cancer Cell Metastasis*. *Science*, 2011. **331**(6024): p. 1559-1564.

158. Ilić, M. and P. Hofman, *Pros: Can tissue biopsy be replaced by liquid biopsy?* Translational lung cancer research, 2016. **5**(4): p. 420-423.
159. Rad, H.S., et al., *The Pandora's box of novel technologies that may revolutionize lung cancer.* Lung Cancer, 2021. **159**: p. 34-41.
160. Crowley, E., et al., *Liquid biopsy: monitoring cancer-genetics in the blood.* Nat Rev Clin Oncol, 2013. **10**(8): p. 472-84.
161. Herath, S., et al., *The Role of Circulating Biomarkers in Lung Cancer.* Frontiers in Oncology, 2022. **11**.
162. Chen, X.-X. and F. Bai, *Single-cell analyses of circulating tumor cells.* Cancer biology & medicine, 2015. **12**(3): p. 184-192.
163. Arechederra, M., M.A. Ávila, and C. Berasain, *Liquid biopsy for cancer management: a revolutionary but still limited new tool for precision medicine.* Advances in Laboratory Medicine / Avances en Medicina de Laboratorio, 2020. **1**(3).
164. de Wit, S., G. van Dalum, and L.W. Terstappen, *Detection of circulating tumor cells.* Scientifica (Cairo), 2014. **2014**: p. 819362.
165. Warburg, O., F. Wind, and E. Negelein, *THE METABOLISM OF TUMORS IN THE BODY.* The Journal of general physiology, 1927. **8**(6): p. 519-530.
166. Warburg, O., *On the origin of cancer cells.* Science, 1956. **123**(3191): p. 309-14.
167. Webb, B.A., et al., *Dysregulated pH: a perfect storm for cancer progression.* Nat Rev Cancer, 2011. **11**(9): p. 671-7.
168. Rivello, F., et al., *Probing single-cell metabolism reveals prognostic value of highly metabolically active circulating stromal cells in prostate cancer.* Science Advances, 2020. **6**(40): p. eaaz3849.
169. DARBRE, P.D., *Hypersensitivity and Growth Adaptation of Oestrogen-deprived MCF-7 Human Breast Cancer Cells.* Anticancer Research, 2014. **34**(1): p. 99-105.
170. Shaw, L.E., et al., *Changes in oestrogen receptor- α and - β during progression to acquired resistance to tamoxifen and fulvestrant (Faslodex, ICI 182,780) in MCF7 human breast cancer cells.* The Journal of Steroid Biochemistry and Molecular Biology, 2006. **99**(1): p. 19-32.
171. Gallego-Ortega, D., et al., *ELF5 Drives Lung Metastasis in Luminal Breast Cancer through Recruitment of Gr1+ CD11b+ Myeloid-Derived Suppressor Cells.* PLOS Biology, 2016. **13**(12): p. e1002330.
172. Valdés-Mora, F., et al., *Single-cell transcriptomics reveals involution mimicry during the specification of the basal breast cancer subtype.* Cell Reports, 2021. **35**(2): p. 108945.
173. Avesar, J., et al., *Nanoliter Cell Culture Array with Tunable Chemical Gradients.* Analytical Chemistry, 2018. **90**(12): p. 7480-7488.
174. Lee, Z.-W., et al., *Intracellular Hyper-Acidification Potentiated by Hydrogen Sulfide Mediates Invasive and Therapy Resistant Cancer Cell Death.* Frontiers in Pharmacology, 2017. **8**(763).
175. Patani, N. and L.A. Martin, *Understanding response and resistance to oestrogen deprivation in ER-positive breast cancer.* Mol Cell Endocrinol, 2014. **382**(1): p. 683-694.
176. Chan, C.M.W., et al., *Molecular changes associated with the acquisition of oestrogen hypersensitivity in MCF-7 breast cancer cells on long-term oestrogen deprivation.* The Journal of Steroid Biochemistry and Molecular Biology, 2002. **81**(4): p. 333-341.

177. Guy, C.T., R.D. Cardiff, and W.J. Muller, *Induction of mammary tumors by expression of polyomavirus middle T oncogene: a transgenic mouse model for metastatic disease.* Mol Cell Biol, 1992. **12**(3): p. 954-61.
178. Lin, E.Y., et al., *Progression to malignancy in the polyoma middle T oncoprotein mouse breast cancer model provides a reliable model for human diseases.* Am J Pathol, 2003. **163**(5): p. 2113-26.
179. Gallego-Ortega, D., et al., *ELF5 Drives Lung Metastasis in Luminal Breast Cancer through Recruitment of Gr1+ CD11b+ Myeloid-Derived Suppressor Cells.* PLoS Biol, 2015. **13**(12): p. e1002330.
180. Valdés-Mora, F., et al., *Single-cell transcriptomics reveals involution mimicry during the specification of the basal breast cancer subtype.* Cell Rep, 2021. **35**(2): p. 108945.
181. Arnold, M., et al., *Current and future burden of breast cancer: Global statistics for 2020 and 2040.* The Breast, 2022. **66**: p. 15-23.
182. Luo, C., et al., *Progress and Prospect of Immunotherapy for Triple-Negative Breast Cancer.* Frontiers in Oncology, 2022. **12**.
183. Goldhirsch, A., et al., *Personalizing the treatment of women with early breast cancer: highlights of the St Gallen International Expert Consensus on the Primary Therapy of Early Breast Cancer 2013.* Ann Oncol, 2013. **24**(9): p. 2206-23.
184. Fares, J., et al., *Molecular principles of metastasis: a hallmark of cancer revisited.* Signal Transduction and Targeted Therapy, 2020. **5**(1): p. 28.
185. Radfar, P., et al., *Rapid metabolomic screening of cancer cells via high-throughput static droplet microfluidics.* Biosensors and Bioelectronics, 2023. **223**: p. 114966.
186. Nieto, M.A., et al., *EMT: 2016.* Cell, 2016. **166**(1): p. 21-45.
187. Kalluri, R. and R.A. Weinberg, *The basics of epithelial-mesenchymal transition.* J Clin Invest, 2009. **119**(6): p. 1420-8.
188. Tafur, D., *The Regulation Of Lactate Metabolism In Epithelial-Mesenchymal Transition Of Human Breast Cancer Cells.* 2017.
189. Warburg, O., F. Wind, and E. Negelein, *THE METABOLISM OF TUMORS IN THE BODY.* J Gen Physiol, 1927. **8**(6): p. 519-30.
190. Sonveaux, P., et al., *Targeting lactate-fueled respiration selectively kills hypoxic tumor cells in mice.* The Journal of clinical investigation, 2008. **118**(12): p. 3930-3942.
191. Goetze, K., et al., *Lactate enhances motility of tumor cells and inhibits monocyte migration and cytokine release.* Int J Oncol, 2011. **39**(2): p. 453-63.
192. Ziebart, T., et al., *Metabolic and proteomic differentials in head and neck squamous cell carcinomas and normal gingival tissue.* J Cancer Res Clin Oncol, 2011. **137**(2): p. 193-9.
193. Végran, F., et al., *Lactate influx through the endothelial cell monocarboxylate transporter MCT1 supports an NF-κB/IL-8 pathway that drives tumor angiogenesis.* Cancer Res, 2011. **71**(7): p. 2550-60.
194. Kim, J. and R.J. DeBerardinis, *Mechanisms and Implications of Metabolic Heterogeneity in Cancer.* Cell Metabolism, 2019. **30**(3): p. 434-446.